The GPCR-G12/13-RhoA signaling axis: a key player in the regulation of MuSC quiescence

INAUGURAL-DISSERTATION

zur Erlangung des Doktorgrades der Naturwissenschaften
- Doctor rerum naturalium -
(Dr. rer. nat.)

vorgelegt dem
Fachbereich für Biologie und Chemie (FB 08)
der Justus-Liebig-Universität Gießen

eingereicht von

Yundong Peng

Gießen, 2023

Die vorliegende Arbeit wurde am Max-Planck-Institut für Herz- und Lungenforschung, W.G. Kerckhoff-Institut in Bad Nauheim angefertigt.

Erstgutachter:

Prof. Dr. Dr. Thomas Braun

Abteilung Entwicklung und Umbau des Herzens

Max-Planck-Institut für Herz- und Lungenforschung

Ludwigstraße 43, 61231 Bad Nauheim

Zweitgutachter:

Disputation am

EIDESSTATTLICHE ERKLÄRUNG

„Ich erkläre: Ich habe die vorgelegte Dissertation selbständig und ohne unerlaubte fremde Hilfe und nur mit den Hilfen angefertigt, die ich in der Dissertation angegeben habe. Alle Textstellen, die wörtlich oder sinngemäß aus veröffentlichten Schriften entnommen sind, und alle Angaben, die auf mündlichen Auskünften beruhen, sind als solche kenntlich gemacht. Bei den von mir durchgeführten und in der Dissertation erwähnten Untersuchungen habe ich die Grundsätze guter wissenschaftlicher Praxis, wie sie in der „Satzung der Justus-Liebig-Universität Gießen zur Sicherung guter wissenschaftlicher Praxis“ niedergelegt sind, eingehalten.“

Bad Nauheim, den

ZUSAMMENFASSUNG

Erwachsene skelettale Muskelstammzellen (MuSCs) verbleiben überwiegend in einem ruhenden Zustand unter Homöostase, was es ihnen ermöglicht für langere Zeit zu überleben und sich selbst zu erneuern. MuSCs reagieren unmittelbar auf Umwelteinflüsse wie erhöhte Muskelbelastung oder Verletzung und ermöglichen ein erhebliches Wachstum nach der Geburt wie auch eine umfassende Regeneration. In den letzten Jahrzehnten ist das wissenschaftliche Interesse an der Aufdeckung der komplexen physiologischen Eigenschaften und molekularen Grundlagen, die die Ruhezustände von Muskelstammzellen (MuSCs) steuern, signifikant gestiegen. Trotz vielfacher Erkenntnisse aus früheren Untersuchungen bestehen grundlegende Fragen hinsichtlich der Mechanismen, wie extrinsische Signale das intrinsische regulatorische Netzwerk von MuSCs steuern und ihren Ruhezustand regulieren.

G-Protein-gekoppelte Rezeptoren (GPCRs) haben sich als einer der wichtigen Regulatoren für die Aufrechterhaltung des Ruhezustands von MuSCs herauskristallisiert. Die spezifische Funktion der GPCRs in ruhenden MuSCs sowie die komplexe regulatorische Schaltung, die ihre Aktivität steuert, sind jedoch weitgehend unerforscht. In dieser Studie habe ich eine umfassende Charakterisierung der Funktion und Expression von GPCRs in ruhenden MuSCs durchgeführt. Unter Verwendung eines multidimensionalen Ansatzes, der pharmakologische Eingriffe und induzierbare Geninaktivierungen umfasst, habe ich kritische G-Proteine identifiziert und zwei GPCR-Liganden, Endothelin-3 (ET-3) und Neurotensin (NT), näher untersucht. ET-3 und NT, welche zum Teil aus der Muskelstammzellnische stammen, binden selektiv an die Rezeptoren EDNRB bzw. NTSR2 und aktivieren dadurch den G12/13-Signalweg in MuSCs. Diese Signalkaskade reguliert die Aktivität von RhoA und ist kritisch für die aktive Aufrechterhaltung der Quiezenz von MuSCs. Insgesamt zeigen meine Ergebnisse die Komplexität der der GPCR-Signalwege, welche den Ruhezustand von MuSCs steuern, und beleuchten die entscheidende Rolle der "GPCRs-G12/13-RhoA"-Achse bei der Aufrechterhaltung des Ruhezustandes von MuSCs. Meine Befunde bergen ein therapeutisches Potenzial, um durch eine Verbesserung der Funktion von MuSC zur Bekämpfung von Myopathien beizutragen.

SUMMARY

Adult skeletal muscle stem cells (MuSCs) predominantly rest in a quiescent state during homeostasis, which enables long-term survival and preserves self-renewal capacity. MuSCs respond promptly to environmental cues, ultimately contributing to the maintenance and regeneration of skeletal muscles throughout an individual's lifespan. Over the past few decades, there has been a surge in scientific interest to unravel the intricate physiological properties and molecular foundations governing the quiescence of muscle stem cells (MuSCs). Despite valuable insights from previous investigations, fundamental questions remain. The molecular mechanisms orchestrating the intrinsic regulatory network of MuSCs, fortifying their quiescent state, are still incompletely understood. G-protein-coupled receptors (GPCRs) have emerged as one of the important regulators for mantaining MuSC quiescence. However, the specific repertoire of GPCRs residing within quiescent MuSCs, as well as the regulatory circuitry governing their activity, remain largely unexplored. In this study, I comprehensively characterized the expression and function of GPCR within quiescent MuSCs. I used a multidimensional approach, encompassing pharmacological interventions and inducible-genetic strategies, resulting in the identification of critical G-proteins and two GPCR ligands, endothelin-3 (ET-3) and neurotensin (NT). These ligands, partially derived from the MuSC niche selectively engage EDNRB and NTSR2 receptors, respectively, thereby activating the G12/13 signaling pathway in MuSCs. I discovered that this signaling cascade is critical to maintain MuSC quiescence by regulating the activity of RhoA. Collectively, my findings unravel the intricate network of GPCR signaling pathways governing MuSC quiescence, illuminating the pivotal role played by the "GPCRs-G12/13-RhoA" axis in preserving the quiescent state of MuSCs. Notably, this novel discovery bears therapeutic potential for improving functionality of MuSC, which will help to treat myopathies.

Contents

1. INTRODUCTION

Skeletal muscle, the largest organ in vertebrates, plays pivotal roles in diverse physiological processes, encompassing locomotion and endocrine regulation. Additionally, skeletal muscles represent a metabolically highly active tissue, accounting for approximately 20% of the organism's total energy expenditure. During embryonic development, myogenesis progresses through two sequential stages: embryonic and fetal myogenesis. Embryonic myogenesis commences with the establishment of myotubes around E9.5, followed by myoblast fusion and the emergence of embryonic myofibers at around E11.5. Subsequently, proliferating myoblasts form secondary (fetal) fibers until E14.5-17.5, which align along already existing primary fibers and become innervated (Lagha et al., 2008; White et al., 2010). Fetal myogenesis reaches completion three weeks after birth in mice, with subsequent muscle mass gain relying predominantly on hypertrophic muscle growth rather than extensive myoblast cell proliferation (Lagha *et al.*, 2008). In the adult stage, skeletal muscle exhibits remarkable regenerative capacity to repair damage resulting from both physiological and pathological muscle injuries (Yin et al., 2013). Regenerative myogenesis, the process of muscle tissue regeneration in adulthood, is predominantly mediated by muscle stem cells (MuSCs) also referred to as "satellite cells." These cells originate from muscle progenitor cells (MPCs) during embryonic myogenesis (Lagha *et al.*, 2008).

1.1 Developmental myogenesis

Myogenesis, the process of muscle development, starts within the somites, which are epithelial cell structures condensating from the paraxial mesoderm. Somites further develop into the sclerotome and the dermomyotome during embryonic development. The dermomyotome eventually gives rise to MPCs and various other tissue progenitor cells, which contribute to different cell types such as endothelial cells of blood vessels, smooth muscle cells, and adipocytes, including brown fat. MPCs derived from the dermomyotome proliferate and migrate away from the dermomyotome. After reaching their destination, myoblasts fuse together, forming multinucleated muscle fibers. This phenomenon corresponds to the process termed "embryonic" or primary myogenesis, which plays a pivotal role in establishing the initial pattern of different muscles.

1.1.1 Pax3 is involved in embryonic myogenesis regulation.

The embryonic myogenesis relies on the precise orchestration of different processes, including migration, proliferation, and differentiation of MPCs. These cellular events are tightly regulated by a network of myogenic transcription factors, including Mrf4, Pax3, MyoD, and Myf5 (Gunther et al., 2013; Relaix et al., 2006; Tajbakhsh et al., 1996). While Myf5, MyoD and Mrf4 determine the identity of myogenic progenitors within somites, Pax3, a paired homeobox-containing transcription factor, primarily governs cell survival, particularly in the hypaxial region of the somite (Franz et al., 1993; Goulding et al., 1994). Moreover, Pax3 serves as a marker for myogenic progenitor cells in a migratory state, poised for transition into muscle cells through the activation of muscle-specific genes (Bober et al., 1994). A delicate equilibrium between the self-renewal of the progenitor pool and the formation of embryonic myofibers must be maintained when Pax3-positive myogenic cells exit the dermomyotome and embark on the formation of different muscle masses (Lagha *et al.*, 2008). Notably, this intricate balance is governed, in part, by the FGF signaling pathway, wherein Pax3 exerts direct control over a specific myogenic enhancer element of Fgfr4 (Lagha *et al.*, 2008). This regulatory element promotes entry of progenitors into the differentiation program. Subsequently, Pax3 initiates transcription of the myogenic factor Myf5, thereby activating downstream transcription factors, including MyoD and Myogenin, by controlling different enhancer elements (Chang et al., 2004; Francetic and Li, 2011; Tajbakhsh *et al.*, 1996). Thus, Pax3 exerts a pivotal role in embryonic myogenesis by finely regulating the dynamic interplay between MPC self-renewal and myogenic cell differentiation, ensuring the proper development of skeletal muscle.

1.1.2 Pax7 maintains skeletal muscle stem cells

During the progression of muscle development, a distinct phase known as fetal myogenesis occurs between E14.5 and E17.5 in mice. This stage involves the fusion of secondary myoblasts, either with one another to form secondary fibers (originally smaller primary fibers) or with primary myofibers. Fetal myogenesis is characterized by the growth,

maturation, and innervation of each muscle anlage. Notably, while Pax3 expression is down-regulated in fetal muscle, it persists in a specific subset of MuSCs, including those residing in the diaphragm(Messina and Cossu, 2009; Relaix *et al.*, 2006). Pax7, a paralog of Pax3, becomes the dominant transcription factor in all myogenic progenitor cells during this stage. In the limb, Pax7 initially co-localizes with Pax3, and genetic tracing experiments have revealed that Pax7-positive cells in the fetal limb originate from cells that previously expressed Pax3 (Hutcheson et al., 2009). Pax7, in turn, activates the transcription factor nuclear factor 1/X (Nfix), which promotes expression of fetal-specific genes such as muscle creatine kinase (MCK) and β-enolase while repressing embryonic genes like slow myosin (Messina et al., 2010). The essential role of $Pax7^{+}$ cells in fetal myogenesis is underscored by the loss of fetal myofibers upon ablation of the Pax7 lineage. Furthermore, during late-stage fetal muscle development, Pax3-derived Pax7-positive cells transition to a MuSC position, indicating their future role as progenitor cells for postnatal skeletal muscles (Kassar-Duchossoy et al., 2005; Relaix *et al.*, 2006). Hence, $Pax3^{+}$ and $Pax7^{+}$ cells play decisive roles in embryonic and fetal limb myogenesis, respectively.

1.1.3 Developmental myogenesis of head muscles

Emerging evidence has shed light on the distinct mode of growth exhibited by head muscles compared to limb and trunk muscles. The bHLH genes MyoR and capsule play pivotal roles in the initial development of mouse masseter muscles, operating independently of Pax3 and Pax7 (Lu et al., 2002). These transcription factors activate the myogenic program governed by MyoD, Myf5, Myogeneinm and Mrf4, initiating the formation of head muscles. The pituitary homeobox 2 (Pitx2) and T-box transcription factor 1 (Tbx1) genes complement this process during embryonic mouse development. Pitx2 mutants fail to develop muscles derived from the first branchial arch and extraocular muscles due to increased cell death in the premyogenic mesoderm (Dong et al., 2006; Gage and Camper, 1997). Inactivation of Pitx2 with $UBC^{CreERT2}$ at later stages prevents this phenotype, indicating that Pitx2 operates upstream of the myogenic factors in head muscle formation (Zacharias et al., 2011). By directly activating Myf5 and MyoD through binding to their regulatory region, known as the “regulatory region,” Pitx2 ensures survival of muscle progenitor cells, allowing muscle cell determination during early stages of extraocular muscle development, essentially

mirroring the role of Pax3 in limb muscle growth. Similarly, individuals with Tbx1 mutations experience problems with myogenesis in the first branchial arch and lack muscles associated with other branches due to severe structural malformations (Kelly et al., 2004; Zacharias *et al.*, 2011). Double mutants of Tbx1 and MyoD revealed that Tbx1 acts upstream of MyoD. Furthermore, Tbx1-mediated head muscle myogenesis has been linked to the Fgf10 and Fgf8 signaling cascades, whose absence leads to decreased proliferation of myogenic progenitor cells (Ng et al., 2002).

1.2 Regenerative myogenesis and muscle stem cells

1.2.1 Characteristics of MuSCs

MuSCs are quiescent mononucleated myogenic cells localized between the basal lamina and the plasma membrane of muscle fibers. Morphologically, MuSCs can be distinguished from fully differentiated myocytes by several characteristics: (1) a relatively high nuclear-to-cytoplasmic ratio and low number of organelles; (2) a smaller nuclear size compared to adjacent myotube nuclei; and (3) an increased amount of condensed heterochromatin in the nucleus, as illustrated in Figure 1.2.1. Immunohistochemical staining, genetic profiling, and mouse transgenic studies have contributed to the identification of molecular and cellular markers capable of discerning MuSCs from other cell types. Notably, the markers CD34, CXCR-4, M-cadherin, Pax7, syndecan-3, syndecan-4, α7-integrin, and c-met serve as reliable markers for MuSCs (Alfaro et al., 2011; Burkin and Kaufman, 1999; Cornelison et al., 2001; Cornelison and Wold, 1997; Ratajczak et al., 2003; Seale et al., 2000). While several of these markers are not exclusively expressed in MuSCs, a combination of such markers enables isolation of pure MuSCs from skeletal muscle (Fukada et al., 2007; Montarras et al., 2005; Pannerec et al., 2013; Zammit et al., 2004).

1.2.2 Origins of MuSCs

MuSCs originate from Pax3 and Pax7 expressing cells, initially derived from the dermomyotome (Relaix *et al.*, 2006; Seale *et al.*, 2000). Inactivation of Pax7 leads to a significant depletion of muscle stem cells in the adult stage and impairs muscle

regeneration following injury (Gunther *et al.*, 2013; Seale *et al.*, 2000). Lineage tracing studies utilizing the MyoD$^{iCre/+}$/*R26R-EYFP* system have demonstrated that nearly all MuSCs in adult muscle have activated MyoD during MuSC development, despite the downregulation of MyoD expression in most adult MuSCs (Kanisicak et al., 2009). These findings strongly support the notion that the majority of adult Pax7^{+} MuSCs originate from the somite and transit through a Pax7^{+}/MyoD^{+} state. Similarly, inactivation of Pax7 in the Myf5 positive lineage using *Myf5$^{Cre/+}$/Pax7$^{loxP/loxP}$* mice has revealed that the majority of adult MuSCs also derive from Myf5-expressing myogenic cells (Gunther *et al.*, 2013). Consistent with this, lineage tracing with a *Myf5^{Cre}/Rosa26YFP* reporter has shown that around 90% of the adult MuSC pool arises from Myf5^{+} precursors (Kuang et al., 2007). Notably, the formation of the MuSC pool in germline Myf5 or MyoD mutant mice suggests that Myf5 or MyoD is dispensable for MuSC formation, likely due to compensatory effects during skeletal muscle development (Gensch et al., 2008).

In contrast, accumulating evidence indicates that some adult MuSCs may have alternative origins distinct from dermomyotome-derived Pax3^{+}/Pax7^{+} progenitors. For example, studies employing TN-APCreERT2 and VE-cadherinCreERT2 alleles have demonstrated that alkaline phosphatase (ALPL) expressing pericytes, but not VE-cadherin-expressing endothelial cells, can give rise to postnatal MuSCs and participate in the normal development of limb muscles (Dellavalle et al., 2011). Additionally, several studies have shown that different types of non-MuSCs can reconstitute the MuSC niche and differentiate into bona fide MuSCs (Pax7-expressing myogenic cells) after transplantation into regenerating skeletal muscles. These cells include hematopoietic stem cells residing in the bone marrow(LaBarge and Blau, 2002), CD45^{-} muscle side population (SP) cells (Asakura et al., 2002), PW1^{+} interstitial cells (Mitchell et al., 2010), Sca1^{+}/CD34^{+} fibro-adipogenic progenitors (FAPs) (Joe et al., 2010), and muscle-derived stem cells (MDSCs) (Lee et al., 2000). However, the extent to which these cells contribute to the adult MuSC pool and muscle regeneration under physiological conditions remains largely unknown, and the validity of some of these studies has been questioned.

1.2.3 MuSCs and adult muscle regeneration

The primary role of MuSC is to facilitate muscle regeneration and maintain muscle integrity in adulthood following injury. Muscle regeneration involves a series of interconnected stages, including myofiber necrosis, the inflammatory response, activation, differentiation, and fusion of MuSCs, as well as the maturation and remodeling of newly formed myofibers. In undamaged muscles, MuSCs reside beneath the basal lamina and remain in a quiescent state, exhibiting low mitotic activity. Upon exposure to signals from the damaged environment, MuSCs transition from a quiescent to an activated state, initiating proliferation (MuSC activation). This transition is accompanied by the down-regulation of Pax7 and rapid activation of myogenic transcription factors, namely Myf5 and MyoD. The proliferating MuSCs and their progeny are commonly referred to as adult myoblasts. Subsequent differentiation of myoblasts is characterized by the up-regulation of Mrf4, Myogenin, and myosin heavy chain, leading to the formation of multinucleated myofibers or their fusion with damaged myofibers, thereby promoting muscle regeneration (Zammit *et al.*, 2004). Certain activated stem cells, which do not proliferate or differentiate, maintain Pax7 gene expression while down-regulating MyoD expression (Rudnicki et al., 1993). These cells eventually exit the cell cycle and regain markers associated with myogenic quiescence (Nagata et al., 2006). Maintaining MuSC homeostasis is crucial for muscle regeneration, both in physiological conditions such as extensive exercise and pathological conditions including myotoxin-induced injury and degenerative diseases (Parise et al., 2008). Reaquisition of MuSC quiescence ensures an adequate supply of myoblasts for fusion and the maintenance of the quiescent MuSC pool.

The essential and decisive role of MuSCs in muscle regeneration is strongly supported by the complete abrogation of muscle regeneration following depletion of the entire MuSC pool (all $Pax7^+$ cells) in adulthood (Gunther *et al.*, 2013; Sambasivan et al., 2011). However, studies have also reported that some non-myogeninc cell types can undergo myogenic differentiation and contribute to muscle regeneration when transplanted into regenerating muscle (LaBarge and Blau, 2002; Mitchell *et al.*, 2010). Nonetheless, the contribution of these cells to adult muscle regeneration appears to be negligible compared to that of MuSCs, indicating that the physiological significance of non-MuSC-based myogenesis depends on Pax7 expression and/or the presence of a substantial number of canonical MuSCs.

1.3 Regulation of MuSC homeostasis

The process of adult muscle regeneration, driven by muscle stem cells (MuSCs), is tightly regulated to ensure precise temporal and spatial control of gene expression in response to genetic and environmental cues. This regulatory mechanism involves the interplay of various muscle-specific transcription factors, epigenetic modifiers, and interactions with the MuSC niche. These factors collectively govern the maintenance of MuSC quiescence, the activation of MuSCs, their re-entry into the cell cycle, and subsequent differentiation following muscle injury. The orchestrated regulation of different processes guarantees the appropriate coordination of molecular events required for effective muscle regeneration (Dobreva and Braun, 2010; Yablonka-Reuveni et al., 2008).

1.3.1 Transcriptional regulation of MuSC homeostasis

The regulation of MuSC homeostasis is governed by a well-established transcriptional network. The activation of MyoD and Myf5 by Pax7 specifies a population of stem cells committed to the differentiation program, while $Pax7^{+}/MyoD^{-}$ cells return to a quiescent state to replenish the MuSC pool (Rudnicki et al., 2008). Down-regulation of Pax7 in $Pax7^{+}/MyoD^{+}$ or $Pax7^{+}/Myf5^{+}$ population coincides with the ability of MyoD and/or Myf5 to induce transcription of downstream genes and promote terminal differentiation (Olguín and Pisconti, 2012). Deficient skeletal muscle regeneration observed in MyoD knockout mice further supports the crucial role of MyoD in myoblast proliferation and SC differentiation (Cornelison *et al.*, 2001). Notably, cyclin-specific genes, known targets of MyoD, play a vital role in MuSC activation, marking the initial step of myogenesis in maintaining the stemness of muscle stem cells (Zammit *et al.*, 2004).

1.3.2 Epigenetic regulation of MuSC homeostasis

Emerging evidence highlights the contribution of epigenetic mechanisms to MuSC identity and homeostasis. Epigenetic regulation involves a complex interplay of post-translational modifications of histones, chromatin remodeling, nucleosome organization, and DNA

modifications. These events collectively maintain MuSC homeostasis and facilitate appropriate responses to external signals (Giordani and Puri, 2013).

Histone acetylation, a dynamic process regulated by histone acetyltransferases and histone deacetylases (HDACs), is closely associated with transcriptional activation. CREB-binding protein (CBP)/p300 and PCAF, two nuclear histone acetyltransferases, transactivate the MyoD promoter by acetylating histones in regulatory regions as well as MyoD itself (Polesskaya et al., 2000). In contrast, HDACs, categorized into three distinct classes, repress muscle gene transcription by counteracting the activities of histone acetyltransferases during myoblast proliferation (Mal et al., 2001; Puri et al., 2001). Class I HDACs associate with and inhibit MyoD, while class II HDACs, specifically HDAC4 and HDAC5, act as dedicated repressors of MEF2 activity (Fulco et al., 2003; McKinsey et al., 2000). Additionally, the NAD(+)-dependent histone deacetylase Sirt1, a class III HDAC, forms a repressor complex with PCAF and MyoD, silencing muscle gene expression in response to metabolic regulation (McKinsey *et al.*, 2000).

Histone methylation is another crucial epigenetic mechanism modulating the expression of muscle-specific transcriptional regulators at different stages of stem cells. Genome-wide epigenetic profiling in MuSCs has revealed the role of H3K27me3 in suppressing factors associated with non-muscle lineages within the proliferative progenitor population (Liu et al., 2013). Furthermore, quiescent MuSCs maintain a permissive chromatin state with a few genes epigenetically silenced by PcG-mediated H3K27me3, while regulators specifying non-myogenic lineages are marked by bivalent domains at their transcription start sites (Woodhouse et al., 2013). Transitioning from a transcriptionally permissive H3K4me3 mark to a repressive H3K27me3 mark is observed on the Pax7 gene locus as proliferating myoblasts deactivate this critical marker of MuSC identity in preparation for differentiation (Palacios et al., 2010; Woodhouse *et al.*, 2013). Loss of Ezh2, the enzyme responsible for H3K27me3, in $Pax7^{+}$ MuSCs leads to transcriptional deregulation in non-muscle lineages and impairs muscle stem cell expansion while preserving terminal differentiation (Juan et al., 2011; McKellar et al., 2021). Moreover, the TrxG/MLL complex, responsible for H3K4 methylation in the Myf5 enhancer region, interacts with Pax7 to control MuSC proliferation (Juan *et al.*, 2011).

Chromatin-remodeling activities, particularly the recruitment of the SWI/SNF complex to myogenic loci, play a vital role in activating the muscle differentiation program (Simone et al., 2004). The differentiation-activated p38 kinase phosphorylates BAF60c, promoting the incorporation of MyoD-BAF60c into a Brg1-based SWI/SNF complex. The ATPase activity of Brg1 and Brm in the complex is essential for chromatin remodeling and the transcriptional activation of MyoD target genes (Forcales et al., 2012; Simone *et al.*, 2004). Furthermore, IGF1 signaling-mediated local hyperacetylation of muscle genes by p300/CBP and PCAF HATs is required for the remodeling activity of the SWI/SNF complex, linking signaling transduction to chromatin remodeling in muscle gene expression (Forcales *et al.*, 2012). The transition from condensed heterochromatin to open euchromatin accompanies the differentiation of MuSCs into myocytes, suggesting the involvement of epigenetic mechanisms in regulating high-order chromatin structure and facilitating the transition from heterochromatin to euchromatin during MuSC homeostasis (Serra et al., 2007).

A comprehensive understanding of the genome-wide alterations of DNA or histone modifications in stem cells will provide further insights into the modulation of the myogenic gene expression program and the maintenance of SC homeostasis. Epigenetic regulations play a crucial role in orchestrating MuSC identity and function in response to various environmental cues.

1.3.3 The muscle stem cell niche regulates MuSC homeostasis

Muscle stem cells (MuSCs) reside within a highly specialized microenvironment known as the niche, comprising the extracellular matrix (ECM), vascular and neural networks, neighboring cell populations, and diffusible signaling molecules. The dynamic interplay between MuSCs and their niche regulates critical processes such as quiescence, self-renewal, proliferation, and differentiation through cell-cell interactions and autocrine/paracrine signaling mechanisms (Chang et al., 2016).

A key constituent of the MuSC niche is the myofiber, which directly interacts with MuSCs and is proposed to emit a "quiescent" signal either through physical association or the release of chemical compounds. Removal of the myofiber plasmalemma triggers activation

and proliferation of quiescent MuSCs (Guerci et al., 2012). Recent studies have uncovered numerous factors involved in MuSC homeostasis that are either presented on or secreted by myofibers. For instance, the myofibers express and secrete cytokines IL6 and IL4, which mediate paracrine control of MuSC proliferation and fusion, respectively. The transcription factor SRF regulates their expression in myofibers (Guerci *et al.*, 2012). Furthermore, myofibers up-regulate the transmembrane Notch ligand Delta in response to muscle injury, which binds to the Notch receptor in MuSCs, activating the Notch signaling cascade, promoting cell proliferation and inhibiting differentiation (Cornelison *et al.*, 2001). Muscle fiber degeneration leads to disruption o the niche and thereby to a loss of inhibitory signals.

Another critical structural feature of the MuSC niche is the basal lamina, an ECM network that envelops the myofibers. It comprises various glycoproteins, including collagen, laminin, entactin, fibronectin, perlecan, and decorin, along with other proteoglycans. Changes in ECM composition have been implicated in providing instructive cues that regulate MuSC homeostasis and muscle regeneration. For example, the absence of collagen VI in *Col6a1*$^{-/-}$ mice diminishes MuSC self-renewal capability and impairs muscle regeneration after injury (Fu et al., 2022). MuSCs express high levels of laminin receptors α7β1 integrin (Itg) and dystroglycan, and their deficiency impairs muscle regeneration in response to injury (Hicks and Pyle, 2022). Laminin-α2 subunit-deficient mice suffer from muscular dystrophy with severely impaired regeneration, which can be rescued by transgenic expression of a functional basement membrane-dystroglycan linkage (Relaix et al., 2021), emphasizing the crucial role of an intact ECM in maintaining MuSC properties and facilitating muscle repair.

The MuSC niche consists of diverse cell types, including Ang1-expressing endothelial cells, fibroblasts, and fibro-adipogenic progenitors (FAPs), which have been shown to influence the behavior of MuSC during regeneration and growth (Joe *et al.*, 2010; Verma et al., 2018). However, whether these cell types constitute the niche itself or impact on MuSC homeostasis by releasing paracrine factors that are involved in the proliferation and differentiation of MuSC progeny remains to be determined.

Mechanical and structural properties of the niche also play a crucial role in MuSC function. It has been observed that removing MuSCs from the niche and maintaining them in vitro leads to a loss of stem cell characteristics (Gilbert et al., 2010; Hicks and Pyle, 2022).

However, recent work by Gilbert et al. demonstrated that culturing isolated MuSCs on elastic surfaces, which mimic the softness of adult skeletal muscle, better preserves their stem cell properties compared to rigid surfaces (Gilbert *et al.*, 2010).

In summary, gaining a comprehensive understanding of the muscle stem cell niche will ultimately contribute to the development of techniques for ex vivo cultivation of MuSCs, enabling genetic correction and stem cell therapy for muscle diseases associated with MuSC dysfunction.

1.4 G-protein-coupled receptor in stem cell maintenance and regulation

The precise mechanisms underlying the role of G protein-coupled receptors (GPCRs) for stem cells are not fully understood, despite some clear hints (Doze and Perez, 2013). Recent evidence revealed expression of multiple subtype receptors, including lysophospholipid, cannabinoid, endothelin, chemokine, acetylcholine, frizzled, GABA, dopamine, and glutamate receptors by embryonic stem cells (ESCs), which corresponds to earlier studies on embryonic development (Flock et al., 2017). These findings strongly indicate the active participation of GPCRs in ESC biology.

It is worth noting that both Gs and Gi signaling pathways have been implicated in the biology of ESCs and induced pluripotent stem cells (iPSCs) (Doze and Perez, 2013). Gs signaling influences expression of crucial transcription factors essential for ESC maintenance. Prior investigations have also linked the Gs pathway and cyclic adenosine monophosphate (cAMP) with ESC self-renewal and pluripotency, reinforcing the association between Gs signaling and ESC biology (Doze and Perez, 2013; Yu and Brown, 2015). Moreover, Gi signaling contributes to the characteristic morphology and structural features exhibited by human pluripotent cell colonies, thereby further substantiating the involvement of GPCRs in stem cell biology (McCudden et al., 2005). Collectively, these findings suggest an role of GPCRs in regulating stem cell function.

1.4.1 GPCR family

GPCRs play a crucial role in signal transduction in eukaryotes and are involved in a wide range of cellular responses to hormones, neurotransmitters, and environmental signals (Sriram and Insel, 2018). Within the human genome, approximately 800 genes belong to the GPCR superfamily (Rosenbaum et al., 2009). Several classification systems have been proposed to categorize these receptors, including the widely used A-F (Class A: Rhodopsin-like, class B: Secretin receptor family, class C: Metabotropic glutamate/pheromone, class D: Fungal mating pheromone receptors, class E: Cyclic AMP receptors, class F: Frizzled/Smoothened) and GRAFS systems (Attwood and Findlay, 1994; Yu and Brown, 2015). In this thesis, the evolutionary exploration of GPCRs is approached using the GRAFS classification system. Based on sequence similarity and phylogenetic inference, the GRAFS system classifies the human GPCR repertoire into five primary families: Glutamate (G), Rhodopsin (R), Adhesion (A), Frizzled/taste2 (F), and Secretin (S) (Krishnan, 2015; Rosenbaum *et al.*, 2009; Yu and Brown, 2015) (refer to Figure 1). In addition to these main families, smaller GPCR families exist such as the GPR108 family, the intimal thickness-related receptor family, the ocular albinism receptor family, and the Dictyostelium discoideum cAMP receptor family (Krishnan, 2015; Sriram and Insel, 2018). These families, however, do not fall within the GRAFS system and are typically referred to as the "others" category. While most GPCR families are found in metazoans, recent mining efforts have revealed the presence of certain families in pre-metazoan organisms. Notably, homologs of Frizzled, Glutamate, Adhesion, and cAMP families have been identified in Dictyostelium discoideum. Nevertheless, previous explorations of GPCRs have predominantly focused on metazoans, and a comprehensive investigation into GPCRs across non-metazoan lineages is lacking (Congreve et al., 2020). Moreover, the curation of GPCR repertoires in non-bilaterian metazoans and their evolutionary relationships with bilaterian GPCRs remain an unresolved areas of research.

Structurally, GPCRs consist of a seven-transmembrane α-helical segment, an extracellular N-terminus, an intracellular C-terminus, and alternating extracellular and intracellular loops connecting the helices (Congreve *et al.*, 2020). While the 7TM domain segments show relative conservation within the GRAFS families, the N-termini and extracellular loops

exhibit significant diversity, enabling GPCRs to bind ligands with various properties (Hamann et al., 2015). Upon ligand binding, GPCRs undergo conformational changes that activate heterotrimeric G proteins, leading to intracellular responses (Rosenbaum *et al.*, 2009).

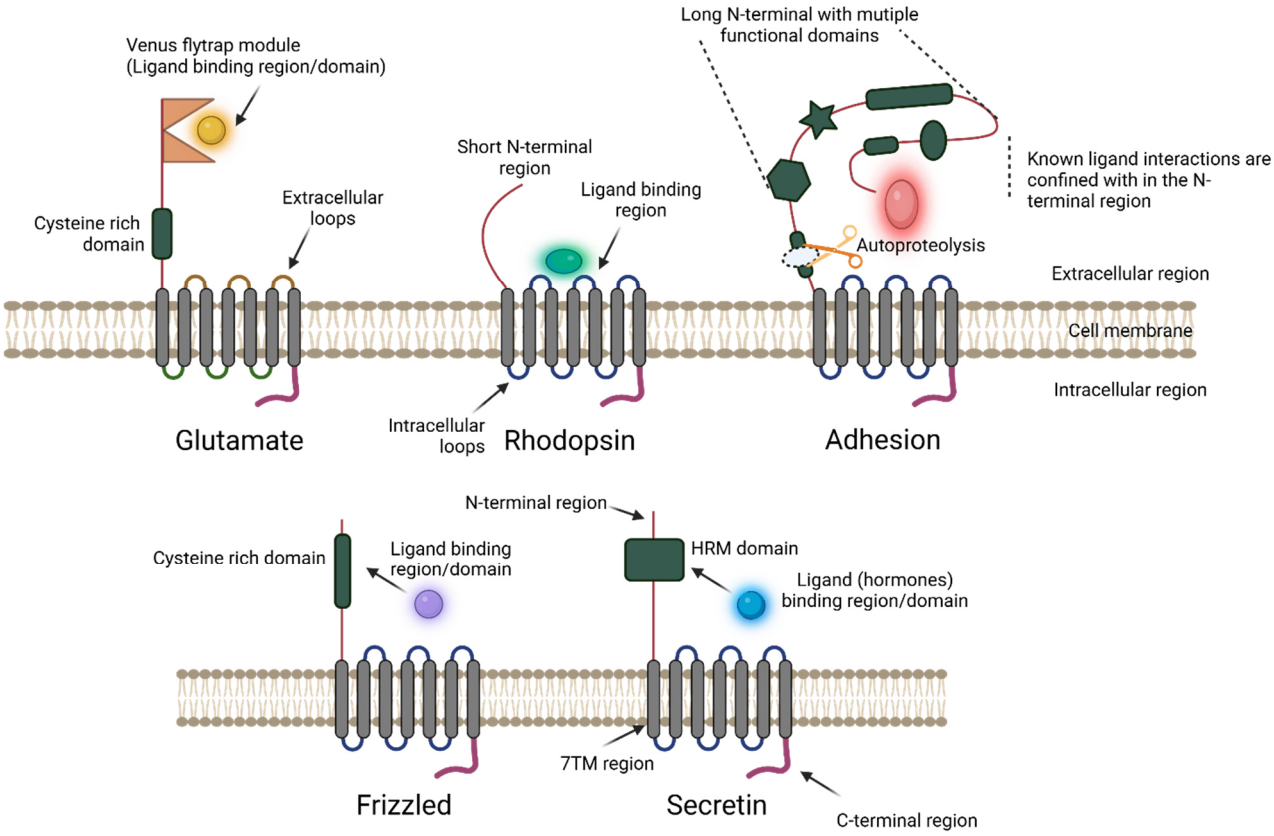

Figure 1 A simplified schematic figure depicting the most common or generic structural architecture of GRAFS GPCR families, which are divided into five major families: Glutamate, Rhodopsin, Adhesion, Frizzled/Taste2, and Secretin. The **Glutamate family** (top left) features a large extracellular ligand-binding domain and primarily responds to neurotransmitters like glutamate, initiating intracellular G protein signaling upon ligand binding. The **Rhodopsin family** (top middle) is the most diverse, with shorter extracellular domains where ligands bind within the transmembrane region, triggering G protein activation or other signaling cascades. This family includes receptors for light, hormones, and neurotransmitters. The **Adhesion family** (top right) has extended extracellular regions with adhesion-like domains and is involved in cell-cell and cell-matrix interactions. A unique feature of this family is **autoproteolysis**, where self-cleavage occurs within the GPCR, facilitating receptor activation and signaling related to cell adhesion, migration, and communication. The **Frizzled/Taste2 family** (bottom left) includes Frizzled receptors that interact with Wnt proteins,

playing critical roles in cell differentiation through the Wnt signaling pathway, and Taste2 receptors involved in taste perception; both can signal through G proteins or β-arrestin pathways. Finally, the **Secretin family** (bottom right) has a prominent extracellular domain for binding peptide hormones like glucagon, often leading to G protein-coupled cAMP production upon activation, influencing various physiological processes such as metabolism and immune responses. This classification highlights the structural distinctions and unique signaling mechanisms of each GPCR family, emphasizing their diverse physiological roles. *Adapted and modified from Krishnan et al., 2015.*(Krishnan, 2015).

1.4.2 GPCR Signalling

Upon ligand binding, conformational changes occur in the GPCR, allowing it to physically interact with heterotrimeric G proteins for subsequent activation. Heterotrimeric G proteins mediate the coupling between membrane receptors and intracellular effectors (Congreve *et al.*, 2020). Comprising three subunits (α, β, and γ), these proteins are initially associated in a basal state, with the α subunit binding to guanosine diphosphate (GDP) (Flock *et al.*, 2017; Inoue et al., 2019). The different subfamilies of heterotrimeric G proteins, including Gi, Gs, Gq, and G12/13, are defined by their specific α isoforms. Upon activation, GPCRs serve as guanine nucleotide exchange factors (GEFs) for G proteins, facilitating the exchange of GDP for guanosine triphosphate (GTP) on the α subunit (Doze and Perez, 2013). This leads to the dissociation of the subunits into an α-GTP monomer and a β/γ dimer, which then interact with their respective effectors. Eventually, GTP hydrolysis by the GTPase activity of the α subunit converts GTP back to GDP (Husted et al., 2017). The activated G protein subunits modulate the release of second messengers and various downstream intracellular signaling pathways, including adenylyl cyclase, phospholipases A2, C, and D, calcium mobilization, mitogen-activated protein (MAP) kinases, phosphoinositide 3-kinase (PI3K), and the activation of small GTPases such as Rho and Rac (O'Hayre et al., 2014; Shen et al., 2015). These signaling events regulate and adapt cellular functions in response to external stimuli.

In addition to heterotrimeric G proteins, monomeric G proteins from the Ras GTPase superfamily, such as Ras, Rho, Arf, Rab, and Ran play essential roles in intracellular signaling (Yu and Brown, 2015). Unlike heterotrimeric G proteins, small G proteins are primarily

localized in the cytoplasm and do not require activation by GPCRs (Sriram and Insel, 2018).

1.4.3 GPCR signalling in regulation of stem cell properties

1.4.3.1 Role of GPCRs in embryonic stem cells

GPCR signaling pathways play a pivotal role in the maintenance and regulation of embryonic stem cells (ESCs). Lysophosphatidic acid (LPA) and sphingosine-1-phosphate (S1P) are integral components in preserving ESCs' pluripotent state (Flock *et al.*, 2017). Mouse ESCs express specific receptor subtypes, including LPAR1-3 and LPAR5, as well as S1PR1-5, while human ESCs express LPAR1-5 and S1PR1-3 (Brockmann et al., 2017; Husted *et al.*, 2017; Krishnan, 2015; Rothe et al., 2019). LPA promotes mouse ESCs' self-renewal by activating extracellular signal-regulated kinase (ERK) 1/2 and inducing c-fos expression, highlighting its role in ESC self-renewal (Sriram and Insel, 2018). Similarly, S1P treatment of mouse ESCs activates ERK1/2, likely mediated by S1PR5, through Gi-, PKC-, and c-Src-dependent mechanisms, associated with both ESC proliferation and differentiation, illustrating its pleiotropic nature (Flock *et al.*, 2017; Husted *et al.*, 2017; Rothe *et al.*, 2019; Tischner et al., 2017). LPA also regulates the expression of c-myc, a key pluripotency gene involved in ESC self-renewal and reprogramming to induced pluripotent stem cells (iPSCs) (Doze and Perez, 2013; McCudden *et al.*, 2005; Siehler, 2009; Yu and Brown, 2015).

Long-term serum-free culture of human ESCs was initially achieved by supplementing S1P along with platelet-derived growth factor (PDGF) and a mouse embryonic fibroblast (MEF) feeder layer (Doze and Perez, 2013). While MEF support for human ESCs potentially involves the release of bioactive sphingolipids, it is insufficient without exogenous supplementation of S1P and PDGF (Bruno et al., 2018; Loh et al., 2012). Moreover, S1P alone is inadequate for maintaining human ESCs, likely due to the down-regulation of key pluripotency genes OCT-4 and NANOG (O'Hayre *et al.*, 2014). Similar to mouse ESCs, the mechanism in human ESCs involves Gi- and ERK1/2-dependent pathways, resulting in the inhibition of apoptosis and pro-survival effects (Flock *et al.*, 2017). Blocking the ERK1/2 pathway abolishes the anti-apoptotic effect of S1P, consistent with S1P-induced up-

regulation of anti-apoptotic genes and down-regulation of pro-apoptotic genes (McCudden *et al.*, 2005).

Wnt signaling has also emerged as a pivotal factor in various stem cell systems, including the regulation of embryonic stem cell (ESC) self-renewal (Urtatiz and Van Raamsdonk, 2016). However, the precise contribution of Wnt signaling to ESC behavior remains to be fully elucidated. While human ESCs (hESCs) have been reported to express Wnt1, Wnt3, and Dkk-1, the presence of Wnt ligands or active canonical Wnt signaling in hESCs has not been confirmed (Doze and Perez, 2013; Husted *et al.*, 2017). The effects of Wnt3a or the GSK-3 inhibitor, 6-bromoindirubin-3'-oxime (BIO), on hESC pluripotency and differentiation have been investigated, yielding conflicting findings (Bernardi et al., 2011). Moreover, studies employing Wnt3a, BIO, Frizzled-Related Protein 2 (FRP2), and Dkk-1 have generated conflicting results (Inoue *et al.*, 2019).

Wnt3a has been suggested to enhance single-cell survival and promote hESC proliferation, possibly in conjunction with unidentified anti-differentiation factors (Sriram and Insel, 2018). Furthermore, the Wnt receptor FZD7 has emerged as a key player in maintaining hESC properties, with mRNA levels exhibiting a remarkable 200-fold increase in hESCs compared to differentiated cell types (Congreve *et al.*, 2020). Knockdown of FZD7 using shRNA induces significant changes in ESC colony morphology and leads to the loss of OCT-4 expression, highlighting the potential role of FZD7 as an ESC-specific surface antigen and a putative regulator of ESC self-renewal (McCudden *et al.*, 2005).

The exploration of Wnt receptor signaling represents a captivating avenue of research, holding great promise for the utilization of pluripotent and other stem cells in translational applications such as tissue engineering and regenerative medicine. However, further investigations are imperative to unravel the intricate mechanisms underlying Wnt signaling in ESCs and to fully comprehend its therapeutic implications. Notably, the upregulation of C-X-C Motif Chemokine Receptor 4 (CXCR4) in the human endometrium suggests its potential involvement in the critical adhesion phase of blastocyst implantation. The biological effects attributed to CXCR4 and its ligand, such as the induction of proliferation, trafficking, locomotion, and adhesion in early stem and progenitor cells, raise intriguing

possibilities regarding its role in the biology of pluripotent stem cells. Although the expression of CXCR4 has been observed in mouse ESCs, there is a notable absence of comprehensive studies investigating CXCR4 signaling in the maintenance of ESCs or induced pluripotent stem cells (iPSCs) to the best of our knowledge (Husted *et al.*, 2017). Thus, a comprehensive examination of CXCR4 signaling in the context of ESC and iPSC maintenance is warranted, considering both indirect evidence and more recent direct findings in related fields. The endothelin (ET) family, comprising ET-1, ET-2, and ET-3, exerts its effects by activating ET_A and ET_Breceptors. Expression of ETs and their receptors has been observed in human embryonic stem cells (hESCs) (Davenport et al., 2016; Siao et al., 2021). However, the precise role, if any, of ET receptor signaling in ESC maintenance remains elusive.

1.4.3.2 Role of GPCRs in mesenchymal stem cells

Mesenchymal stem cells (MSCs) represent a diverse adult stem cell population with a remarkable potential for differentiation into various mesodermal lineages such as adipocytes, osteoblasts, and chondrocytes (Ullah et al., 2015). Their regenerative prowess and immunomodulatory capabilities have positioned them at the forefront of tissue repair and regeneration, with G protein-coupled receptors (GPCRs) playing a pivotal role in enhancing their therapeutic efficacy in regenerative medicine (Chechekhin et al., 2022; Pant et al., 2021).

A range of GPCRs have been identified as crucial regulators of MSC functions, including proliferation, migration, and differentiation (Chechekhin *et al.*, 2022). Among them, the sphingosine-1-phosphate receptor 1 (S1PR1) stands out as a central player, orchestrating the pro-regenerative abilities inherent to MSCs (Kong et al., 2014). Activation of S1PR1, facilitated by its ligand sphingosine-1-phosphate (S1P), not only fosters MSC migration to injury sites but also promotes tissue repair by modulating inflammatory responses and guarding against oxidative stress-induced apoptosis (Kong *et al.*, 2014). Furthermore, GPR56 (ADGRG1) facilitates MSC osteogenesis, a process vital for bone regeneration and repair, through its interaction with collagen III (Moreno et al., 2017).

Delving deeper into the role of GPCRs, it is evident that they hold significant sway in the functioning of specific MSC subsets, including adipose-derived mesenchymal stem cells (AMSCs) and bone marrow-derived mesenchymal stem cells (BMMSCs) (Mohamed-Ahmed et al., 2018). AMSCs, isolated from adipose tissue, rely heavily on GPCRs for regulating activities such as adipogenic differentiation and lipid metabolism (Chechekhin *et al.*, 2022; Liu et al., 2016). For instance, while the activation of FFAR2 inhibits adipogenic differentiation and reduces lipolysis in adipocytes, GPR120 fosters adipogenic differentiation, highlighting the potential of GPCRs as targets in AMSC regulation (Ivan et al., 2017; Lin et al., 2021).

Similarly, BMMSCs, commonly utilized in regenerative medicine, have their differentiation and migration processes overseen by GPCRs. These receptors facilitate the differentiation of BMMSCs into various cells, including osteoblasts and chondrocytes, through the activation of specific GPCRs like P2Y2 and P2Y6 (Li et al., 2016; Szustak and Gendaszewska-Darmach, 2020). Moreover, GPCRs such as CXCR4 enhance the migration of BMMSCs to injury sites, underlining the critical role GPCRs play in guiding the therapeutic application of BMMSCs (Luo et al., 2022).

1.4.3.3 Roles of GPCRs in epidermal stem cells

Epidermal stem cells (EpdSCs) reside in specialized niches pivotal in determining their fate. These niches are characterized by their interaction with the extracellular matrix (ECM), particularly the basement membrane (BM) that separates the epidermal and dermal compartments. The ECM acts as a fundamental regulator of EpdSC maintenance, mobilization, and differentiation (Chermnykh et al., 2018). Mechanical signaling, both from external sources and intrinsic cell surface properties, profoundly impacts biological processes, including stem cell fate determination (De Belly et al., 2022). Notably, the behavior of somatic stem cells, especially those in the epidermis, is influenced by mechanical signals. For instance, the YAP/TAZ regulation by cell shape and ECM rigidity can dictate whether EpdSCs remain undifferentiated or activate a terminal differentiation program (Fuchs and Blau, 2020). The mechano-activation of YAP/TAZ promotes epidermal stemness by inhibiting Notch signaling, a key factor for epidermal differentiation (Fuchs and

Blau, 2020).

Building on this, G-protein coupled receptors (GPCRs) emerge as pivotal players in the realm of epidermal stem cells. These receptors transduce extracellular signals into intracellular responses, serving as key regulators that ensure epidermal stem cells adeptly adapt to changing conditions, maintain tissue homeostasis, and activate repair mechanisms (Pedro et al., 2020). GPCRs can activate a myriad of intracellular signaling cascades through both G protein-dependent and independent mechanisms. The choice of pathway is often contingent on the specific GPCR, its ligand, and the cellular context, influencing a range of cellular processes from gene expression to cytoskeletal dynamics. Notably, the Hedgehog signaling pathway, mediated through the GPCR Smoothened (SMO), plays a crucial role in tissue patterning during embryonic development and remains active in certain adult tissues, including the skin. Dysregulation of this pathway, especially aberrant activation of SMO, has been linked to conditions like basal cell carcinoma (Rezza et al., 2016). Additionally, the Hippo signaling pathway, with its key effectors YAP and TAZ, regulates organ size by controlling cell proliferation and apoptosis (Zhang et al., 2011). In epidermal stem cells, GPCRs modulate the Hippo pathway, influencing cell behavior from proliferation to tissue repair (Zhang *et al.*, 2011). Furthermore, the WNT signaling pathway, fundamental in stem cell regulation and tissue homeostasis, is influenced by certain GPCRs, which can either enhance or inhibit the pathway, thereby determining epidermal stem cell fate (Veltri et al., 2018). The intricate interplay between GPCRs and these signaling pathways underscores their significance in skin health and potential disease states.

1.4.3.4 Role of GPCRs in hematopoietic stem cells

Hematopoietic stem cells (HSCs) are multipotent cells responsible for the formation of blood cells in the body (Till and Mc, 1961). The regulation of HSCs is a complex process, influenced by various factors, including G protein-coupled receptors (GPCRs). In the context of HSCs, several GPCRs have been identified and studied for their potential roles and implications. G-protein coupled receptor 56 (Gpr56) has been identified as a potential HSC

regulator based on its differential expression in quiescent relative to proliferating HSCs (Rao et al., 2015; Saito et al., 2013). Gpr56 is abundantly expressed by hematopoietic stem and progenitor cells (HSPCs) during both embryonic definitive hematopoiesis and in the adult bone marrow, with expression levels decreasing substantially upon HSPC differentiation (Rao *et al.*, 2015).

In Acute Myeloid Leukemia (AML) with high ecotropic viral integration site-1 (EVI1) expression, GPR56 has been identified as a novel marker (Birdwell et al., 2021). GPR56 is associated with high cell adhesion and anti-apoptotic activities in EVI1 high AML through the activation of RhoA signaling (Daga et al., 2019). Furthermore, GPR56 plays a significant role in the maintenance of quiescence and cellular adhesion of EVI1 high AML and HSCs in the bone marrow niche (Daga *et al.*, 2019). A variety of GPCRs, including CXCR4, CysLT1, S1P1, CB2, and C3aR, are expressed in HPCs (Mohle and Drost, 2012). While the role of CXCR4 in stem cell homing is established, the function of other GPCRs is only partially understood (Zhang et al., 2016). There exists a crosstalk between these GPCRs, influencing HPC trafficking.

Inappropriate activation of Wnt/β-catenin signaling in MLL-rearranged acute myeloid leukemia (AML) suggests that other developmental signaling pathways, including GPCRs, may induce activation or downstream signaling of β-catenin (Wagstaff et al., 2022). GPR84, a proinflammatory GPCR, has been identified as a potential LSC-specific candidate target, suggesting its potential clinical relevance in predicting disease prognosis (Dietrich et al., 2014). The cannabinoid receptors CB1 and CB2, members of the GPCR family, have been identified in murine embryonic stem (mES) cells. These receptors play a role in the differentiation of mES cells into multiple hematopoietic lineages during embryoid body (EB) formation in vitro (Jiang et al., 2007). The G protein-coupled receptor (GPCR), chemokine CXC-type receptor 4 (CXCR4), and its ligand, CXCL12, mediate the retention of polymorphonuclear neutrophils (PMNs) and HSPCs in the bone marrow (Zhang *et al.*, 2016). Agents that disrupt CXCL12-mediated chemoattraction of CXCR4-expressing cells mobilize PMNs and HSPCs into the peripheral circulation, offering therapeutic potential for HSPC collection before autologous bone marrow transplantation (ABMT) (Zhang *et al.*, 2016).

1.4.3.5 Role of GPCRs in neural stem cells

Neural stem cells (NSCs) play a pivotal role in shaping the neural framework and facilitating the repair mechanisms of the nervous system (Zhao and Moore, 2018). These cells exhibit a range of behaviors, including growth, transformation, movement, and resilience, all of which are influenced by an array of G protein-coupled receptors (GPCRs) (Doze and Perez, 2012).

Within the realm of GPCRs, adrenergic receptors (ARs) have emerged as significant influencers of NSC activities (Gupta et al., 2009). The a1-ARs, for instance, are known to promote the growth and movement of neural progenitor cells (Gupta *et al.*, 2009). In contrast, specific agonists, such as clonidine, have shown to limit the growth of hippocampal progenitors when interacting with a2-ARs (Gupta *et al.*, 2009).

Cannabinoid receptors, notably CB1 and CB2, are central to the growth dynamics of both embryonic and adult rodent NSCs (Rodrigues et al., 2019). Additionally, chemokine receptors, with an emphasis on SDF-1 and CXCR4, play a role in guiding and nurturing developing granule cells, particularly in regions like the cerebellum and hippocampus (Ho et al., 2017b).

Dopaminergic receptors, with the D2 receptor standing out, have been linked to the growth patterns observed in adult neural structures(Kippin et al., 2005). Systemic treatments with D2-like agonists have been reported to amplify the growth of precursor cells in specific neural zones (Daadi, 2019).

Other noteworthy GPCRs include the vasoactive intestinal peptide receptors, neuropeptide Y receptors, purinergic receptors, and Wnt receptors (Doze and Perez, 2012; Geloso et al., 2015). Each of these receptors has a unique role in guiding the behavior and transformation of NSCs, ensuring the proper development and maintenance of neural structures(Doze and Perez, 2012).

1.4.3.6 GPCR Signalling in MuSC functions

GPCRs have emerged as key regulators of various stages of muscle satellite cell (MuSC) behavior, including quiescence, activation, proliferation, and differentiation. During quiescence, the calcitonin receptor (CALCR) plays a critical role in maintaining MuSCs in a quiescent state by responding to calcitonin and soluble collagen V (Baghdadi et al., 2018a). This response is mediated by activation of the Gsa protein, leading to an increase in the cAMP-PKA pathway as a second messenger (Yamaguchi et al., 2015; Zhang et al., 2019). In addition, the adhesion-type GPCR, GPR116 (also known as Adgrf5 or Adhesion G Protein-Coupled Receptor F5), maintains MuSC quiescence by activating beta-arrestin1 nuclear translocation, which then interacts with CREB to enhance CREB transcriptional activity and promote the expression of cell cycle inhibitors such as p27Kip1 (Sénéchal et al., 2022). Eliazer et al. reported that Wnt-4 secreted by myofibers can suppress MuSC activation through a paracrine mechanism by promoting RhoA activity in quiescent MuSCs, thereby inhibiting YAP-mediated MuSC activation (Eliazer et al., 2019). In this process, the Frizzled receptor-mediated WNT-PCP (planar cell polarity) signaling pathway is implicated in the activation of RhoA in MuSCs (Eliazer *et al.*, 2019). Fzd7, which is highly enriched on the surface of quiescent MuSCs, interacts with Wnt7a during muscle injury repair to promote symmetric MuSC division by regulating the polarized distribution of Vangl2, thereby mediating the maintenance and expansion of the MuSC pool during repair (Smith et al., 2017).

There are other GPCRs that, although also enriched on the surface of quiescent MuSCs, tend to facilitate the normal activation process and responsiveness of quiescent MuSCs to activation signals. For example, CXCR4 and prostaglandin E receptor 4 (EP4) have been shown to be critical for the proper activation of injury-mediated MuSCs. CXCR4 protects MuSCs from TNF-alpha-mediated apoptotic signals during the inflammatory phase of skeletal muscle regeneration by synergizing with the HGF/c-Met pathway, thereby promoting normal MuSC activation and muscle repair (Perez et al., 2009). EP4 has been identified as an important mediator of MuSCs response to activation signals. After muscle injury, the inflammatory cytokine prostaglandin E2 (PGE2) interacts with EP4 to activate the cAMP/phospho-CREB signaling pathway, which further activates the proliferation-inducing

transcription factor Nurr1 to promote MuSC activation and rapid expansion (Ho et al., 2017a). Interference with S1P synthesis significantly inhibits injury-mediated MuSC activation and proliferation, and further studies have shown that S1P1-4 receptors regulate S1P-mediated MuSC behavior (Donati et al., 2013). However, Fortier et al. found that S1pr3, which is highly enriched in quiescent MuSCs, inhibits MuSC activation and cell cycle entry, suggesting that S1PR3 may also be involved in a unique regulatory pathway independent of the S1P-S1PR signaling axis (Fortier et al., 2013).

Numerous GPCRs and their downstream signaling pathways have been reported to be involved in the regulation of MuSC proliferation and differentiation. Early in vitro studies indicated that pertussis toxin (PTX), a classical inhibitor of G-protein i/o (Gi/o), could inhibit FGF2-mediated MuSC proliferation, suggesting that Gi/o may be an important hub in the GPCR downstream signaling network regulating MuSC proliferation (Fedorov et al., 1998). Consistent with this, Gαi2 knockout mice exhibited severe impairments in muscle development and injury repair (Minetti et al., 2014). While direct *in vivo* evidence for the involvement of several other major GPCR-coupled G-protein cascades in the regulation of MuSC proliferation and differentiation is scarce, numerous GPCRs associated with them, particularly those typically coupled to G-protein 12/13 (G12/13), such as CXCRs (chemokine receptors), S1PRs (Sphingosine-1-phosphate receptors), ATs (Angiotensin II receptor), PARs (Protease-activated receptors), etc., have been shown to play irreplaceable roles in these processes (Auvergne et al., 2016; Donati *et al.*, 2013; Perez *et al.*, 2009; Yoshida et al., 2013; Yoshida et al., 2014). In addition, some GPCRs can also activate their downstream signaling pathways independently of G proteins to regulate MuSC proliferation and differentiation. A human study found that activated MuSCs during skeletal muscle injury repair secrete obestatin to activate GPR39 on their cell surface, which then activates the scaffolding proteins β-arrestin 1 and 2 through a G-protein-independent downstream signaling pathway, enhancing mitosis-related ERK1/2 and JunD activities to promote expansion of the activated MuSC population (Santos-Zas et al., 2016).

Collectively, these studies underscore the critical role of the GPCR receptor system in regulating the behavior of MuSCs at various stages of their physiological process. As a key interface connecting systemic regulatory networks, GPCRs are likely indispensable

components for MuSCs to participate in the coordinated regulation of organismal homeostasis.

2. OBJECTIVES

Skeletal muscles contain a rare, specialized subset of myofiber-associated adult stem cells called MuSCs, which are derived from a population of proliferative $Pax7^{+}$ muscle precursors during early embryonic development. In resting muscle these cells are in a quiescent state. Upon muscle injury or excessive exercise, MuSCs exit quiescence, activate, proliferate and differentiate eventually generating new myofibers. The aim of this study was to understand the molecular mechanisms controlling quiescence of MuSCs in adult mice. Previous studies have shown that quiescent MuSCs are characterized by highly activated RhoA and other GPCR-related signaling transduction pathways. Therefore, I reasoned that distinct groups of GPCRs regulate MuSC quiescence. To identify and elucidate GPCR-dependent processes that control MuSC quiescence and thereby skeletal muscle regeneration, I have addressed following objectives:

(1) Identification of unknown GPCRs and their counterpart ligands that are specifically enriched in MuSCs

(2) Investigating which G-protein signaling pathways is required for maintaining MuSC quiescence state in both physiological and pathological conditions.

(3) Identification of molecular targets mediating the effects of GPCR signaling pathways in the control of MuSC quiescence.

(4) Addressing the potential role of GPCRs and its coupled G-proteins in myopathies and muscle diseases.

3. MATERIALS

3.1 Chemicals and Enzymes

Table 3.1: Specific reagents

Reagent	Manufacturer
Cardiotoxin (# C-9759)	Sigma-Aldrich Chemie GmbH, Steinheim
Collagen type 1 (# 354236)	BD Biosciences Pharmingen, San Diego, USA
Collagenase type 2 (# 4176)	Worthington Biochemical Corporation, Lakewood, United States
Collagenase P (# 11213857001)	Roche Diagnostics GmbH, Mannheim, Germany
Complete Protease Inhibitor Cocktail Tablets	Roche Diagnostics GmbH, Mannheim, Germany
Dispase (# 354235)	BD Biosciences Pharmingen, San Diego, USA
DMSO	Sigma-Aldrich Chemie GmbH, Steinheim
DNase I (# 11284932001)	Roche Diagnostics GmbH, Germany
Dithiothreitol (DTT)	AppliChem GmbH, Darmstadt
Ethidium bromide	Sigma-Aldrich Chemie GmbH, Steinheim
Eosin Y solution, aqueous	Sigma-Aldrich Chemie GmbH, Steinheim
Hematoxylin Gill	Sigma-Aldrich Chemie GmbH, Steinheim
Skimmed milk powder	Roth GmbH, Karlsruhe, Germany
Paraformaldehyde (PFA)	Fluka Chemie GmbH, Buchs
Percoll (# P4937)	Sigma-Aldrich Chemie GmbH, Steinheim
Ponceau S	Fluka Chemie GmbH, Buchs
Protein Standard (Novex ® Sharp Protein Standard)	Invitrogen GmbH, Karlsruhe
Rnase,Dnase-free(#11119915001)	Roche Diagnostics GmbH, Mannheim, Germany
Tissue-Tek ® O.C.T. PolyfreezeTM freezing	Miles Inc., Diagnostic Division, Elkhart, United States
TRIZOL ® reagent	Invitrogen GmbH, Karlsruhe

Matrigel	BD Biosciences, Greiner
Mowiol 4-88	Fluka Chemie GmbH, Buchs
Protein A Agarose	Roche Diagnostics GmbH, Germany
Protein G Agarose	Roche Diagnostics GmbH, Germany
Chelex®100 Resin	BioRad Laboratories GmbH, Munchen
Rhotekin-RBD protein(# PAK01)	Cytoskeleton, Inc
Pak1-PBD protein(# PAK01)	Pak1-PBD protein
ROCK inhibitor – Y-27632(Y27) (# 72304)	StemCell Technologies
Rho inhibitor I – Exoenzyme C3 (# CT04-A)	Cytoskeleton, Inc
Endothelin 3 (ET-3)(# AS-24323)	Eurogentec
Neurotensin(NT)(# 1909)	Tocris
Formin inhibitor – SMIFH2 (# HY-16931)	MedChemExpress
EDNRB inhibitor – BQ788 (# 1500)	Tocris
NTSRs inhibitor – SR142948A (# SML0015)	Sigma-Aldrich
YAP inhibitor – verteporfin (VP) (# 5305)	Tocris
Coelenterazine 400a (# 70217-82-2)	Cayman

3.2 Ready-reaction systems

Table 3.2: Used Kits

Kits	Manufacture
Click-iT EdU Cell Proliferation Kit	Invitrogen GmbH,Germany
	Roche Diagnostics GmbH, Germany
RhoA G-LISA Activation Assay (Luminescence Format) 96 Assays	BioRad Laboratories GmbH, Germany
Masson's trichrome	Sigma-Aldrich Chemie GmbH, Germany
Absolute ™ SYBR ® Green Fluorescein Mix	Thermo Fisher Scientific, USA
GPCR Compound Library	Selleck Chemicals GmbH, Germany
MinElute PCR Purification Kit	QIAGEN GmbH, Germany
Qubit® dsDNA HS Assay Kit	Invitrogen GmbH, Germany

3.3 Buffers and Solutions

All buffers and solutions were prepared with water that previously available via a Treatment system (MilliQ Plus Water System, Millipore GmbH, Schwalbach/Ts) to the quality grade "double-distilled”.

Table 3.3: Standard buffers

Standard buffers	Composition
PBS	137 mM NaCl, 2.7 mM KCl, 10 mM Na2HPO4, 2 mM KH2PO4
PBST	PBS containing 0.1% Tween 20
SDS running buffer (10x)	250 mM Tris base, 1% SDS, 1.9 M Glycine
Semi-dry transfer buffer	25 mM Tris base, 192 mM Glycine, 20% Methanol
Whole cell extraction buffer	100mM Tris-HCl, pH 7.9, 1M MgCl2, 1M KCl, 0.1M EDTA, protease inhibitor cocktail
Red blood cell lysis buffer	1.5M NH4Cl, 100 mM KHCO3, 10 mM EDTA,add 5 µg/ml Dnase I before use

3.4 Culture Medium

Table 3.4: Culture media Mediums Composition

Growth medium for FACS isolated MuSCs	DMEM-GlutaMAX containing 20% fetal calf serum (FCS), 1%Penicillin/Streptomycin, and 5 ng/mL basic fibroblast growth factor (bFGF)
Growth medium for freshly isolated myofibers	GlutaMAX ™ DMEM with 4.5 g / l glucose 20% fetal calf serum, 100 U / ml penicillin / streptomycin 15 µg/µl Fibroblast growth supplement (FGS)
Screening medium	DMEM-GlutaMAX medium supplemented with 20% fetal calf serum (FCS) and basic fibroblast growth factor (bFGF) at a concentration of 5 ng/mL

3.5Oligonucleotides

The oligonucleotides used in this work were from Sigma-Aldrich Chemie GmbH, Steinheim based.

Table 3.5: List of primers for genotyping or qRT-PCR.

Genotyping	Primers	Sequence(5'-->3')
Pax7 CreERT2	*Forward*	ACTAGGCTCCACTCTGTCCTTC
	Reverse	GCAGATGTAGGGACATTCCAGTG
Pax7 nGFP	*Forward*	CTGCATGTACCACGAGTCCA
	Reverse	GTCAGCTGCCACTTCTGGTT
G12 KO	*G12 F*	AAA GTC GCT CTG AGT TGT TAT
	G12 WT R	GGA GCG GGA GAA ATG GAT ATG
	G12 KO R	CAT CAA GGA AAC CCT GGA CTA CTG
	mdx_Forward	GCGCGAAACTCATCAAATATGCGTG TTAGTGT
	mdx WT Reverse	GATACGCTGCTTTAATGCCTTTAGTC ACTCAGATAGTTGAAGCCATTTTG
	mdx MUT Reverse	CGGCCTGTCACTCAGATAGTTGAAGC CATTTTA
G13 loxp	*Forward*	GAACTTTGACTTCGTCACGG
	Reverse	ACAACACCTCCTGGTCAGAGG
Gq KO	*Gq F*	GAAGAACGAGATCAGCAG
	Gq WT R	GCTCTGGATACACCTGAGTCT
	Gq MUT R	TCGGCCTTCTTCTAGGTTCTGCTC
G11 loxp	*Forward*	GGATAGTGAAACAGGGGCAA
	Reverse	TGTAAATATTAAAGGCGCATAAC
RhoA loxp	*Forward*	CTATGGATCTACTTAGGGGCTTC
	Reverse	CCAGAACTTCCTCTGGTTTCTGG
caRhoA	*Forward*	AAA GTC GCT CTG AGT TGT TAT
	Reverse	GGA GCG GGA GAA ATG GAT ATG
qRT-PCR		

Edn3	*Forward*	CCCTGGTGAGAGGATTGTGTC
	Reverse	CCTTGTCCTTGTAAGTGAAGCAC

Nts	*Forward*	GCAAGTCCTCCGTCTTGGAAA
	Reverse	TGCCAACAAGGTCGTCATCAT
MyoD1	*Taqman assay*	Mm00440387_m1, Thermo Fisher
Calcr	*Forward*	GCAACGCTTTCACTTCTGAGA
	Reverse	GTTCCCACTGCATTGTCCACA
Ntsr2	*Forward*	TTCACCGCGCTCTATTCGC
	Reverse	AGGGGTAGTGGGACCACAC
Ntsr1	*Forward*	CAGTTCGGACTGGAGACGATG
	Reverse	ACCAGCACCTTGGAATAAATGTC
Ednrb	*Forward*	GTGGCTTCTTGGGGGTATGG
	Reverse	TCTTAGTGGGTGGCGTCATTA
Ednra	*Forward*	TACAAGGGCGAGCTGCATAG
	Reverse	GGCGTGCTGATTTCCAAAGG
Pecam1	*Forward*	ACGCTGGTGCTCTATGCAAG
	Reverse	TCAGTTGCTGCCCATTCATCA
Lyve1	*Forward*	CAGCACACTAGCCTGGTGTTA
	Reverse	CGCCCATGATTCTGCATGTAGA
Pax7	*Taqman assay*	mm01354484_m1, Thermo Fisher
S1pr3	*Forward*	ACTCTCCGGGAACATTACGAT
	Reverse	CAAGACGATGAAGCTACAGGTG
Gpr116	*Forward*	GGGTTTCGGTCTTGCCACA
	Reverse	CTTCCTGCACCTTCTGATCCC
Ccrl2	*Forward*	GCCCCGGACGATGAATATGAT
	Reverse	CACCAAGATAAACACCGCCAG
P2ry14	*Forward*	AGCAGATCATTCCCGTGTTGT
	Reverse	AGCCACCACTATGTTCTTGAGA

Gpr50	*Forward*	AGAGCAACATGGGACCTACAA
	Reverse	GCCAGAATTTCGGAGCTTCTTG
Tshr	*Forward*	ATACCCAGTCTTGCATTTTCGAG
	Reverse	CGAAGTCATGTAAGGGTTGTCTG
P2ry1	*Forward*	GAGGTGCCTTGGTCGGTTG
	Reverse	CGGCAGGTAGTAGAACTGGAA
Bdkrb1	*Forward*	CCCCTCCCAACATCACCTC
	Reverse	GGACAGGACTAAAAGGTTCCCC
Agtr2	*Forward*	AACTGGCACCAATGAGTCCG
	Reverse	CCAAAAGGAGTAAGTCAGCCAAG
Gabbr1	*Forward*	GCACAGGACACAATGAAAACAG
	Reverse	AGCAAATGTACTCGACTCCCA
Ptger4	*Forward*	ACCATTCCTAGATCGAACCGT
	Reverse	CACCACCCCGAAGATGAACAT
Casr	*Forward*	CTGACCAGCGAGCCCAAAA
	Reverse	GCTGCTACTCCAAAATGGATAGG
Gpr37l1	*Forward*	GGGCTGCCACCTCATCTTTAG
	Reverse	GATGGATGGGCTTGGGATATTC
Gpr4	*Forward*	GCTGGGCGTCTACCTGATG
	Reverse	AGGCGATGCTGATATAGATGTTG
Gapdh	*Forward*	AGGTCGGTGTGAACGGATTTG
	Reverse	TGTAGACCATGTAGTTGAGGTCA
Gapdh	*Taqman assay*	Mm999999915_g1, Thermo Fisher
Fzd4	*Forward*	TGCCAGAACCTCGGCTACA
	Reverse	ATGAGCGGCGTGAAAGTTGT

3.6 Plasmids & Virus

Table 3.6: List of primers for plasmids & virus.

	Description	**Source**
Cre Recombinase Adenovirus (Ad-CMV-iCre)	This recombinant adenovirus containing the Cre recombinase, a Type I topoisomerase derived from P1 bacteriophage, which exerts site-specific recombination of DNA between loxP sites. These loxP sites are characterized by a 34 bp DNA sequence that confers a defined directionality.	Vector Biolabs
Adeno CMV Null Adenovirus (Ad-CMV-Null)	This adenvoirus contains an empty CMV promoter. The viral backbone is E1/E3 deletion, serotype 5 adenovirus.	Vector Biolabs
TRUPATH	It is a repertoire of 20 plasmids harboring the genetic information encoding the alpha, beta, or gamma subunits of the heterotrimeric G protein complex was assembled to facilitate the	Addgene Gift from Bryan Roth (Addgene kit #1000000163)

	monitoring of heterotrimer dissociation.

3.7 Antibodies

Table 3.7: List of antibodies used in this thesis, related to the experimental procedures

Mouse anti-PAX7	Developmental Studies Hybridoma Bank (DSHB)	Ca# AB_528428, RRID:AB_528428
Rat anti-LAMININ α2	Santa Cruz Biotechnology	Ca# sc-59854, RRID:AB_784266
Rabbit anti-MYOD	Abcam	Ca# ab64159, RRID:AB_2266875
Mouse anti-MYOGENIN	BD Biosciences	Ca# 556358, RRID:AB_396383
Rabbit anti-mCherry	Abcam	Ca# ab183628, RRID:AB_2650480
Mouse anti-ET-3	Santa Cruz Biotechnology	Ca# sc-81944, RRID:AB_2096417
Mouse anti-NT	GeneTex	Ca# GTX37368, RRID:AB_11169919
Mouse anti-MYH3	Developmental Studies Hybridoma Bank (DSHB)	Ca# AB_528358, RRID:AB_528358
Rat anti-CALCR	Abcam	Ca# ab11042, RRID:AB_297696
Rabbit anti-G protein alpha 12	GeneTex	Ca# GTX114147, RRID:AB_11170944
Mouse anti-G protein alpha 13	Abnova	Ca# H00010672-M01, RRID:AB_425862
Rabbit anti-EDNRB	Thermo Fisher Scientific	Ca# PA3-066, RRID:AB_2540493
Rabbit anti-NTSR1	Thermo Fisher Scientific	Ca# PA3-214, RRID:AB_10979876
Rabbit anti-NTSR2	Millipore	Ca# AB15134, RRID:AB_301679
Rabbit anti-AGTR2	Thermo Fisher Scientific	Ca# PA3-210, RRID:AB_11007512
Rabbit anti-S1PR3	Cayman Chemical	Ca# 10006373, RRID:AB_10006373
Rabbit anti-KI67	Abcam	Ca# ab15580, RRID:AB_443209
Rabbit anti-pMLC2	Cell Signaling Technology	Ca# 3671, RRID:AB_330248
Mouse anti-MYH1	Developmental Studies Hybridoma Bank (DSHB)	Ca# AB_2235587, RRID:AB_2235587

Rat anti-α TUBULIN	Santa Cruz Biotechnology	Ca# sc-53029, RRID:AB_793541
Rabbit anti-LYVE1	Abcam	Ca# ab14917, RRID:AB_301509
Rabbit anti-PECAM1	Abcam	Ca# ab7388, RRID:AB_305905
Rabbit anti-DYSTROPHIN	Abcam	Ca# ab15277, RRID:AB_301813
Rabbit anti-BDKRB1	Thermo Fisher Scientific	Ca# PA5-18988, RRID:AB_10980507
Goat anti-GPR50	Santa Cruz Biotechnology	Ca# ab189051
Rabbit anti-GAPDH	Cell Signaling Technology	Ca# 2118, RRID:AB_561053
Rabbit anti-Histone H3	Abcam	Ca# ab18521, RRID:AB_732917
Alexa Fluor 488 goat anti-rabbit IgG (H+L)	Thermo Fisher Scientific	Ca# A-11008, RRID:AB_143165
Alexa Fluor 594 goat anti-rabbit IgG (H+L)	Thermo Fisher Scientific	Ca# A-11012, RRID:AB_2534079
Alexa Fluor 488 goat anti-mouse IgG (H+L)	Thermo Fisher Scientific	Ca# A-11001, RRID:AB_2534069
Alexa Fluor 594 goat anti-rat IgG (H+L)	Thermo Fisher Scientific	Ca# A-11007, RRID:AB_10561522
Alexa Fluor 555-conjugated anti-GST tag	Thermo Fisher Scientific	Ca# MA4-004-A555, RRID:AB_2610642
Alexa Fluor 488 goat anti-mouse IgG2b	Thermo Fisher Scientific	Ca# A-21141, RRID:AB_2535778
Alexa Fluor 488 goat anti-mouse IgG1	Thermo Fisher Scientific	Ca# A-21121, RRID:AB_2535764
FITC-conjugated anti-Mouse Integrin α7	MBL international corporation	Ca# K0046-4, RRID:AB_1279097
GFP Booster Atto488	Chromotek	Ca# gba488-100, RRID:AB_2631386
Alexa Fluor 594 goat anti-mouse IgG (H+L)	Thermo Fisher Scientific	Ca# A-11005, RRID:AB_2534073
Rabbit anti-YAP	Cell Signaling Technology	Ca# 4912, RRID:AB_2218911
Alexa Fluor 594 goat anti-mouse IgG1 (H+L)	Thermo Fisher Scientific	Ca# A-21125, RRID:AB_2535767
DAPI	Thermo Fisher Scientific	Cat# D3571, RRID:AB_2307445

3.8 Cell lines

Table 3.8: List of primers for cell lines.

HEK293T ATCC CRL-11268 ™	A specific cell line originally derived from human embryonic kidney cells. These cells constitutively express the simian virus 40 (SV40) large T antigen. 293T cells are suitable for the production of virus particles (DuBridge et al., 1987).

3.9 Mouse lines

Table 3.9: List of mouse lines used in this study.

C57BL6	Jackson Laboratories	Strain #:000664
Pax7^{CreER}	Jackson Laboratories	Strain #:017763
Gnaq$^{-/-}$; Gna11 $^{flox/flox}$	From corresponding lab	**(**Wettschureck et al., 2001**)**
Gna12$^{-/-;}$ Gna13 $^{flox/flox}$	From corresponding lab	**(**Moers et al., 2003**)**
RhoA $^{flox/flox}$	From corresponding lab	**(**Melendez et al., 2011**)**
Dmd $^{mdx-4Cv/Y}$	Jackson Laboratories	Strain #:001801
Pax7^{nGFP}	Jackson Laboratories	Strain #:036759
R26$^{LSL-caRhoA}$	Generated in this paper	Mentioned in the method part

4. METHODS

4.1 Animal Procedures

Male mice aged 8-12 weeks were subjected to intraperitoneal administration of tamoxifen (Sigma) at a dosage of 0.05 mg/g body weight. The tibialis anterior muscles were injected with cardiotoxin (0.06 mg/ml, Sigma) in a 50 µl volume. Anesthesia was induced in adult mice (8-12 weeks old) for both injury techniques, followed by shaving of the left hindlimb. The protocol for MuSC engraftment was adapted from a published procedure (Zhang et al., 2015b), and the host mice were anesthetized. Prior to engraftment, the donor cells were quantified using a haemocytometer, with non-viable cells stained using 0.4% Trypan Blue (Gibco) excluded from the count. Subsequently, the donor MuSCs were centrifuged at 1200 × g, 4°C for 20 minutes and suspended in DMEM media (Life Technologies) before being transplanted into the TA muscle using a 5-µL microcapillary pipette (Drummond). All procedures related to animal care and handling were conducted in strict adherence to the "Guide for the Care and Use of Laboratory Animals" published by the US National Institutes of Health. The study protocol received approval from the Animal Rights Protection Committee of the State of Hessen (Darmstadt, Germany) and the Institutional Animal Care and Use Committee of Sichuan Agricultural University (Chengdu, China).

4.2 Generation of *R26* $^{LSL\text{-}caRhoA}$ mouse

Transgenic mice carrying the conditional allele *R26LSL-caRhoA* (Tg: *Rosa26 locus*: *Loxp-stop-Loxp-caRhoA*) were generated from a plasmid construct (pcDNA3, #12968, Addgene) containing the cytomegalovirus enhancer, cytomegalovirus promoter, promotor for bacteriophage T7 RNA polymerase, and a bovine globin polyadenylation signal. The plasmid construct was modified to incorporate the CMV early enhancer/chicken β actin (CAG) promoter and loxp-stop-loxp sequence upstream of the caRhoA gene, which encodes a constitutively active mutant (Q63L) of human RhoA protein fused with enhanced GFP at the N-terminus. Subsequently, the modified DNA fragment was inserted into the *Rosa26* locus of the mouse genome (Figure 7A). The construct was inserted into the *Rosa26* locus of (129S6/SvEvTac x C57BL/6J)F1-derived embryonic stem cells via homologous recombination, using electroporation. Recipient blastocysts were injected with correctly

targeted ES cells, and the resulting chimeric males were mated with C57BL/6J females to produce founder animals. To ensure a consistent genetic background, all mice were backcrossed into the C57BL6 strain for at least 3 generations. The genotyping primers used in this thesis are provided in table 3.5.

4.3 MuSC isolation & culturing

MuSCs were isolated using a previously described FACS-based purification method (Zhang et al., 2015a). Limb and trunk muscles were minced, digested with 100 CU Dispase and 0.2% type II collagenase, and filtered sequentially through 100-, 70-, and 40-µm strainers. The cells were then separated using a discontinuous Percoll gradient, with mononuclear cells collected from the 70%/30% interphase. These cells were sorted via FACS, either by immunostaining for CD11b−, CD45−, CD31−, CXCR4+, and CD34+ markers, or by GFP fluorescence in Pax7ZsGreen mouse-derived MuSCs. The purified MuSCs were subsequently cultured in either growth medium 1 (GM1) or screening medium (SM). GM1 consisted of DMEM-GlutaMAX supplemented with 20% fetal calf serum (FCS), 1% penicillin/streptomycin, and 5 ng/mL basic fibroblast growth factor (bFGF). SM comprised DMEM-GlutaMAX supplemented with 20% knock-out serum (KSR), 1% penicillin/streptomycin, and 1% chicken embryo extract (CEE) (Gunther et al., 2013). To investigate the effects of specific factors, cultured MuSCs were subjected to various treatments, including ± ET-3, ± NT, ± BQ887, ± SRA43611, ± Cell Permeable Rho Inhibitor (C3 Transferase), and other compounds as listed in table 3.1. Additionally, EdU, a thymidine analog, was added to the GM or SM at a final concentration of 10 µM, 3 hours prior to fixation of the cultured MuSCs. The incorporation of EdU was analyzed using the Click-iT EdU kit (Invitrogen) following the manufacturer's instructions. Time-lapse imaging and analysis were performed using the Incucyte Live-Cell Imaging System and associated software (Essen Instruments).

4.4 Adenovirus-mediated Cre deletion of floxed sequences in MuSC

FACS isolated MuSCs from *Gna12*$^{-/-}$*Gna13* $^{loxp/loxp}$ or *Gna11*$^{-/-}$*Gnaq* $^{loxp/loxp}$ mice were cultured in screening medium (SM). To induce Cre-mediated deletion of Gna13 or Gnaq in the mutant MuSCs in vitro, the cells were exposed to Ad-Cre virus (Vector Biolabs) for a

minimum of 2 days. Adenoviruses lacking Cre expression (Ad-Null) were used as control treatments for MuSCs.

4.5 Single myofiber isolation & culturing

Freshly isolated or pre-fixed myofibers were obtained by enzymatic digestion of FBD or EDL muscles using collagenase 2 (0.02%, Roche). For pre-fixed samples, mice were perfused with 0.5% paraformaldehyde (PFA) prior to muscle digestion. The isolated myofibers were cultured in growth medium 2 (GM2: DMEM-GlutaMAX medium supplemented with 20% fetal calf serum (FCS) and 5 ng/mL basic fibroblast growth factor (bFGF)). Upon muscle excision, the drugs specified in the key resource table were instantaneously added to both the digestion tubes and culturing plates for immediate exposure. The myofibers were then cultured for 0, 8, or 24 hours in the absence or presence of the respective drugs. Subsequently, the myofibers were fixed with 4% paraformaldehyde (PFA) for 10 minutes in preparation for further analysis.

4.6 Immunocytochemistry

Myofibers, cryosections, or cultured MuSCs were fixed using a 4% paraformaldehyde (PFA) solution for a duration of 10 minutes. Following fixation, the samples were permeabilized with 0.1% Triton X-100 for 15 minutes. Subsequently, the specimens were blocked in a 3% bovine serum albumin (BSA) solution for 30 minutes and then incubated with the respective antibodies (refer to table 3.7 for antibody details) overnight at 4°C. Immunofluorescence signals were visualized using secondary antibodies conjugated with Alexa488 or Alexa594. A fluorescence microscope (AXIO observer Z1, Zeiss) equipped with objective lenses of 63×, 40×, and 20× was utilized for fluorescence signal detection and recording. The fluorescence intensity was quantified using ImageJ software, allowing for subsequent statistical analysis of the acquired data.

4.7 RhoA G-LISA activation assay

To assess the activity of RhoA in cultured MuSCs, the RhoA G-LISA Activation Assay kit (BK121, Cytoskeleton) was utilized to measure the Rho-GTP levels. Cultured MuSCs were

lysed using the provided lysis buffer for a duration of 10 minutes on ice. Total cell extracts were then collected and adjusted to a protein concentration of 1 mg/ml to enable quantitative detection of active and total RhoA, following the manufacturer's instructions. Luminescence intensity was measured using the LB940 Mithras plate reader (Berthold Technologies) at a wavelength of 490 nm.

4.8 In situ binding assays for assessment of Rho & Rac GTPase activity

The isolation and fixation of myofibers were previously described in the method section(4.5). Following fixation, the myofibers were subjected to blocking with 3% bovine serum albumin (BSA) and subsequently incubated at room temperature for 1 hour with GST-tagged PAK-P21 binding domain (PBD) proteins (Cytoskeleton Inc., PAK01) or GST-tagged Rhotekin-Rho binding domain (RBD) proteins (Cytoskeleton Inc., RT01), which specifically bind to active-Rac/Cdc42 or active-Rho, respectively. After three washes with PBS, the myofibers were incubated with fluorophore-conjugated anti-GST antibodies (Invitrogen) at room temperature for 1 hour. Cell nuclei were stained using DAPI (Life Technologies).

4.9 BRET2 assays

HEK 293T cells were transfected after reaching a density of 600,000 to 800,000 cells per well in a 6-well plate using a plasmid cocktail consisting of receptor, Gα12(134)-RLuc8/Gα13(126)-RLuc8, Gβ3, and Gγ9-GFP2 in a 1:1:1:1 plasmid DNA ratio, following a previously published protocol (Olsen et al., 2020). The following day, the medium of the transfected cells was replaced daily with selection medium (DMEM supplemented with 10% fetal calf serum (FCS), 1% Penicillin/Streptomycin, and 200 µg/mL G418) for 3 days. The full-length cDNA of human EDNRB and NTSR2 genes were cloned from EDNRB-Tango (#66458, Addgene) and NTSR2-Tango (#66458, Addgene) plasmids, respectively, and subsequently fused with an empty pcDNA3.1(+) vector.

One day after selected cells were plated in 96-well plates, the culture medium was replaced with 60 µL of assay buffer (1× Hank's balanced salt solution (HBSS) + 20 mM HEPES, pH 7.4), followed by the addition of 10 µL of freshly prepared 50 µM coelenterazine 400a (Nanolight Technologies). After a 5-minute equilibration period, the cells were treated with 30 µL of

the drug for an additional 5 minutes. The plates were then analyzed using an LB940 Mithras plate reader (Berthold Technologies) with 395 nm (RLuc8-coelenterazine 400a) and 510 nm (GFP2) emission filters, with an integration time of 1 second per well. The plates were read sequentially five times, and the measurements from the sixth read were used for all analyses. BRET2 ratios were calculated as the ratio of GFP2 emission to RLuc8 emission.

4.10 RNA sequencing

RNA sequencing (RNA-seq) analysis was performed following established protocols (Zhang *et al.*, 2015a). Total RNA was extracted using the RNAeasy Mini kit (QIAGEN) and its quality and integrity were assessed using the LabChip Gx Touch 24 (PerkinElmer). For the VAHTS Stranded mRNA-seq, 300 ng of total RNA was used for library preparation according to the manufacturer's protocol (Vazyme). Sequencing was carried out on an Illumina NextSeq500 instrument with v2 chemistry, generating an average of 30 million reads per library with 1x75bp single-end reads. Raw reads were subjected to quality assessment, adaptor content analysis, and duplication rate estimation using FastQC 0.10.1. Trimmed reads were aligned to the Ensemble mouse genome version mm10 (GRCm38) using STAR 2.4.0a. Gene-level read counts were obtained using the featureCounts 1.4.5-p1 tool from the Subread package, and only reads partially mapping within exons were considered. DESeq2 version 1.62 l was used to identify differentially expressed genes based on criteria including an absolute fold change of $\geqslant$2, a Benjamini-Hochberg corrected p-value $\leqslant$ 0.05, and a minimum combined mean of 5 reads. GO and KEGG analyses were performed using the "clusterProfiler" package in R, while principal component analysis (PCA) was conducted on the rlog-transformed count data using the "plotPCA" function from the R package "DESeq2". Pearson correlation coefficients were calculated to assess the relationship between replicate groups, and gene set enrichment analysis was performed using gene sets extracted from MSigDB.

4.11 Western blot assay

Freshly isolated or cultured MuSCs were rinsed with PBS and subjected to lysis in cell lysis buffer for a duration of 10 minutes. The resulting lysate was sonicated to ensure protein solubilization. Subsequently, the proteins were separated by SDS-PAGE and transferred

onto nitrocellulose membranes (Millipore, Billerica, MA). The membranes were probed with specific primary antibodies targeting G12, G13, Histone-3 (H3), MYH3, ET-3, NT, and GAPDH. Following an overnight incubation at 4 °C, HRP-conjugated secondary antibodies were applied for signal detection using the enhanced chemiluminescence (ECL) detection system (Pierce). Protein quantification was conducted using ImageJ software, enabling accurate measurement of the protein levels.

4.12 RT-qPCR assays

RT-qPCR analysis was conducted using SYBR Green or TaqMan probe-based assays. Total RNA was extracted from the samples using the RNAeasy Mini kit (QIAGEN) following the manufacturer's instructions. Subsequently, cDNA was synthesized using the PrimeScript™ II 1st strand cDNA Synthesis Kit (Takara). TaqMan probe-based RT-qPCR was performed using the TaqMan Fast Advanced Master Mix (Thermo Fisher), and the assay IDs for the commercial TaqMan probes used to detect the target genes can be found in Table 3.5. For SYBR Green-based RT-qPCR, the Applied Biosystems™ PowerUp™ SYBR™ Green Master Mix (Thermo Fisher) was utilized, and the primer sequences can be found in Table 3.5 as well. The relative expression levels of the target genes were determined using the comparative threshold method, with Gapdh serving as the internal control. Data analysis was performed using the ΔΔCt method to calculate fold changes in gene expression.

4.13 Histological analysis

The muscles were harvested at designated time points, as indicated in each figure, and promptly frozen by immersion in isopentane chilled with liquid nitrogen. Subsequently, 8 µm thick sections of the muscle samples were prepared using a cryomicrotome and subjected to Hematoxylin & Eosin staining following established protocols (Gunther *et al.*, 2013).

4.14 Statistics

The figure legends provide comprehensive statistical details pertaining to the conducted experiments. Statistical evaluations followed established procedures and depended on type

of analysis. For comparisons among multiple groups, the one-way ANOVA test was employed, whereas unpaired two-tailed Student's t-test was utilized for comparisons between two groups. Normal distribution of recorded data points was confirmed before using parametric statistical tests such as ANOVO or Student’s t-test. Statistical significance was determined with a threshold of P values < 0.05, represented as significant ($*p < 0.05$, $**p < 0.01$, $***p < 0.001$). The results are presented as the mean ± standard error of the mean (s.e.m.). Data analysis was carried out using GraphPad Prism 9 software.

5. RESULTS

5.1 Quiescent MuSCs display a distinct repertoire of GPCRs

GPCRs, such as the CalcR, have been described to act as crucial regulators preventing MuSCs from exiting quiescence (Sénéchal *et al.*, 2022; Yamaguchi *et al.*, 2015). However, the precise composition of the quiescent MuSC-specific GPCR signaling network remains elusive, and a comprehensive characterization of GPCRs and their ligands in MuSC is still missing. To unveil the repertoire of GPCRs, specific for quiescent MuSCs, I initially screened six publicly available bulk-RNAseq datasets that compared transcriptomic profiles between quiescent and activated MuSCs. Through comparative analysis, I identified 39 known GPCRs showing high expression levels in quiescent versus activated MuSCs across at least two datasets (Figure 2A). Subsequent qRT-PCR analysis confirmed robust expression (fold change >2) of 19 of these GPCR targets in quiescent MuSCs. Furthermore, immunofluorescence staining validated the presence of seven GPCRs in quiescent MuSCs (Figure 2B-C), prefentially in the plasma membrane (Figure 2D). Collectively, these findings identified a group of G-protein coupled receptors that is specifically expressed in quiescent but absent in proliferating MuSCs, suggesting a potential role in maintaining the quiescent state.

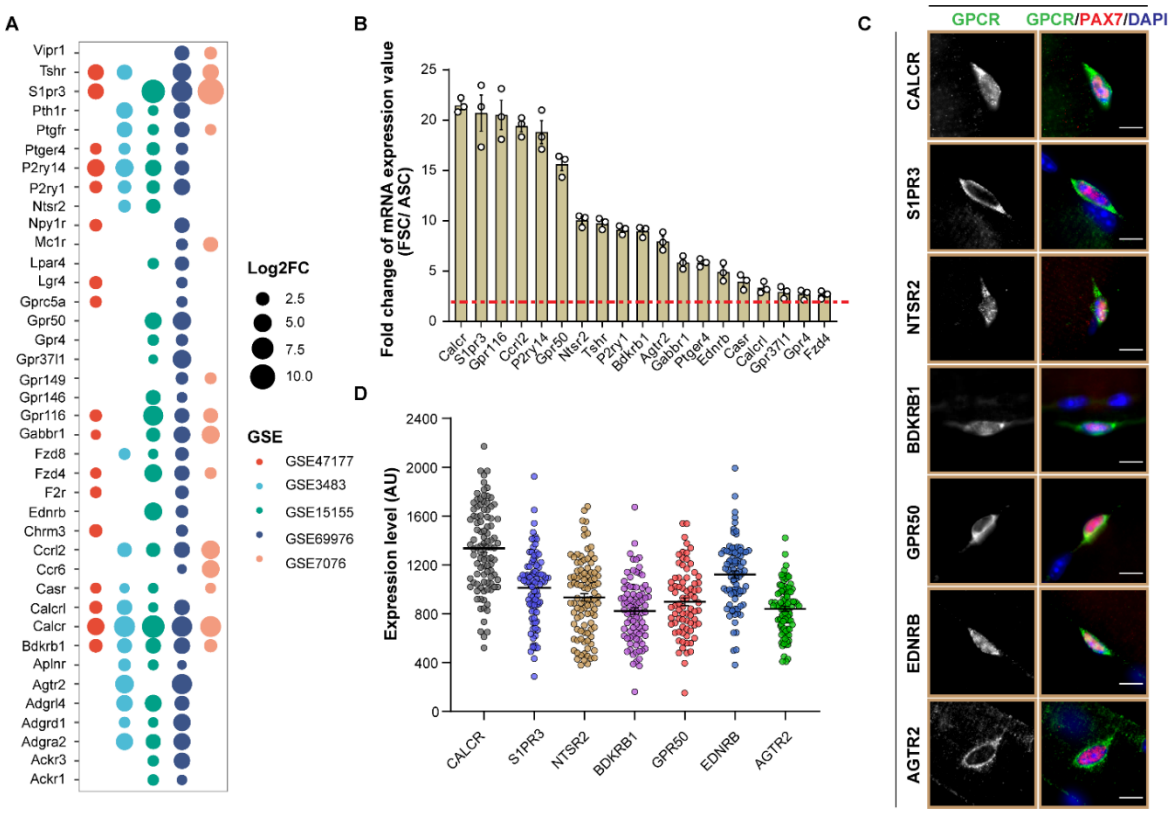

Figure 2 Screening for GPCRs that are highly expressed in quiescent MuSCs and downregulated upon activation.

A. Comparative analysis of gene expression profiles of activated and quiescent MuSCs derived from 5 publicly available microarray datasets to identify the GPCR repertoire in quiescent MuSC. Selected GPCRs show significant higher expression level ($p<0.05$, Log2_foldchange >1) in quiescent/freshly isolated MuSCs compared to G-alert/activated MuSCs in at least 2 different datasets;

B. RT-qPCR expression analysis of selected *GPCRs* in freshly isolated MuSCs (FSC) and after 24 h culturing (ASC), using TaqMan assays or SYBR Green with specific primers. Expression levels were normalized to *Gapdh* (Fold change>2, t-test: $p < 0.05$, n = 3, 2-months-old male mice)

C-D. Representative images ((PAX7 (red), DAPI (blue), and GPCR (green)) (C) and quantification (D) of GPCRs intensity in MuSCs using freshly isolated single myofibers dissected from FDB muscle of WT mice (n = 3, 2-months-old male mice). Scale bars in (C) represent 5 µm.

5.2 ET-3 and NT are potent inducers of MuSC quiescence

The GPCR compound library serves as a comprehensive collection of pharmacological tools designed for high throughput screening, enabling the identification of ligands targeting GPCRs with unknown roles in biological processes (Zhang et al., 2012). To gain deeper insights into the functional diversity of MuSC-specific GPCRs and their contributions to maintaining MuSC quiescence, I employed a customized GPCR compound library consisting of 259 compounds that target 23 subfamilies of GPCRs. This library encompasses both natural and synthetic agonists or antagonists. My objective was to elucidate functional

GPCRs and ligand-GPCR interactions involved in the maintenance of MuSC quiescence. To investigate the potential of these targeted compounds to suppress or delay MuSC proliferation and myogenic commitment in vitro, I devised a cell-based screening strategy (Figure 3A). To assess proliferation and myogenic commitment, I performed an EdU-based cell proliferation assay on MuSCs after a five-day co-incubation with the test compounds, quantifying the proportion of $PAX7^+$ $MYOD^+$ cells. I defined a hit cutoff based on the effects of mOSM (100 µg/mL) on MuSCs (Figure 3B-C). Consequently, I identified 12 functional GPCR subfamilies potentially involved in in maintaining quiescence of MuSCs, including adrenergic receptors (ARs), dopamine receptors (D1R and D2R), metabotropic glutamate receptor subtype 1 (mGluR1), and histamine receptor H2R, among others (Figure 4B). Intriguingly, two natural GPCR ligands, Endothelin-3 (ET-3) and Neurotensin (NT), were found to hinder myogenic commitment and expansion of MuSCs *ex vivo* even at very low concentrations (Figure 3D). Importantly, their respective binding receptors (EDNRB and NTSR2) are expressed on the cell surface of quiescent MuSCs (Figure 2C), strongly suggesting pro-quiescence functions in vivo. Similar effects were observed when ET-3/NT were co-incubated with isolated single myofibers from the mouse flexor digitorum brevis (FDB) muscle *in vitro* (Figure 4C-D).

The robust regenerative capacity of muscle stem cells (MuSCs) is typically compromised following ex vivo expansion under standard culture conditions (Gilbert *et al.*, 2010; Montarras *et al.*, 2005). Thus, my objective was to investigate whether MuSCs maintained their stem cell properties for self-renewal and muscle regeneration after ex vivo growth in the presence of ET-3 or NT, followed by engraftment into a mouse model of Duchenne muscular dystrophy (*Dmd* $^{mdx\text{-}4Cv/Y}$ mice). To achieve this, MuSCs were isolated from *Pax7nGFP*$^{+/+}$ mice, which express GFP specifically in the nucleus of $PAX7^+$ cells, and cultured with ET-3 or NT for 5 days. Subsequently, these cells were engrafted into the TA muscle of 18 Gy irradiated hindlimbs of Mdx mice after three rounds of CTX injection, simulating the muscular dystrophy characterized by cycles of myofiber degeneration and regeneration (Figure 3E). The self-renewal and long-term regenerative capacities of donor MuSCs were quantitatively assessed by enumerating the number of GFP^+ nuclei and $DYSTROPHIN^+$ myofibers following the final regeneration cycle. Since freshly isolated muscle stem cells possess a superior regenerative potential compared to cultured cells (Sacco et al., 2008; Zismanov et al., 2016), I compared the engraftment of cultured donor satellite cells (with

and without ET-3/NT treatment) with freshly isolated donor satellite cells. Treatment with ET-3 or NT enhanced the engraftment of MuSC leading to increased numbers of DYSTROPHIN^{+} myofibers and GFP^{+} nuclei of donor origin compared to the untreated group, comparable to the engraftment of freshly isolated MuSCs (Figure 3E-F). In conclusion, treatment with either NT or ET-3 preserved the self-renewal and regenerative capacities of freshly isolated MuSCs in vitro, thereby enhancing the efficacy of therapeutic MuSC transplantation.

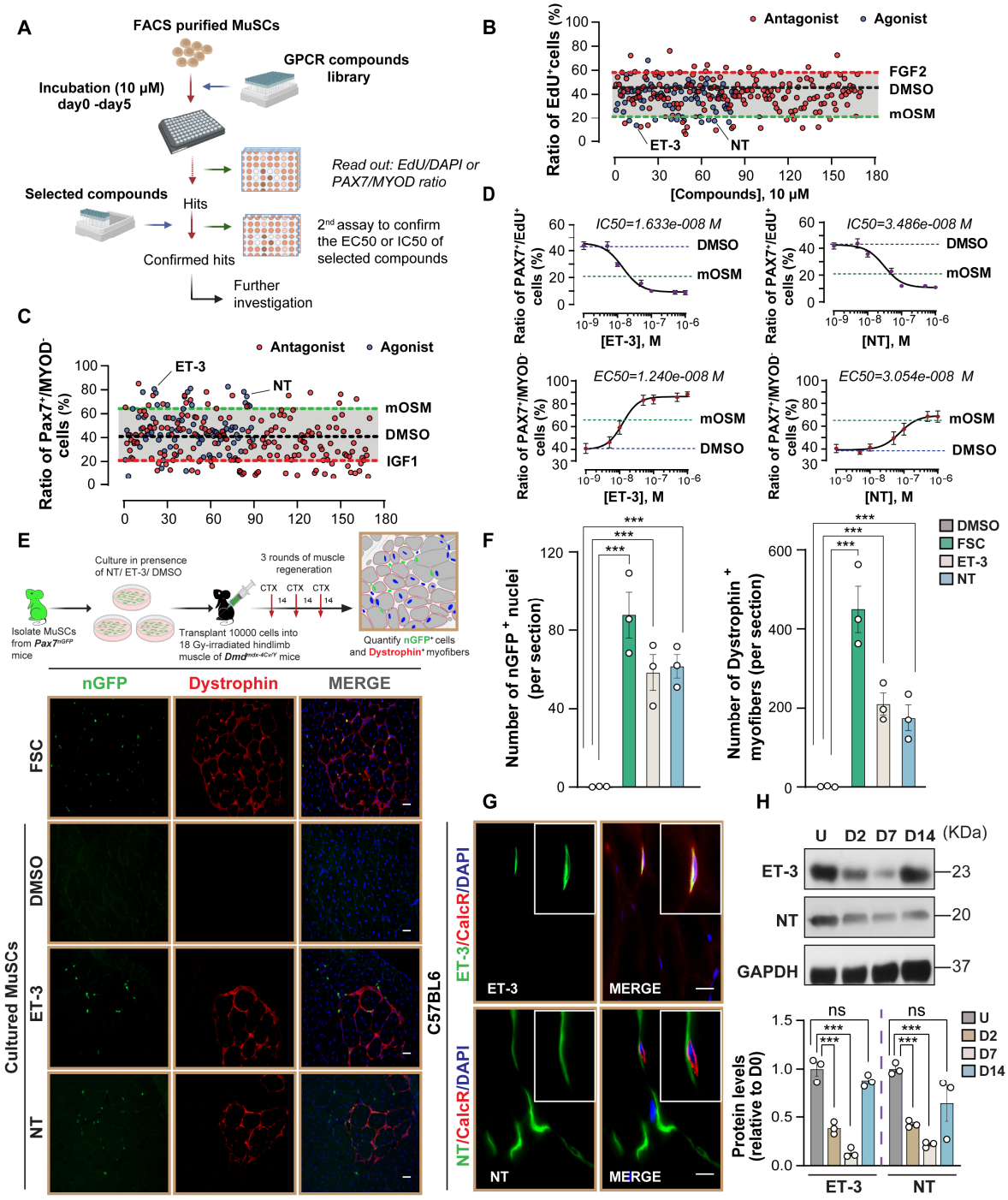

Figure 3 *In vitro* GPCR compound screening assays identified ET-3 and NT as regulators of MuSC quiescence.

A. Schematic representation of the GPCR compound screening strategy developed to identify GPCR compounds and the target GPCRs which can potentially inhibit MuSC activation.

B-C. Scatter plots indicating the ratio of EdU^+ (B) or $PAX7^+$ $MYOD^-$ (C) MuSCs following 5 days *in vitro* treatment with 259 synthetic and natural GPCR compounds (10µM). The red dots represent the GPCR antagonists and the blue dots represent the agonists. The green dashed lines represent the threshold value of positive selection (mOSM treatment), and the red dashed lines represent the threshold value of negative selection (FGF2 or IGF1 treatment), the black dashed lines represent the values of DMSO treated MuSCs.

D. ET-3 or NT (1 nM – 1 µM) *in vitro* mediated inhibitory effects on proliferation (upper panel) and myogenic activation (lower panel) of MuSCs.

E-F. *In vitro* MuSCs cultured in the presence of ET-3 or NT retain long-term regenerative capacity to differentiate and self-renew after intramuscular engraftment into a mouse model of Duchenne muscular dystrophy (*Dmd* $^{mdx\text{-}4Cv/Y}$). The upper panel in (E) is the schematic outline of MuSCs engraftment, the lower panel in (E) are representative images of GFP-fluorescence (green) and immunostaining for DYSTROPHIN (red), DAPI (blue) on TA muscle transverse sections from *Dmd* $^{mdx\text{-}4Cv/Y}$ mice engrafted with fresh isolated MuSC (FSC) or cultured in the presence of DMSO, ET-3, and NT for 5 days, after 3 consecutive CTX-induced injuries, quantifications of GFP^+ nuclei and $DYSTROPHIN^+$ myofibers (t-test: ***$p < 0.001$, n = 3, 2-months-old male mice, 5 sections per sample) are shown in (F). Scale bars in (E) represent 50 µm.

G. Representative images of immunostaining for CALCR (red), ET-3/NT (green), and DAPI (blue) on TA muscle transverse sections of C57BL6 mouse. Scale bars represent 5 µm.

H. Western blot analysis for ET-3/NT expression level in TA muscle, either uninjured (U) or at the indicated days (D0, D2, D7, D14) after CTX injury, quantification of the relative protein levels (One-way ANOVA: ***$p < 0.001$, ns: no significant, n = 3, 2-months-old male mice) are shown in the lower panel.

To explore the potential sources of ET-3 and NT within the muscle stem cell (MuSC) niche, I conducted an analysis using the "scmuscle" database (scrna-seq.org), an extensive omics resource. The database provides information about transcription in individual skeletal muscle cells under various conditions, providing a comprehensive view of Edn3 (the gene encoding ET-3) and Nts (the gene encoding NT) expression across different cell types within skeletal muscle(McKellar *et al.*, 2021). My findings revealed abundant expression of both Edn3 and Nts in skeletal muscle. Notably, the expression of Edn3 was significantly higher in quiescent MuSCs compared to other cell types in skeletal muscle, strongly suggesting quiescent MuSCs as the primary source of ET-3 within the niche (Figure 4E). In contrast, Nts expression was primarily observed in lymphatic and capillary endothelial cells, with lymphatic endothelial cells being the predominant cell type (Figure 4E), which is in line with

previous observations of substantial enrichment of Nts in lymphatic endothelial cells within adipose tissue (Li et al., 2021). To further validate these expression patterns, I conducted qRT-PCR and immunohistochemical analyses on murine skeletal muscles (Figure 3G and Figure 4F-I), thereby confirming the MuSC-niche origin of ET-3 and NT. Furthermore, by examining the expression of ET-3 and NT at different stages of muscle regeneration, I observed a downregulation of both ET-3 and NT following muscle injury, with gradual restoration towards the final stage of regeneration (Figure 3H). These observations suggest that ET-3 and NT are more actively produced by quiescent MuSCs or their niche cells under homeostatic conditions. Overall, the high expression levels of ET-3 and NT in quiescent MuSCs and niche cells, along with their decline following muscle injury, suggest a role of ET-3 and NT in the regulation of MuSC quiescence.

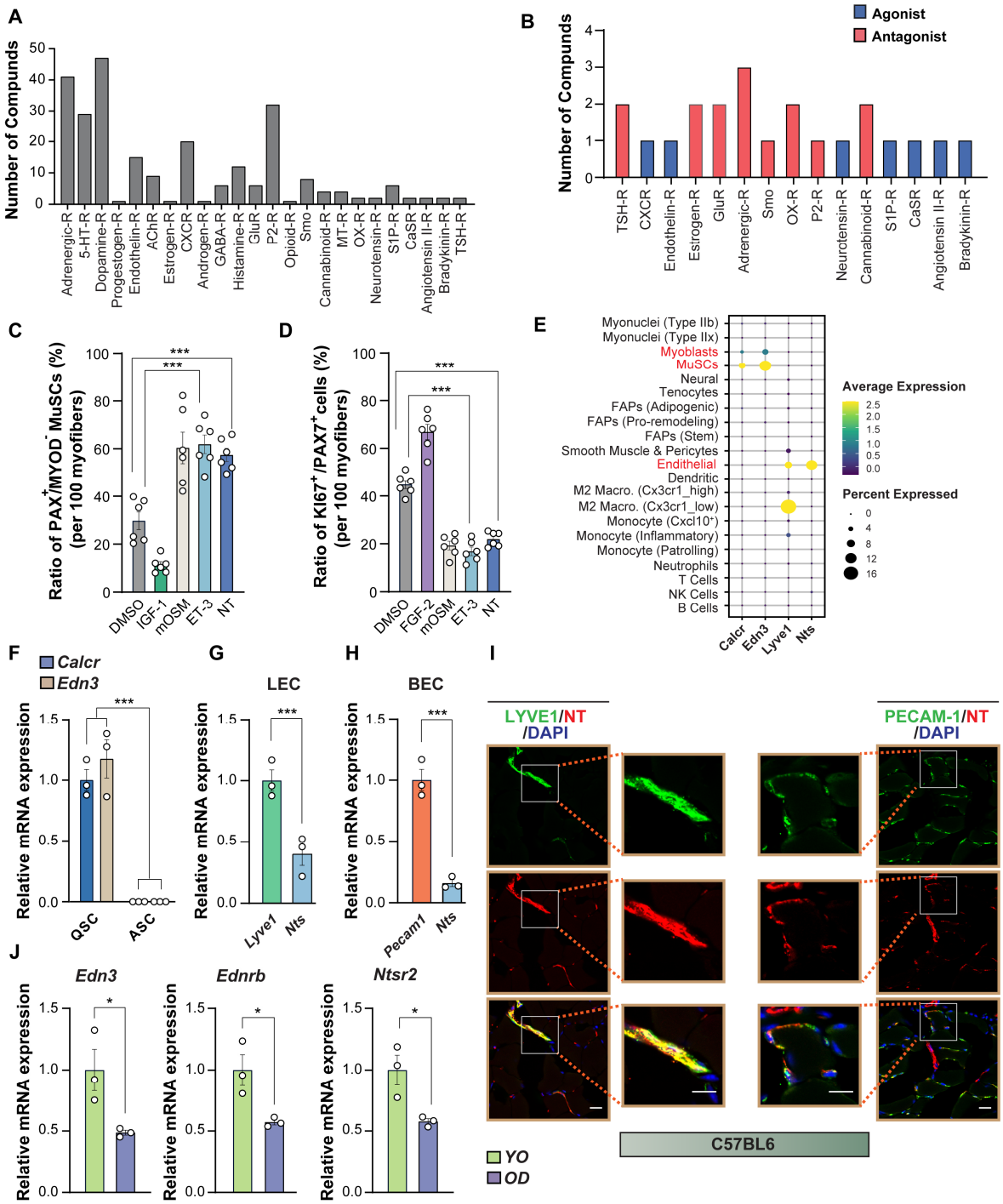

Figure 4 Origin of ET-3 and NT in mouse skeletal muscle

A. Composition of the customized GPCR compound library
B. Selected compounds and their target GPCR subfamilies.
C-D. Quantification of the ratio of PAX7$^+$/MYOD$^-$ (C) and PAX7$^+$ KI67$^+$ (D) MuSCs on isolated myofibers from FDB muscles 24 h after culturing in presence of DMSO, IGF1/FGF2, mOSM, ET-3, and NT. (One-way ANOVA: ***p<0.01, 5 independent experiments, 100 myofibers per group).

E. Single-cell RNA-seq data from whole muscle of adult mice. Dot plots display expression of *Calcr, Edn3, Lyve1, and Nts* by different cell-type clusters. Dot size shows the frequency of cells expressing non-zero transcript level. Dot color shows average expression level.

F. RT-qPCR analysis of *Calcr* and *Edn3* expression in freshly isolated MuSCs (FSC) and 24h after culturing (ASC). Expression levels were normalized to *Gapdh* (One-way ANOVA: ***p < 0.001, n = 3, 2-months-old male mice).

G. RT-qPCR analysis of *Lyve1* and *Nts* expression in lymphatic endothelial cells (LEC). Expression levels were normalized to *Gapdh* (t-test: ***p < 0.001, n = 3, 2-months-old male mice).

H. RT-qPCR analysis of *Pecam1* and *Nts* expression in blood vessel endothelial cells (BEC). Expression levels were normalized to *Gapdh* (t-test:***p < 0.001, n = 3, 2-months-old male mice).

I. Representative images of immunostaining for NT (red), DAPI (blue), and LYVE1 or PECAM-1 (green) on TA muscle transverse sections of C57BL6 mouse. Scale bars represent 10 µm.

J. RT-qPCR analysis of *Edn3*, *Ednrb*, and Ntsr2 expression in freshly isolated young (YO, 2 months old male C57BL6 mice) and old (OD, 24 months-old male C57BL6 mice) MuSCs. Expression levels were normalized to Gapdh (One-way ANOVA: *p < 0.05, n=3).

5.3 ET-3/EDNRB and NT/NTSR2 signaling prevent premature activation of MuSCs *in vivo*

GPCRs usually recognize only a limited set of specific ligands, and ligands bind to only one or a few target receptors. Ligand-receptor binding induces conformational or activity changes in the receptor, enabling signal transmission or initiation of cellular responses. Previous studies have identified two canonical receptors for endothelin (ET), the endothelin receptor A (EDNRA) and the endothelin receptor B (EDNRB). However, ET-3 shows a preference for binding to EDNRB but only a low affinity towards EDNRA(Davenport, 2002). Neurotensin (NT) binds to two specific receptors, NTSR1 and NTSR2, as well as a non-specific receptor, Sortlin (NTSR3) (Geisler et al., 2006). Notably, Sortlin is not considered a signaling receptor and functions mainly as a decoy via soluble NTSR3 (sNTSR3), which is released by shedding the extracellular domain of Sortlin (Mazella, 2001). Consistent with the initial GPCR expression profiling, subsequent qRT-PCR and immunofluorescence staining analyses revealed significant upregulation of EDNRB and NTSR2 in quiescent MuSCs, with no detectable expression of NTSR1 at the transcriptional or protein level (Figure 5A-C). To investigate the involvement of EDNRB and NTSR2 in effects exerted by ET-3 or NT on MuSCs, selective antagonists of EDNRB (BQ788) and NTSR2 (SR142948A) were employed. Co-incubation of single FDB myofibers with BQ788 or SR142948A did not impact MuSC proliferation or MYOD expression ratio (Figure 5D-E). However, the addition of BQ788 to the culture medium after ET-3 treatment abolished the inhibitory effects of ET-3 on MuSC proliferation and MyoD expression (Figure 5F-G). Similar results were observed when

SR142948A was added to the growth medium of single FDB myofibers treated with NT (Figure 5F-G). These findings suggest that EDNRB and NTSR2 are expressed in quiescent MuSCs and mediate the inhibitory effects of ET-3 or NT on MuSC activation.

To further confirm the roles of EDNRB and NTSR2 in maintaining MuSC quiescence in vivo, BQ788 or SR142948A was administered into the TA muscle of WT mice to pharmacologically interfere with the activation of EDNRB or NTSR2 in MuSCs. After 7 days of exposure to BQ788 or SR142948A in the TA muscle of WT mice, 33% of MuSCs in BQ788-treated mice and 65% in NT-treated mice had moved out of the stem cell niche and were located in the interstitial space, outside the basal lamina, and a higher proportion of MuSCs showed KI67 and MYOD expression compared to the control group (Figure 5H-L). These results clearly indicate that the activation of EDNRB and NTSR2 is essential for MuSCs to maintain their quiescent state and niche location.

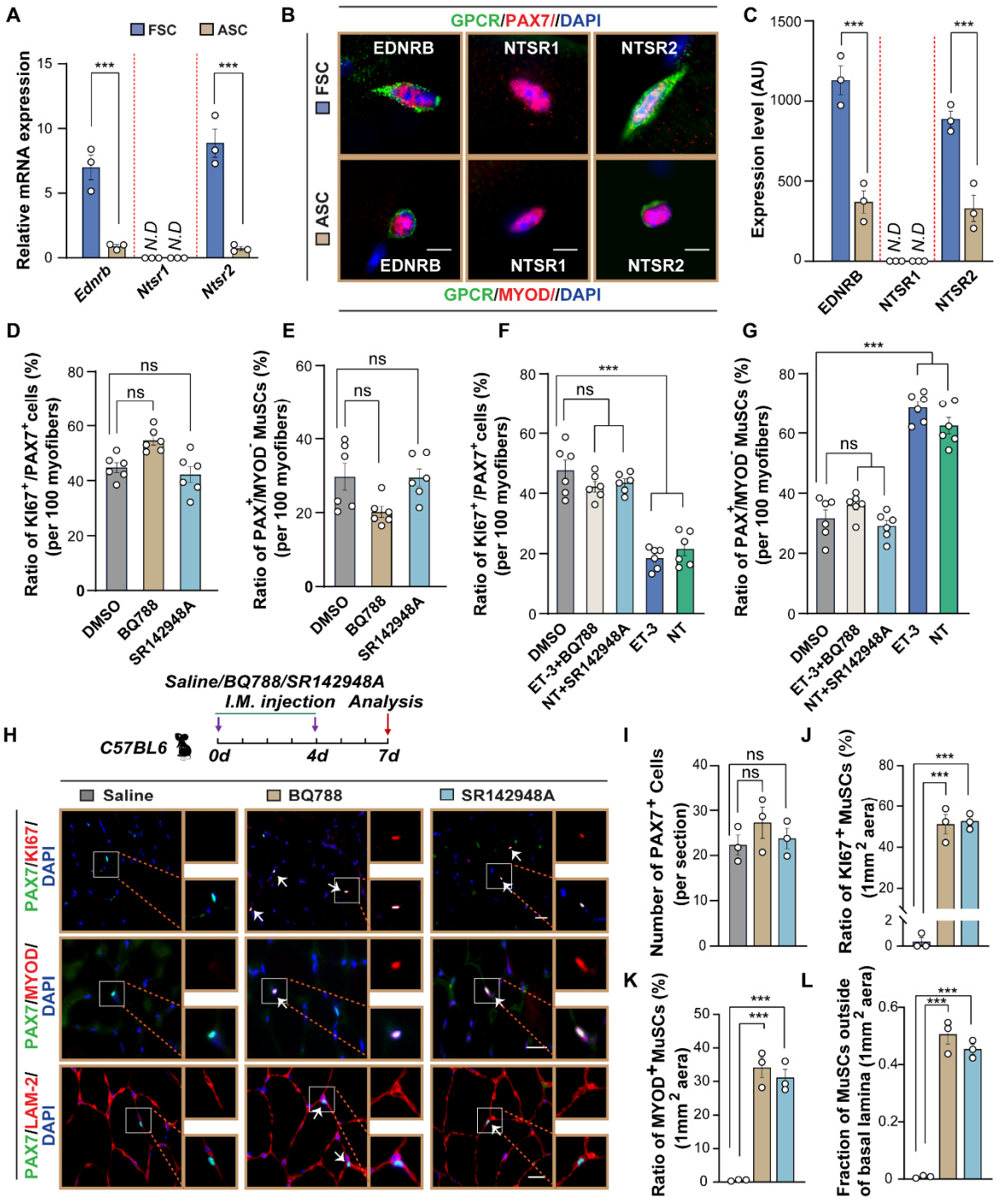

Figure 5 Activation of EDNRB or NTSR2 mediates the pro-quiescence effects of ET-3 or NT on MuSCs.

A. Taqman-assay based RT-qPCR analysis of *Ednrb*, *Ntsr1*, and *Ntsr2* expression in freshly isolated MuSCs (FSC) and 24h cultured activated stem cells (ASC). (t-test: ***p < 0.001, *N.D* (not detected) n = 3, 2-months-old male mice)

B-C. Representative images of immunostaining for EDNRB/NTSR1/NTSR2 (red), PAX7 (green) and DAPI (blue) on isolated myofibers from FDB muscles of WT mice at 0h (upper panel) and 24h (lower panel) of culturing. The quantification of GPCRs intensity (t-test: ***p < 0.001, *N.D.* (not detected), n = 3, 2-months-old male mice) are shown in (C). Scale bars in (B) represent 50 µm.

D-E. Quantification of the ratio of $PAX7^+$ $KI67^+$ (D) and $PAX7^+$ $MYOD^-$ (E) MuSCs on isolated myofibers from FDB muscles after 24 hours culturing in presence of DMSO, BQ788 or

SR142948A. (One-way ANOVA: ns: no significant, 6 independent experiments, 100 myofibers per group).

F-G. Quantification of the ratio of $PAX7^+$ $KI67^+$ (F) and $PAX7^+$ $MYOD^-$ (G) MuSCs on isolated myofibers from FDB muscles after 24 hours culturing in presence of DMSO, ET-3, NT, ET-3+BQ788 or NT+SR142948A. (One-way ANOVA: ***p < 0.001, ns: no significant, 6 independent experiments, 100 myofibers per group).

H-L. Pharmacological inhibition of EDNRB or NTSR2 mediates precocious activation of MuSCs *in vivo*. The upper panel in (H) depicts the schematic outline of the experimental design, and the lower panel in (H) are representative images of immunostaining for KI67/MYOD /LAMININ-2 (red), PAX7 (green), and DAPI (blue) on transverse sections of WT mice TA muscle after intramuscular injection of saline, BQ788, or SR142948A. Quantification of $PAX7^+$ cells (I) and the ratio of $KI67^+$ MuSCs ($PAX7^+$ $KI67^+$ cells) (J), $MYOD^+$ MuSCs ($PAX7^+$ $MYOD^+$ cells) (K), and the fraction of MuSCs localized outside the basal lamina (L) (One-way ANOVA: ***p < 0.001, ns: no significant, n = 3, 2-months-old male mice, 5 sections per sample) are shown on the right. Scale bars in (H) represent 50 µm.

5.4 ET-3 and NT suppress MuSC activation by stimulation of Rho and G12/13 signaling

To gain a deeper understanding of the molecular mechanisms underlying the inhibitory effects of ET-3 and NT on MuSC activation, I conducted RNAseq analysis on FACS-purified MuSCs treated with ET-3 or NT for 5 days in vitro. Notably, the transcriptomic data analysis revealed a high correlation between the transcriptome of ET-3 and NT-treated MuSCs. The R-value of 0.86 was significantly higher compared to the control group (Figure 6A). Furthermore, a substantial overlap was observed in the upregulated and downregulated genes between the ET-3 and NT treatment groups, accounting for 21% and 56%, respectively, suggesting shared molecular targets, suppressing MuSC activation (Figure 6B). Functional enrichment analysis using Gene Ontology (GO), Kyoto Encyclopedia of Genes and Genomes (KEGG), and Gene Set Enrichment Analysis (GSEA) demonstrated regulation of genes related to Rho signaling pathways, indicating the potential involvement of Rho family members as key effectors mediating the inhibitory effects of ET-3 and NT on MuSC activation (Figure 6C-E).

To further investigate the effects of ET-3 and NT on Rho signaling in MuSCs, I examined the levels of active-Rho (Rho-GTP) following treatment. Both ET-3 and NT significantly increased active-Rho levels in MuSCs compared to the control group after 5 days of treatment (Figure 6F). A similar increase of active-Rho levels was observed in MuSCs from freshly isolated single flexor digitorum brevis (FDB) myofibers treated with ET-3 or NT for 8 hours. Notably, the level of upregulation was comparable to treatment with Wnt4, a known RhoA-inducer

(Figure 6G-H). Moreover, the inhibitory effects of ET-3 and NT on MuSC activation were blocked by the Rho inhibitor C3 Transferase (C3), further corroborating the crucial role of Rho family members as downstream effectors of G protein-coupled receptor (GPCR) signaling pathways activated by ET-3 and NT in enforcing MuSC quiescence (Figure 6I-G).

It is well-established that GPCRs mediate their functions by engaging different heterotrimeric G proteins upon binding to specific ligands. Among the GPCR-coupled G proteins, Gq/11 and G12/13 have been reported as major regulators of Rho activity (Vogt et al., 2003). Previous studies have also associated both NTSR2 and EDNRB with G12/13 or Gq/11 in various physiological processes (Holst et al., 2004; Liu and Wu, 2003; Urtatiz and Van Raamsdonk, 2016). Therefore, I investigated whether EDNRB and NTSR2 require recruitment of Gq/11 or G12/13 to activate Rho and initiate pro-quiescence signaling pathways in MuSCs. To achieve targeted knockout of Gnaq or Gna13 in MuSCs, I utilized Cre-recombinase adenoviruses (Ad-Cre) in MuSCs isolated from *Gna11*$^{-/-}$*Gnaq* $^{loxp/loxp}$ or *Gna12*$^{-/-}$*Gna13* $^{loxp/loxp}$ mice, allowing inactivation of Gq/11 or G12/13 (Figure 6K and Figure 7A). Treatment of MuSCs from *Gna12*$^{-/-}$ *Gna13* $^{loxp/loxp}$ mice with ET-3 or NT significantly increase the proportion of EdU or MYOD positive MuSCs compared to control cells infected with adenovirus containing an empty CMV promoter (Ad-Null) (Figure 6M, and Figure 7C). However, no significant differences were observed in MuSCs from *Gna11*$^{-/-}$*Gnaq* $^{loxp/loxp}$ mice under the same conditions (Figure 6L and Figure 7B). Additionally, the level of active-Rho in G12/13-deficient MuSCs did not significantly increase following treatment with ET-3 or NT, in contrast to control MuSCs infected with Ad-Null (Figure 7D). These findings strongly indicate that G12/13 is essential for ET-3-EDNRB or NT-NTSR2 binding-induced activation of Rho-related quiescence signaling in MuSCs.

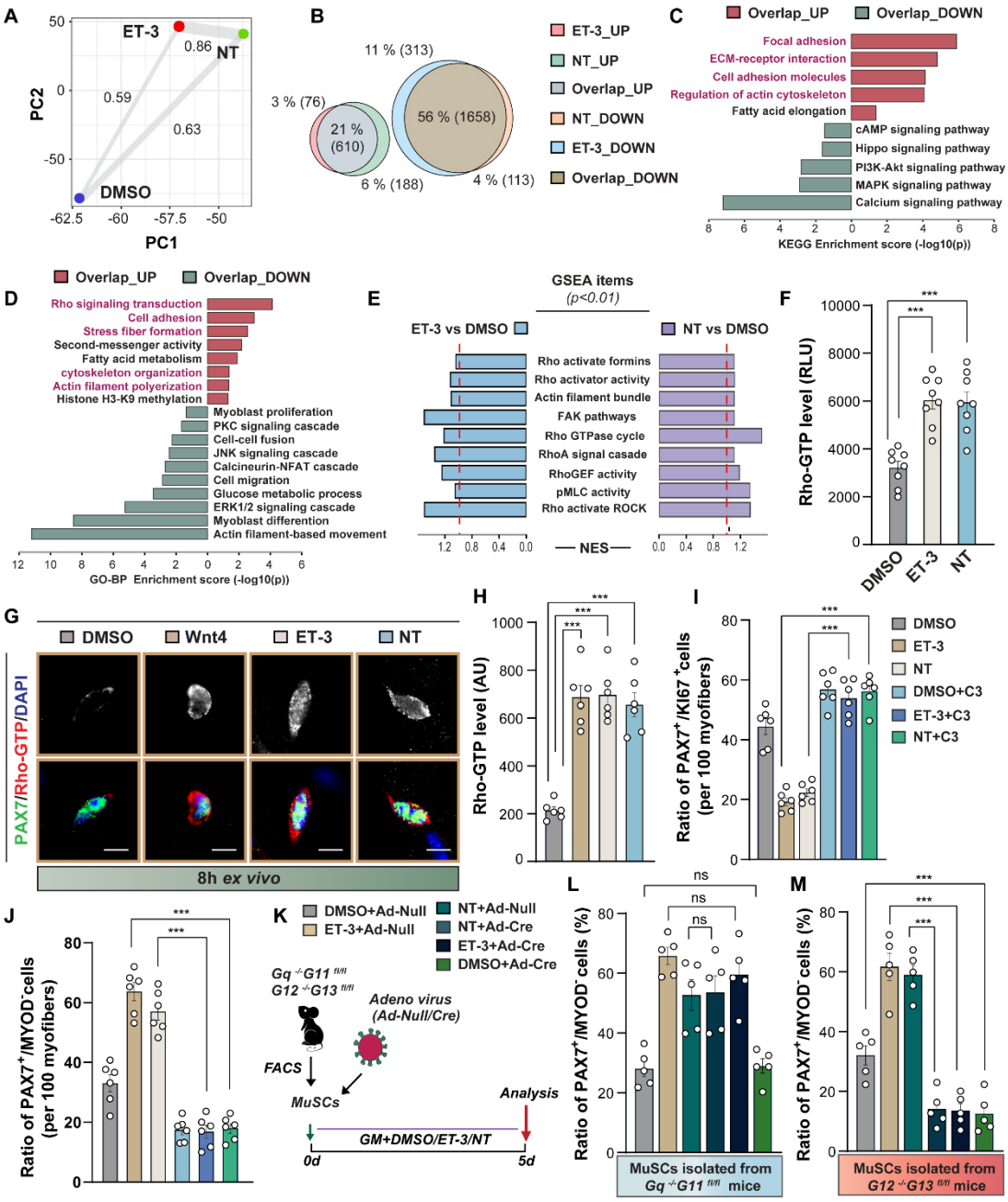

Figure 6 ET-3 and NT prevent MuSC activation via RhoA and G12/13 signaling.

A. Principal component analysis of global transcriptomes of DMSO, ET-3 and NT treated MuSCs (*in vitro* culturing for 5days) and Pearson's values illustrating the correlation between samples. Each dot represents the mean of three biological samples.

B. Venn diagram depicting the overlap between differentially expressed upregulated (left panel, genes with $p < 0.05$ and $Log2FC > 1$) or downregulated (right panel, genes with $p < 0.05$ and $Log2FC < -1$) genes in ET-3 or NT treated MuSCs compared to the DMSO group.

C-E. KEGG (C), Gene ontology of biological process (GO-BP) term enrichment (D) and gene set enrichment analysis (GSEA) (E) of upregulated and downregulated genes, overlapping between ET-3 or NT treated MuSCs compared to DMSO group.

F. Rho activity in MuSCs cultured in the presence of DMSO, ET-3, or NT for 5 days. The level of activated RhoA-GTP was quantified by luminescence measurements at 490 nm. (One-way

ANOVA: ***p < 0.001, ns: no significant, eight independent experiments, 3 replicates per group)

G-H. Representative images (Rho-GTP (red), PAX7 (green), and DAPI (blue)) (G) and quantification (H) of active Rho levels in MuSCs on isolated myofibers from FDB muscles of WT mice following 8 hours culturing in presence of DMSO, ET-3 or NT. (One-way ANOVA: ***p < 0.001, 6 independent experiments, at least 100 MuSCs were measured in each group). Scale bars in (G) represent 5 µm.

I-J. Quantification of the ratio of $PAX7^{+}$ $KI67^{+}$ (I) and $PAX7^{+}$ $MYOD^{-}$ (J) MuSCs on isolated myofibers from wild type FDB muscles after 24 hours in presence of DMSO, ET-3, or NT, with or without Rho inhibitor (C3). (One-way ANOVA: ***p < 0.001, 6 independent experiments, 100 myofibers per group).

K-M. ET-3 and NT prevent MuSC activation through G12/13 signaling. The schematic experimental outline is depicted in (K), and quantifications of the ratio of $PAX7^{+}$/$MYOD^{-}$ MuSCs isolated from $Gq^{-/-}G11^{fl/fl}$ (L) or $G12^{-/-}G13^{fl/fl}$ (M) mice infected with Ad-null or Ad-Cre virus cultured in presence of DMSO, ET-3, or NT for 5 days *in vitro*, are shown on the right (One-way ANOVA: ***p < 0.001, ns: no significant, n = 5, 2-months-old male mice, 3 replicates per group).

To investigate whether activation of EDNRB and NTSR2 by ET-3 and NT, respectively, leads to enhanced coupling between these receptors and Gα12 or Gα13, I employed TRUPATH biosensors, which are optimized bioluminescence resonance energy transfer (BRET2) Gαβγ biosensors (Olsen et al., 2020). The dissociation of Gα12 or Gα13 subunit and Gβγ heterodimer was monitored by measuring the BRET2 signal upon agonist-induced activation of G protein-coupled receptors (GPCRs) (Figure 7E). Reduction in the BRET2 signal indicates receptor-mediated G protein dissociation. HEK cells overexpressing full-length EDNRB or NTSR2 were transfected with plasmid vectors expressing Gβ3, Gγ9-GFP2, and Gα12(134)-RLuc8 or Gα13(126)-RLuc8 proteins. In HEK cells overexpressing EDNRB, ET-3 treatment induced a significant dose-dependent reduction in BRET signals for both Gα12 and Gα13 compared to controls (Figure 7F-G). Similar effects were observed in HEK cells overexpressing NTSR2 stimulated with NT (Figure 7H-I). These findings suggest that the binding of ET-3 to EDNRB or NT to NTSR2 directly activates G12/13 signaling.

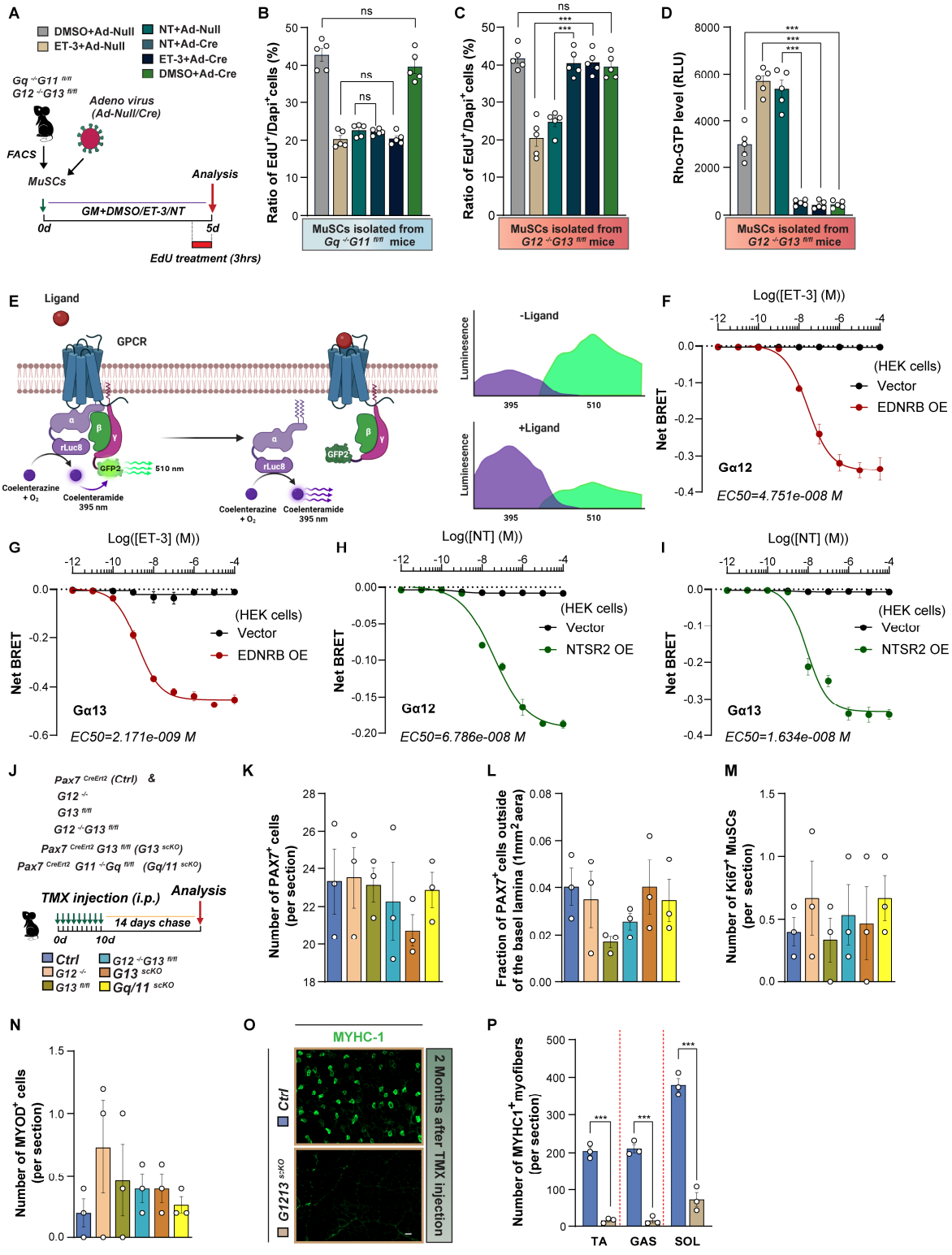

Figure 7 EDNRB or NTSR2 interacts with both Gα12 and Gα13 upon ET-3 or NT stimulation.

A-C. ET-3 and NT prevent MuSC activation through G12/13 signaling. The schematic outline of the experimental design is shown in (A), and quantifications of the ratio of EdU⁺ MuSCs isolated from *Gq*$^{-/-}$*G11*$^{fl/fl}$ (B) or *G12*$^{-/-}$*G13*$^{fl/fl}$ (C) mice infected with Ad-null or Ad-Cre virus culturing in presence of DMSO, ET-3, or NT for 5 days *in vitro*, are shown on the right (One-way ANOVA: ***p < 0.001, ns: no significant, n = 5, 2-months-old male mice, 3 replicates per group).

D. Rho activity in Ad-null or Ad-Cre virus infected *G12*$^{-/-}$*G13*$^{fl/fl}$ MuSCs cultured in presence of DMSO, ET-3, or NT for 5 days. The level of activated RhoA-GTP was quantified by luminescence measurements at 490 nm (One-way ANOVA: ***p < 0.001 n=5, 2-months-old male mice, 3 replicates per group).

E. Schematic representation of TRUPATH assay for measuring heterotrimeric G protein dissociation by bioluminescence resonance energy transfer 2 (BRET2).

F-G. ET-3 concentration response curves for activation of (F) Gα12(134)-RLuc8/Gβ3γ9-GFP2, (G) Gα13(126)-RLuc8/Gβ3γ9-GFP2, BRET biosensors in control (vector) or EDNRB overexpressed HEK cells (5 independent experiments, 3 replicates per group).

H-I. NT concentration response curves for activation of (H) Gα12(134)-RLuc8/Gβ3γ9-GFP2, (I) Gα13(126)-RLuc8/Gβ3γ9-GFP2, BRET biosensors in control (vector) or EDNRB overexpressed HEK cells (5 independent experiments, 3 replicates per group).

J. Schematic experimental design of (K-N).

K-N. Quantifications of all PAX7^{+} cells (B), the fraction of PAX7^{+} MuSCs localized outside the basal lamina (C), KI67^{+} MuSCs (D), and MYOD^{+} cells (E), in the TA muscles of control, *G12*$^{-/-}$, *G13*$^{fl/fl}$, *G12*$^{-/-}$ *G13*$^{fl/fl}$, and *Gq/11*^{scKO} mice (n=3, 2-months-old male mice, 5 sections per muscle sample).

O-P. Immunofluorescence staining for MYHC-1 (green), DAPI (blue) in TA muscles of control and *G1213*^{scKO} mice 2 months after tamoxifen (TMX) injection (O), and quantification of MYHC-1^{+} myofibers in TA, GAS, and SOL muscles is shown in (P) (t-test: ***p<0.01, n=3, 17-weeks-old male mice, 5 sections per muscle sample). Scale bars in (O) represent 50 µm.

5.5 G12/13 signaling is crucial for preserving quiescence and preventing decline of MuSCs.

Subsequently, I aimed to elucidate the impact of G12/13 signaling on the regulatory framework of MuSC quiescence. To address this, I generated MuSC-specific conditional knockout mice for G12/13 (referred to as *G1213*^{scKO}) (Figure 8A-B). Following ten consecutive days of tamoxifen administration, *G1213*^{scKO} mice displayed a notable increase in MuSC numbers, with 80% of them localized outside the basal lamina of myofibers, in contrast to the control group (Figure 8C-D). Further analysis confirmed the accumulation of PAX7/MYOD or PAX7/KI67 double-positive cells in TA muscles of *G12/13*^{scKO} mice under homeostatic conditions (Figure 8E-G), implying a crucial role of G12/13 signaling for maintaining quiescence and keeping MuSC in the niche.

Additionally, I observed a substantial increase in eMYHC (MYH3) protein levels within the TA muscle of *G1213*^{scKO} mice, along with the presence of centrally localized nucleiin myofibers (Figure 8J-L). Expression of eMYHC and central localization of nuclei are indicative for recent fusion of MuSCs to myofibers. By employing genetic lineage tracing, I confirmed that all central-localized myonuclei were derived from G12/13-inactivated MuSCs, which

also contributed to the substantial ratio of mCherry+ nuclei in the periphery of myofibers (Figure 8M-O), suggesting that the activated G12/13 KO-MuSCs not fused with adjacent myofibers. Consistently, the number of MyoG-positive nuclei increased considerably in *G1213^{scKO}* mice (Figure 8H-I), further proving activation of myogenesis in mutant mice. Collectively, these findings underscore the critical role of G12/13 signaling in maintaining MuSC quiescence and shed light on how GPCR signals control quiescence and activation of MuSC, which is crucial for maintaining proper muscle homeostasis. However, the overall morphology of muscles did not change during the first weeks after inactivation of *G12/G13* and *Gq/11* (Figure 10J-N).

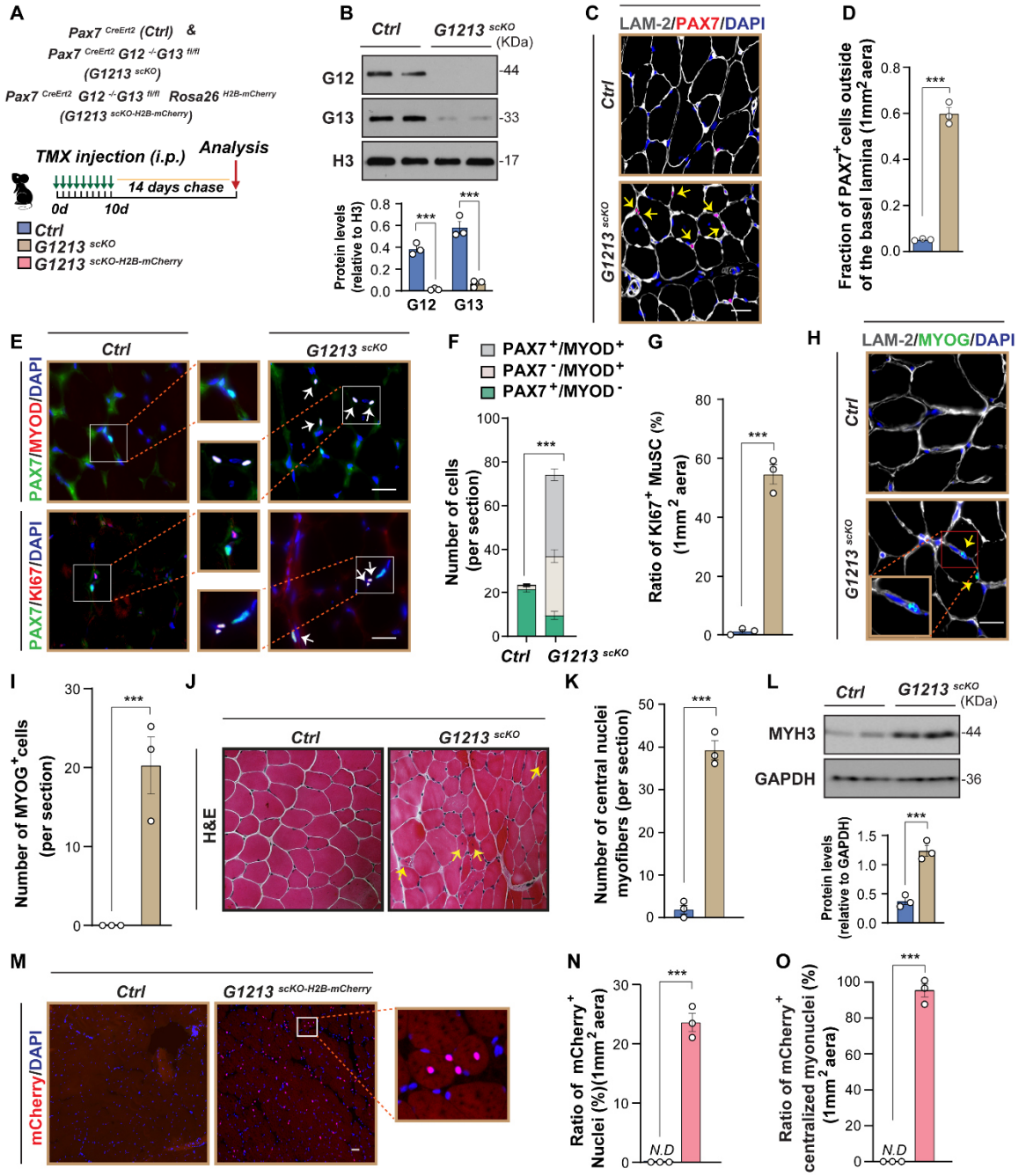

Figure 8 Absence of G12/13 leads to activation and differentiation of muscle stem cells *in vivo*.

A. Principal schematic representation of the experimental design of (B-O).
B. Western blot analysis of G12, G13 and Histone3 (H3) expression in freshly isolated control and *G1213^{scKO}* MuSCs. Quantification is shown on the lower panel, the protein level of G12 and G13 are normalized to H3 (One-way ANOVA: ***p < 0.001, n = 3, 2-months-old male mice).
C-D. Immunofluorescence staining for PAX7 (red), LAMININ-2 (LAM-2) (grey), and DAPI (blue), in TA muscles of control and *G1213^{scKO}* mice (C), and quantification of the fraction of MuSCs localized outside the basal lamina (D) (t-test: ***p<0.01, n=3, 2-months-old male mice, 5 sections per muscle sample). Scale bars in (C) represent 10 µm.
E-G. Immunofluorescence staining for PAX7 (green), MYOD/KI67 (red), and DAPI (blue), in TA muscles of control and *G1213^{scKO}* mice (E). The quantifications are shown on the right (F-G) (t-test: ***p<0.01, n=3, 2-months-old male mice, 5 sections per muscle sample). Scale bars in (E) represent 20 µm.
H-I. Immunofluorescence staining for MYOG (green), LAMININ-2 (LAM-2) (grey), and DAPI (blue), in TA muscles of control and *G1213^{scKO}* mice (H). The quantification is shown in (I) (t-test: ***p<0.01, n=3, 2-months-old male mice, 5 sections per muscle sample). Scale bars in (H) represent 10 µm.
J-K. H&E staining of muscle sections from TA muscles of control and *G1213^{scKO}* mice (J). Quantification of central nuclei myofibers is shown in (K) (t-test: ***p<0.01, n=3, 2-months-old male mice, 5 sections per muscle sample). Scale bars in (J) represent 20 µm.
L. Western blot analysis for MYH3 and GAPDH expression level in TA muscles of control and *G1213^{scKO}* mice (J). Quantification is shown on the lower panel. The protein level of MYH3 is normalized to GAPDH (t-test: ***p<0.01, n=3, 2-months-old male mice).
M-O. Immunofluorescence staining for mCherry (red) and DAPI (blue) in TA muscles of control and *G1213^{scKO}* mice (M). The quantifications of the ratio of H2B-mCherry^{+} nuclei (N) and H2B-mCherry^{+} centralized myonuclei (O) are shown on the right (t-test: ***p<0.01, n=3, 2-months-old male mice). Scale bars in (M) represent 20 µm.

To investigate the long-term consequences of G12/13 depletion in MuSCs, I administered tamoxifen to young (2 months old) *G1213^{scKO}* mice for ten consecutive days to inactivate G12/13 in MuSCs and subsequently allowed the mice to age (Figure 9A). At 20 months of age, *G1213^{scKO}* mice exhibited reduced body weight and muscle mass compared to the control group (Figure 9B). The aged control mice displayed 44% greater tibialis anterior muscle mass and 40% greater gastrocnemius muscle mass than aged *G1213^{scKO}* mice (Figure 9C-D). The muscle loss was accompanied by distortion of the muscle morphology, reflected by disorganized myofiber sizes and structure (Figure 9E-F). Furthermore, a significant reduction in the number of MuSCs was observed in the tibialis anterior muscle of aged *G1213^{scKO}* mice (Figure 9G-H). Aged mutant MuSCs exhibited notable proliferative defects compared to control MuSCs (Figure 9I). Overall, these findings strongly suggest that G12/13 signaling is indispensable for maintaining the MuSC pool and ensuring proper MuSC function during aging. Impairment of G12/13 signaling within MuSCs may thus contribute

to age-related muscle loss by compromising skeletal muscle homeostasis.

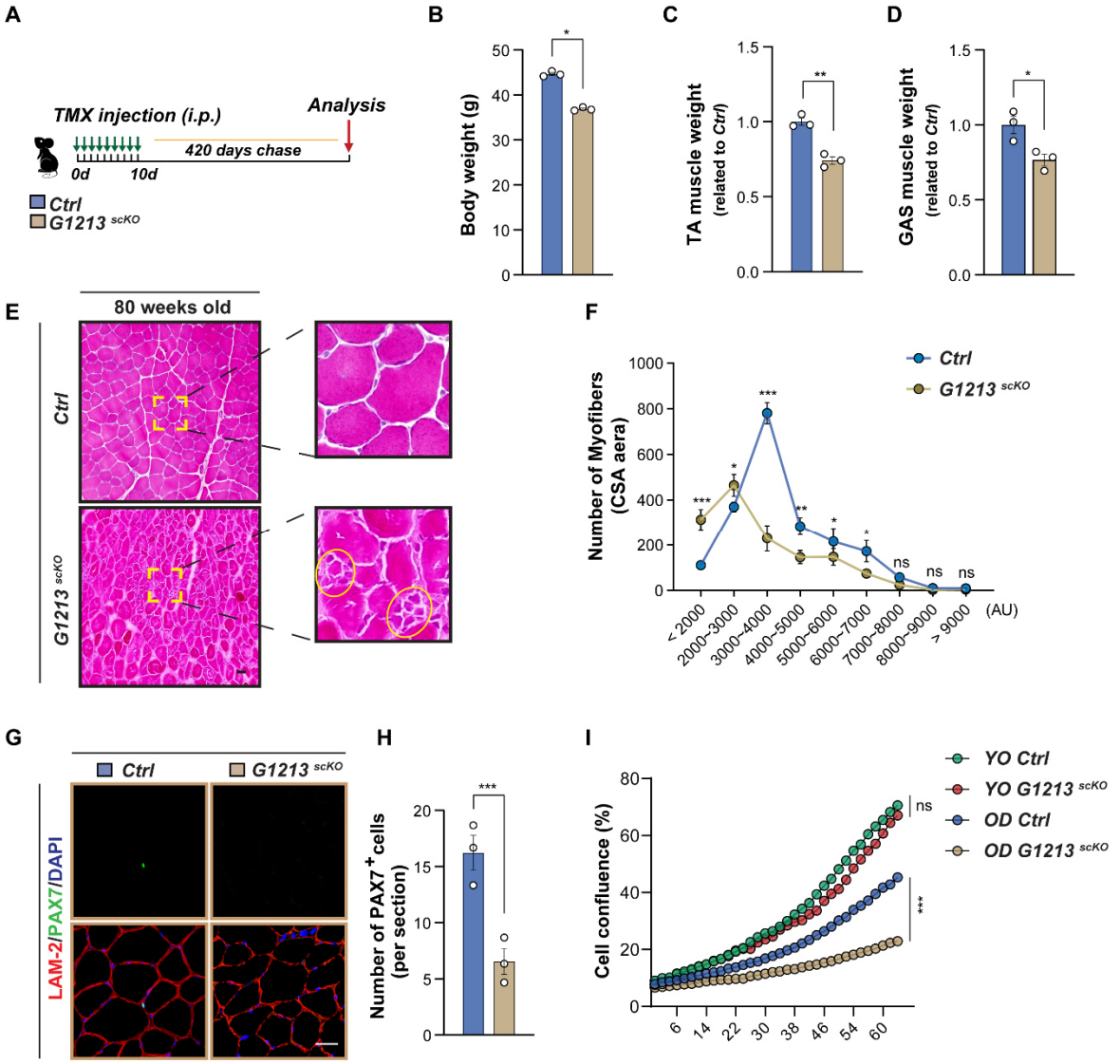

Figure 9 Long-term ablation of G12/13 in MuSCs reduces the MuSC pool and accelerates age-related muscle loss.

A. Schematic representation of the experimental design in (B-H).
B. Body weight of control and *G1213*^{scKO} mice. (n=3, 80-weeks-old male mice)
C. Weight of control and *G1213*^{scKO} mice TA muscles. (n=3, 2-months-old male mice)
D. Weight of control and *G1213*^{scKO} mice GAS muscles. (n=3, 2-months-old male mice)

E-F. H&E staining of muscle sections from TA muscles of control and *G1213*^{scKO} mice (E). Distribution of myofibers with different cross-sectional areas (CSA) in TA muscles of control (blue) and *G1213*^{scKO} (yellow) mice is shown in (F) (One-way ANOVA-test: ***p < 0.001, **p < 0.01, *p < 0.05, ns: no significant, n = 3, 2-months-old male mice, 3 sections per sample). Scale bars in (E) represent 50 µm.

G-H. Immunofluorescence staining for PAX7 (green), LAMININ-2 (LAM-2) (red), and DAPI (blue), in TA muscles of control and *G1213*^{scKO} mice (G), and quantification of PAX7^{+} cells is shown in (H) (t-test: ***p<0.01, n=3, 80-weeks-old male mice, 5 sections per muscle sample). Scale bars in (G) represent 10 µm.

I. Proliferation of young (YO, 2 month old male mice) and old (OD, 80-weeks-old male mice) control and *G1213^{scKO}* MuSCs assessed by time-lapse imaging (Statistical significance at the last time point, one-way ANOVA-test: ***p < 0.001, ns: no significant, n = 3, 3 repeats per group).

5.6 Disabling RhoA in quiescent MuSC *in vivo* recapitulates the phenotypes of *G1213^{scKO}* mice

The results strongly suggested that members of the Rho family function are essential components of the ET-3/NT-GPCRs-G12/13 signaling axis for maintaining MuSC quiescence. Consistently, I observed a significant reduction in active-Rho levels and phosphorylated-Myosin Light Chain (pMLC), a downstream target of Rho, in MuSCs isolated from *G12/13^{scKO}* mice compared to controls (Figure 10A-D). However, the specific Rho proteins responsible for governing the downstream regulatory hierarchy of G12/13 in quiescent MuSCs remained unidentified. Previous studies have shown that RhoA is a canonical responder to G12/13 signaling in various cellular contexts, and its downregulation in MuSCs in vivo leads to premature activation under homeostasis conditions, consistent with the findings in *G1213^{scKO}* mice (Eliazer *et al.*, 2019; Siehler, 2009; Sternweis et al., 2007). These findings strongly suggest that RhoA, downstream of G12/13, is critical for maintaining quiescence.

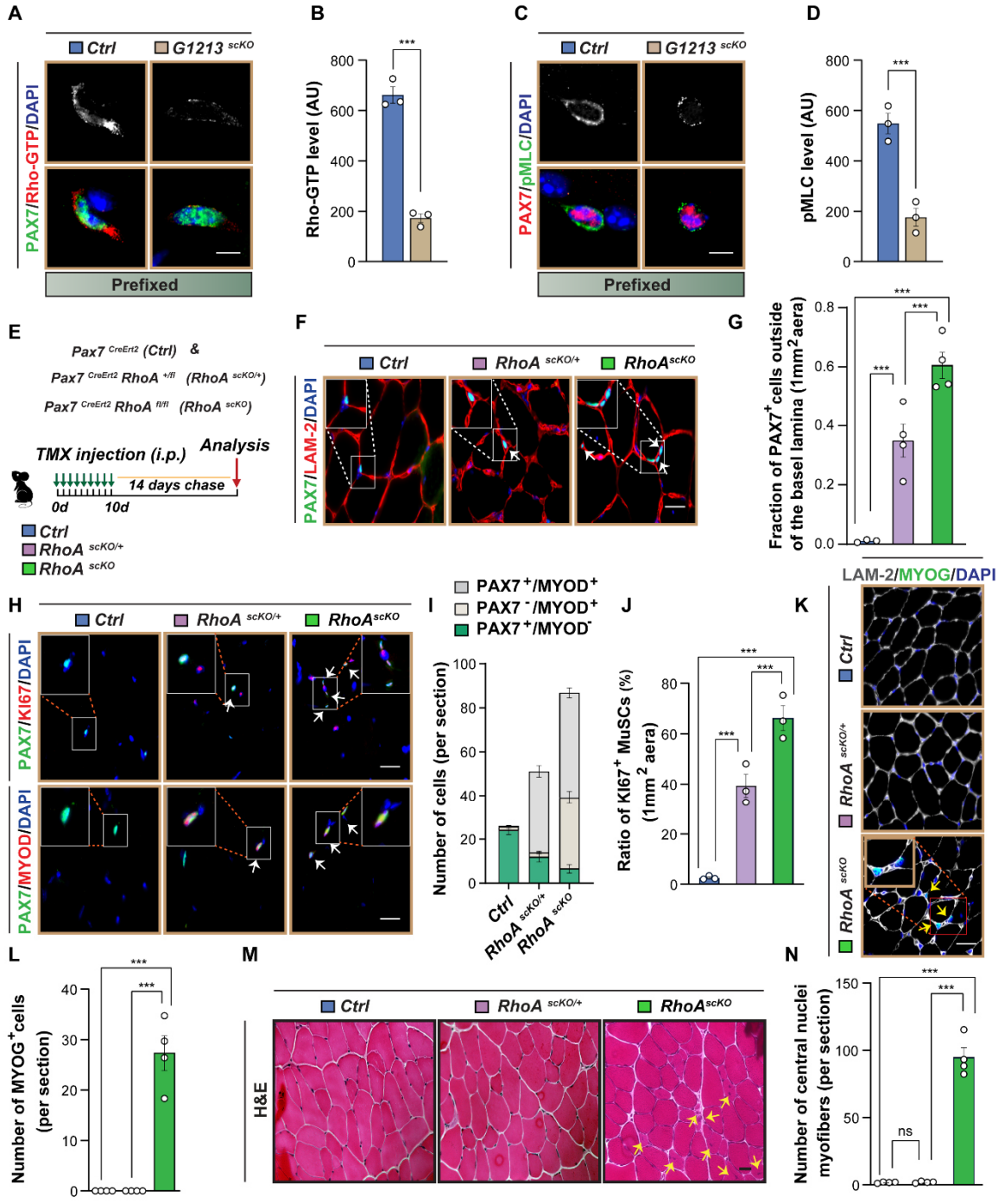

Figure 10 *In vivo* inactivation of RhoA signaling in quiescent MuSC phenocopies effects of *G12/13* inactivation

A-B. Representative images (Rho-GTP (red), DAPI (blue), and PAX7 (green)) (A) and quantification (B) of active Rho levels in MuSCs on isolated myofibers from prefixed FDB muscles of control and *G1213*^{scKO} mice. (t-test: ***p < 0.001, n=3, 2-months-old male mice). Scale bars in (G) represent 5 µm.

C-D. Representative images (PAX7 (red), DAPI (blue), and pMLC (green)) (C) and corresponding quantification (D) of pMLC levels in MuSCs on isolated myofibers from prefixed FDB muscles of control and *G1213*^{scKO} mice. (t-test: ***p < 0.001, n=3, 2-months-old male mice). Scale bars in (C) represent 5 µm.

E. Schematic experimental design of (F-N).

F-G. Immunofluorescence staining for PAX7 (red), LAMININ-2 (LAM-2) (red), and DAPI (blue), in TA muscles of control, *RhoA*$^{scKO/+}$ and *RhoA*^{scKO} mice (F), and the quantification of the fraction of MuSCs localized outside the basal lamina is shown in (D) (One-way ANOVA: ***p<0.01, n=3, 2-months-old male mice, 5 sections per muscle sample). Scale bars in (F) represent 10 µm.

H-J. Immunofluorescence staining for PAX7 (green), MYOD/KI67 (red), and DAPI (blue), in TA muscles of control, *RhoA*$^{scKO/+}$ and *RhoA*^{scKO} mice (H). Quantifications are shown on the right (I-J) (One-way ANOVA: ***p<0.01, n=3, 2-months-old male mice, 5 sections per muscle sample). Scale bars in (J) represent 20 µm.

K-L. Immunofluorescence staining for MYOG (green), LAMININ-2 (LAM-2) (grey), and DAPI (blue), in TA muscles of control, *RhoA*$^{scKO/+}$ and *RhoA*^{scKO} mice (K). Quantification is shown in (L) (One-way ANOVA: ***p<0.01, n=3, 2-months-old male mice, 5 sections per muscle sample). Scale bars in (K) represent 20 µm.

M-N. H&E staining of muscle sections from TA muscles of control, *RhoA*$^{scKO/+}$ and *RhoA*^{scKO} mice(J). Quantification of central nuclei myofibers is shown in (N) (One-way ANOVA: ***p<0.01, n=3, 2-months-old male mice, 5 sections per muscle sample). Scale bars in (J) represent 20 µm.

Earlier studies already demonstrated that RhoA is involved in the regulation of MuSC quiescence, but a complete inactivation of RhoA has not been attempted before (Castellani et al., 2006). To fully inactivate RhoA in quiescent MuSCs in vivo, a tamoxifen-inducible, MuSC-specific genetic approach was persued, yielding *RhoA*^{scKO} mice (Figure 10E). In comparison to heterozygous (*RhoA*$^{scKO/+}$) mice, *RhoA*^{scKO} mice exhibited a significant increase in MuSC abnormalities. Specifically, the number MYOD-positive MuSCs increased by 20% rise and the number of MuSC outside the niche by 35% (Figure 10F-J). Furthermore, a higher number of MYOG-positive nuclei and nuclei centrally located within myofibers were observed in the TA muscle of *RhoA*^{scKO} mice (Figure 10K-N), mirroring the phenotypic traits observed in *G1213*^{scKO} mice. These findings indicate that RhoA serves as the primary downstream effector of G12/13, with G12/13 playing a predominant role in RhoA activation in quiescent MuSCs.

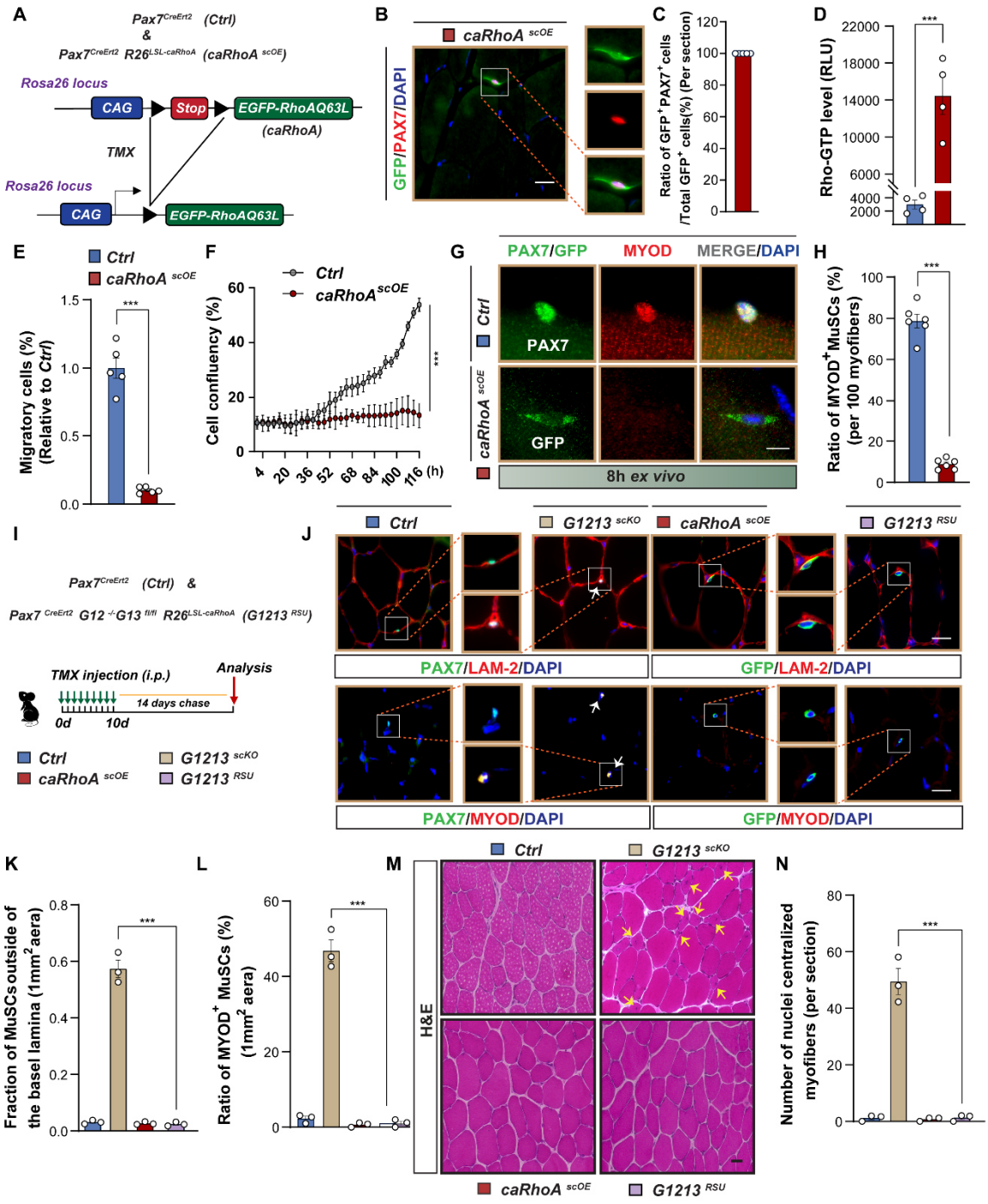

Figure.11 The G12/13 signaling axis maintains MuSC quiescence by activation of RhoA

A. Schematic representation of the caRhoA overexpression allele.

B-C. Immunofluorescence staining for PAX7 (red), DAPI (blue), or GFP-fluorescence (green) in TA muscles of *caRhoA*^{scOE} mice (B). Quantification of the percentage of Pax7^{+}cells in total GFP^{+} cells is shown in (C) (n=5, 2-months-old male mice, 5 sections per muscle sample). Scale bars in (B) represent 10 µm.

D. Rho activity in control and *caRhoA*^{scOE} MuSCs cultured for 5 days. The level of activated RhoA-GTP was quantified by luminescence measurements at 490 nm. (t-test: ***p < 0.001 n=4, 2-months-old male mice, 3 replicates per group)

E. Transwell cell migration assay to measure the motility of control and *caRhoA*^{scOE} in cultured MuSCs for 5 days (t-test: ***p < 0.001 n=5, 2-months-old male mice, 3 replicates per group).

F. Time-lapse imaging of MuSCs proliferation. MuSCs from control are represented by grey dots, MuSCs from *caRhoA*^{scOE} mice by red dots (Statistical significance at the last time point, one-way ANOVA: ***p < 0.001 n=3, 2-months-old male mice, 3 replicates per group).

G-H. Immunofluorescence staining for PAX7 (green), MYOD (red), DAPI (blue), or autofluorescence GFP (green) in MuSCs on isolated myofibers from FDB muscles of control and *caRhoA*^{scOE} mice after 8 hours of culture (G). Quantification of the ratio of MYOD^{+} MuSCs is shown in (H) (t-test: ***p<0.01, n=6, 2-months-old male mice, 100 myofibers were counted per sample). Scale bars in (G) represent 5 µm.

I. Schematic experimental design of (J-L).

J. Immunofluorescence staining for MYOD /LAMININ-2 (red), PAX7 (green), DAPI (blue) , or GFP-fluorescence (green) in the TA muscles of control, *caRhoA*^{scOE}, *G1213*^{scKO}, and *G1213*^{RSU} mice. Scale bars represent 10 µm.

K-L. Quantifications of the fraction of MuSCs localized outside the basal lamina (K) and the ratio of MYOD^{+} (L) MuSCs in TA muscles of control, *caRhoA*^{scOE}, *G1213*^{scKO}, and *G1213* ^{RSU} mice (One-way ANOVA: ***p<0.01, n=3, 2-months-old male mice, 5 sections per muscle sample).

M. H&E staining of muscle sections from TA muscles of control, *caRhoA*^{scOE}, *G1213*^{scKO}, and *G1213* ^{RSU} mice. Scale bar represent 20 µm.

N. Quantifications of central nuclei myofibers in the TA muscles of control, *caRhoA*^{scOE}, *G1213*^{scKO}, and *G1213* ^{RSU} mice (One-way ANOVA: ***p<0.01, n=3, 2-months-old male mice, 5 sections per muscle sample).

5.7 Maintainence of MuSC quiescence by GPCRs-G12/13 signaling depends on RhoA activation

To explore whether elevated levels of active RhoA prevent the loss of MuSC quiescence resulting from disrupted GPCRs-G12/13 signaling, I established a mouse model (*Pax7* ^{CreERT2}; Tg: *R26LSL-caRhoA*) in which a constitutively active mutant (Q63L) of human RhoA protein fused with GFP (caRhoA scOE) is expressed in a conditional MuSC-specific manner (Figure 11A-D). Remarkably, elevated levels of caRhoA prevented activation of MUSC as well as migration and proliferation of freshly isolated MuSCs in vitro (Figure 11E-H). Moreover, expression of caRhoA in MuSC effectively prevented MuSC activation in response to disruption of ET-3-EDNRB or NT-NTSR2-induced signal transduction in vivo, caused by injection of SR142948A or BQ788 into the TA muscle (Figure 12A-D). caRhoA overexpression also fully rescued the phenotype of *G1213*^{scKO} mice, restoring MuSC quiescence and normalizing the number of centrally located nuclei in myofibers (Figure 11I-N and Figure 12E-H). These findings emphasize the critical role of the GPCRs-G12/13-RhoA signaling cascade, initiated by niche ligands (ET-3/NT), in preserving MuSC quiescence, maintaining a robust MuSC population, and sustaining long-term regenerative capacity of adult skeletal muscles.

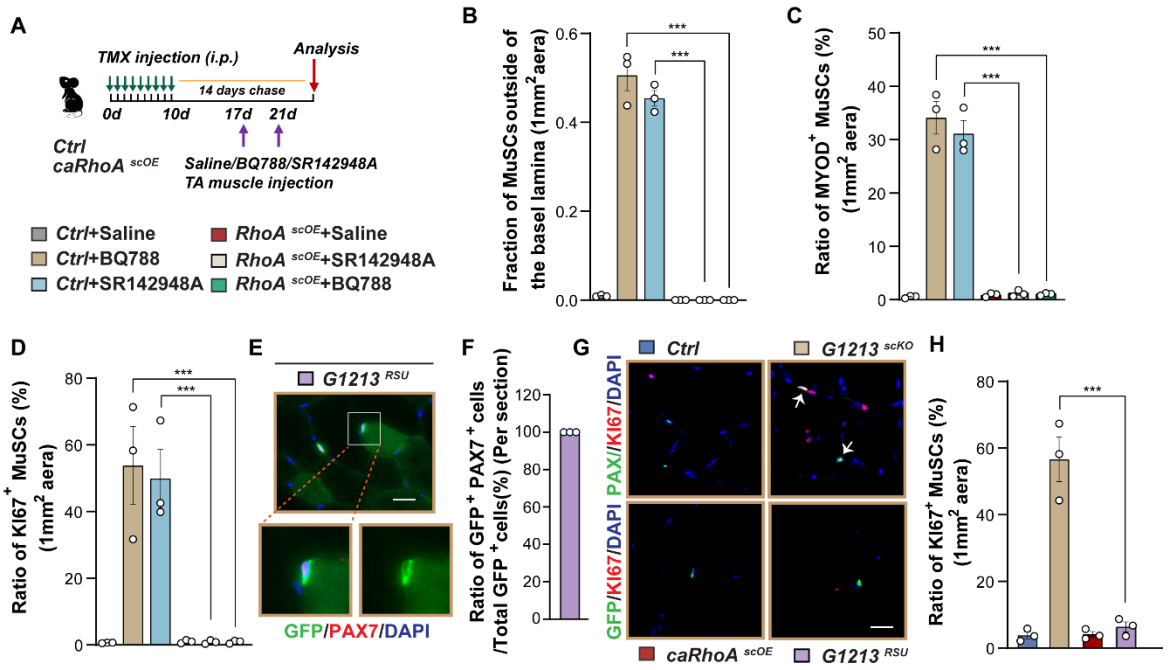

Figure 12 GcRhoA overexpression prevents MuSC activation initiated by administration of BQ788 or SR142948A.

A. Schematic representation of the experimental design in (B-D).

B-D. Quantifications of the fraction of MuSCs localized outside the basal lamina (B) and the ratio of MYOD+ (C) and KI67+ (D) MuSCs in control and *caRhoA*^{scOE} mice TA muscles after intramuscular injection of saline, BQ788, or SR142948A (One-way ANOVA: ***p<0.01, n=3, 2-months-old male mice, 5 sections per muscle sample).

E-F. Immunofluorescence staining for PAX7 (red), DAPI (blue) and GFP-fluorescence (green) in TA muscles of control and *G1213*^{RSU} mice (E). Quantification of the ratio of GFP^{+} Pax7^{+}cells in total GFP^{+} cells is shown in (F) (n=3, 2-months-old male mice, 5 sections per muscle sample). Scale bars in (E) represent 10 µm.

G-H. Immunofluorescence staining for PAX7 (green), KI67 (red), DAPI (blue) or, GFP-fluorescence (green) in TA muscles of control, *caRhoA*^{scOE}, *G1213*^{scKO}, and *G1213*^{RSU} mice (G). Quantification of the ratio of KI67^{+} MuSCs is shown in (H) (One-way ANOVA: ***p<0.001, n=3, 2-months-old male mice, 5 sections per muscle sample). Scale bars in (G) represent 10 µm.

5.8 Active RhoA inhibits cell cycle entry and differentiation of MuSC via Rock and formins

Previous studies revealed that inactivation of YAP1 effectively prevents activation of MuSC after suppression of RhoA (Eliazer *et al.*, 2019). Notably, translocation of YAP1 into nuclei was reduced in both *RhoA*^{scKO} and *G1213*^{scKO} mice, indicating that RhoA stimulates the Hippo pathway (Figure 13F). Several effects of RhoA are mediated by the Rho-associated

protein kinase (ROCK) and by formins, which regulate actin cytoskeleton dynamics and various other functions (Amano et al., 2010; Watanabe et al., 1999). Thus, I investigated whether ROCK, formins, and YAP are part of the RhoA-induced regulatory hierarchy in quiescent MuSCs.

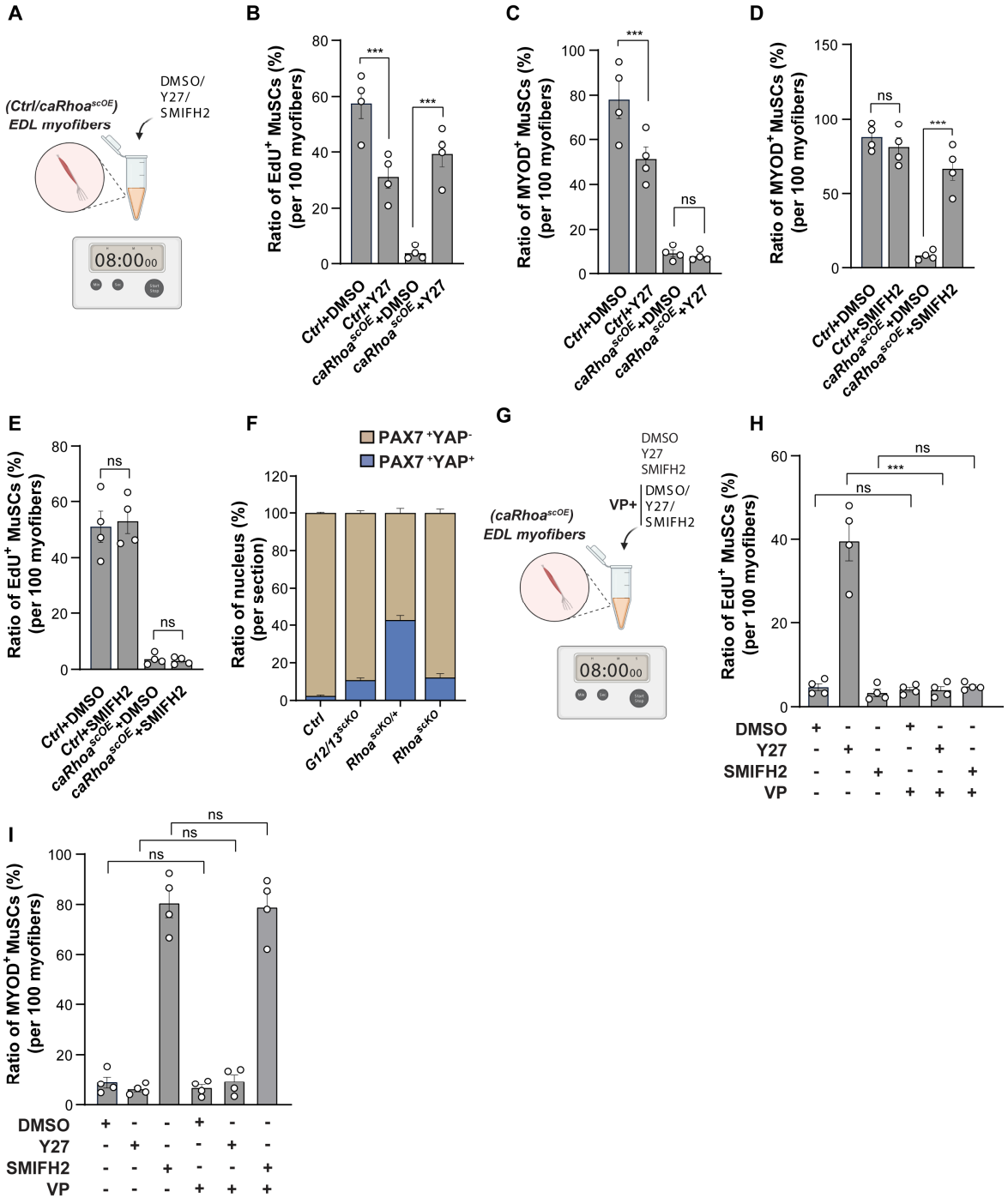

Figure 13 RhoA separately activates ROCK1/2-YAP and Formins in quiescent MuSCs to prevent cell-cycle entry and myogenic differentiation, respectively.

A. Schematic representation of the experimental design in (B-E).

B-C. Quantifications of the ratio of MYOD^{+} (B) and EdU^{+} (C) MuSCs on isolated myofibers from FDB muscles of control and *caRhoA^{scOE}* mice following 8 hours in the presence of DMSO, Y-27632(Y27) (One-way ANOVA: ***p < 0.001, ns: no significant, n = 4, 2-months-old male mice, 3 replicates per group).

D-E. Quantifications of the ratio of MYOD^{+} (D) and EdU^{+} (E) MuSCs on isolated myofibers from FDB muscles of control and *caRhoA^{scOE}* mice after 8 hours in presence of DMSO, SMIFH2 (One-way ANOVA: ***p < 0.001, ns: no significant, n = 4, 2-months-old male mice, 3 replicates per group).

F. Proportion of YAP^{+} MuSCs on muscle sections from TA muscles of control, *G1213^{scKO}*, *RhoA$^{scKO/+}$* and *RhoA^{scKO}* mice (n=3, 2-months-old male mice, 5 sections per muscle sample).

G. Schematic representation of the experimental design of (H-I).

H-I. Quantifications of the ratio of MYOD^{+} (H) and EdU^{+} (I) MuSCs on isolated myofibers from FDB muscles of *caRhoA^{scOE}* mice after 8 hours treatment with DMSO, Y-27632(Y27), or SMIFH2 without or with 5 Mm verteporfin (VP) (One-way ANOVA: ***p < 0.001, ns: no significant, n = 4, 2-months-old male mice, 3 replicates per group).

First, I pharmacologically inhibited ROCK and formin activities using the ROCK inhibitor Y-27632 (Y27) and the general formin inhibitor SMIFH2, respectively, in isolated caRhoA-OE MuSCs (Figure 13A). Suppression of either ROCK or formins abolished different effects of caRhoA on MuSCs. (i) Inhibition of ROCK by Y27 released the proliferation block in caRhoA-overexpressing MuSCs but did not stimulated myogenic differentiation (Figure 13B-C). (ii) Inhibition of formins by SMIFH2 induced expression of MYOD characteristic for myogenic differentiation but had no effects on the arrested proliferation of caRhoA-overexpressing MuSCs (Figure 13D-E). The distinct effects of Y27 and SMIFH2 on caRhoA-overexpressing MuSCs indicate that RhoA controls two different pathways to ensure quiescence. ROCKs for preventing cell cycle entry and formins to suppress myogenic differentiation. Notably, mDia1, a member of the formin family, suppresses expression of MYOD and MYOG, making it likely that activation of mDia1 by caRhoA inhibits myogenic regulatory factors, impeding initiation of the myogenic program in MuSCs (Gopinath et al., 2007; Saleh et al., 2019). On the other hand, RhoA inhibits activation of YAP in quiescent MuSCs by inducing ROCK-mediated phosphorylation of MLC (Eliazer *et al.*, 2019). To further corroborate the involvement of YAP downstream of RhoA in maintaining MuSC quiescence, we inhibited YAP activity using verteporfin (VP). The administration of VP alongside Y27 significantly mitigated the EdU incorporation that was induced by ROCK blockade with Y27, suggesting that ROCK indeed restricts activation of YAP, thereby preventing quiescent MuSCs from entering the cell cycle (Figure 13G-I). However, VP treatment had no effect on the SMIFH2-induced MyoD expression, reinforcing the notion that RhoA orchestrates distinct pathways to synergistically enforce MuSC quiescence (Figure 13G-I). Collectively, these findings

provide compelling evidence for the existence of a complex regulatory network orchestrated by RhoA in quiescent MuSCs, involving ROCK and formins.

5. 9 Activation of RhoA has no effects on cytoplasmic projections of quiescent MuSC

In light of our findings that delineate the distinct roles of ROCK and formin pathways in maintaining MuSC quiescence, we further investigated the interplay between RhoA activity and Rac1, another member of the Rho GTPase family known for its role in cytoskeletal reorganization and cell cycle regulation. A recent report has suggested that a Rac1-to-RhoA activity switch is required for MuSCs to retract their quiescent projections (QPs) and exit the quiescent state. To address whether increased RhoA signaling influences Rac1 activity and the maintenance of QPs, I performed immunofluorescence staining of MuSCs for PAX7 and α-Tubulin on isolated single myofibers from control and *caRhoA*^{scOE} mice.

The results revealed no significant changes in the presence or morphology of QPs between control and *caRhoA*^{scOE} MuSCs (Figure 14A-B), suggesting that the overexpression of constitutively active RhoA does not affect the structural property of QPs, typically associated with MuSC quiescence. Additionally, the level of active Rac-GTP remained unchanged in *caRhoA*^{scOE} MuSCs (Figure 14C-D), indicating that RhoA overexpression does not suppress Rac1 activity *in vivo*. This observation challenges the proposed reciprocal regulation between RhoA and Rac1, and implies that RhoA maintains MuSC quiescence through mechanisms that are distinct and likely independent from Rac1-mediated signaling pathways.

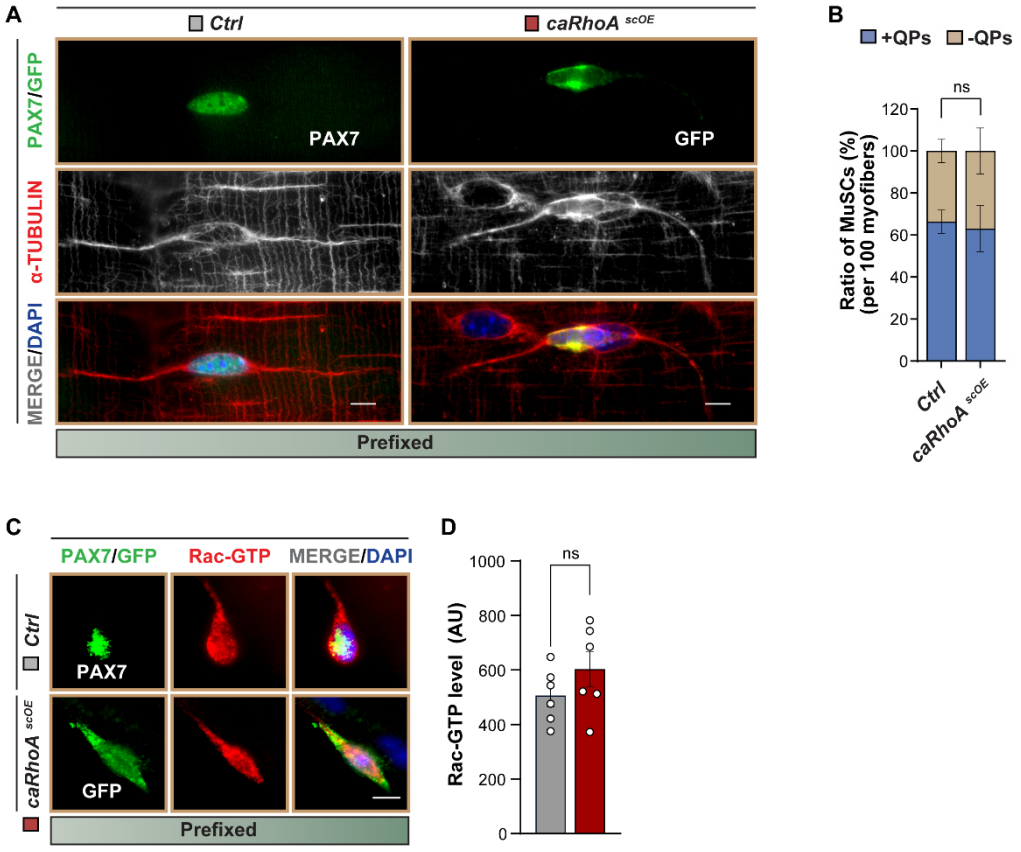

Figure 14 Overexpression of caRhoA has no effect on Rac activity or quiescent-projections (QPs) property of quiescent MuSC.

A-B. Immunofluorescence staining for PAX7 (green), α-TUBULIN (red), DAPI (blue), or autofluorescence GFP (green) on isolated myofibers from prefixed EDL muscles of control and *caRhoA*^{scOE} mice (A), and the proportion of MuSCs with or without quiescent projections (QPs) is shown in (B) (t-test: ns: no significant, n=3, 2-months-old male mice, 100 myofibers per muscle sample). Scale bars in (A) represent 10 µm.

C-D. Representative images (Rac-GTP (red), DAPI (blue), and PAX7/GFP (green)) (C) and quantification of Rho levels in MuSCs on isolated myofibers from prefixed EDL muscles is shown in (D). (One-way ANOVA: ***p < 0.001, 6 independent experiments, at least 100 MuSCs were measured in each group). Scale bars in (C) represent 5 µm.

6. DISCUSSION

G protein-coupled receptors (GPCRs) and their corresponding ligands have been implicated in maintaining quiescence in muscle stem cells (MuSCs) (Baghdadi et al., 2018b; Eliazer *et al.*, 2019; Sénéchal *et al.*, 2022; Yamaguchi *et al.*, 2015). However, a systematic analysis of the function of GPCRs in MUSCs and associated G-proteins was missing so far. In this thesis, I uncovered the expression pattern of GPCRs in quiescent MuSCs and identified ET-3 and NT, two novel ligands originating from the MuSC niche. ET-3 and NT promote and sustain MuSC quiescence by binding to EDNRB and NTSR2, respectively. Mechanistically, the activation of these GPCRs stimulates the G12/13 signaling cascade, thereby triggering RhoA-dependent regulatory mechanisms that establish quiescence in MuSCs. My findings not only offer a comprehensive overview of the diverse repertoire of GPCRs expressed in quiescent MuSCs but also shed light on the intricate regulatory mechanisms employed by extrinsic niche factors to govern MuSC behavior. Furthermore, I explored a fundamental regulatory axis that operates within quiescent MuSCs. I demonstrated that ET-3 and NT enhance the long-term regenerative potential of transplanted MuSCs, which will be helpful for the development of cell therapies targeting conditions such as Duchenne muscular dystrophy (DMD) and other myopathies.

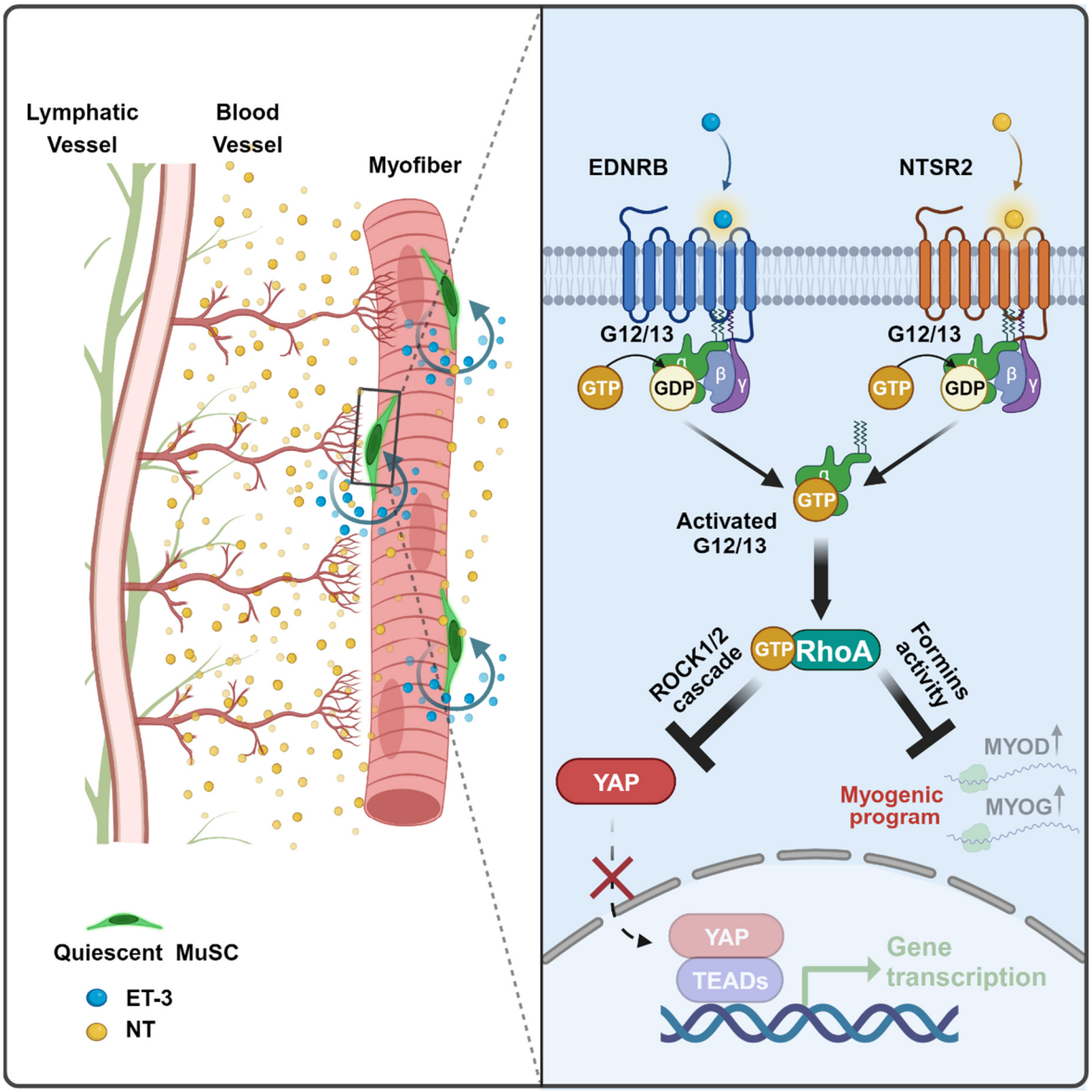

Figure 15 Schematic diagram of MuSC quiescence regulation via ET-3/NT-GPCRs-G12/13-RhoA signaling axis.

The diagram depicts quiescent muscle stem cells (MuSCs, green) situated on a myofiber, with endothelin-3 (ET-3, blue dots) being secreted by the MuSCs themselves and acting in an autocrine fashion by binding to the EDNRB receptor on the MuSC surface. Additionally, neurotrophin (NT, yellow dots) secreted by the endothelial cells of blood vessels affects the MuSCs in a paracrine manner by engaging the NTSR2 receptor. The ligand-receptor activation initiates a cascade via the G12/13 proteins, leading to the activation of RhoA (green). RhoA then exerts its effects through two pathways: it activates the Rho-associated protein kinase (ROCK) cascade, which in turn inhibits the nuclear translocation of YAP (red), consequently reducing the transcriptional activity of the YAP/TEAD complex and downregulating genes associated with cell cycle entry. Concurrently, RhoA

modulates the activity of formin family proteins, suppressing the expression of myogenic regulatory factors MYOD and MYOG, which helps to maintain the quiescent state of MuSCs.

6.1 G12/13-coupled GPCRs are crucial for maintaining quiescence of MuSC

Previous investigations on GPCR-mediated regulation of MuSC quiescence, made limited efforts to elucidate how distinct GPCRs engage specific downstream pathways in quiescent MuSCs. GPCR signals are predominantly transduced and amplified through heterotrimeric G proteins, which subsequently activate specific downstream effectors. Here, I unveiled the critical role of G-protein 12/13 (G12/13) in mediating effects of GPCRs to preserve MuSC quiescence. Stimulation of G12/13 by different GPCRs activates RhoA, which plays a fundamental role to prevent cell cycle entry and differentiation of MuSC. Stimulation of G12/13 is achieved by binding of ET-3 or NT to their respective GPCRs leading to increased RhoA activaty and subsequent promotion of MuSC quiescence. My findings indicate that the combined stimulation of G12/13 by a group of GPCRs is crucial to maintain quiescence of MuSC. Integration of signals from different GPCRs by G12/13 creates redundancy, preventing accidential activation of MuSCs when expression of individual ligands serving distinct GPCRs drops. The virtually complete loss of MuSC quiescence caused by inactivation of G12/13, which is much stronger than inhibition of individual GPCRs, is in agreement with this hypothesis. Essentially, G12/13 act as a funnel, collecting information from all GPCRs that couple to these G-proteins. Previous reports demonstrated that WNT signaling molecules also regulate MuSC quiescence. The receptors for WNTs belong to the frizzled family, which are atypical G-protein coupled receptors, mainly signaling via the WNT/b-catenin, WNT/calcium, or planar cell polarity pathways (Kestler and Kuhl, 2008). Reports about G-protein-dependent signaling by frizzled are scarce and the activity level of Frizzled-mediated G protein signaling seems much lower than that of a typical GPCR (Nichols et al., 2013). However, evidence for the involvement of G12/G13 in frizzled-dependent signaling has been reported (Arthofer et al., 2016; Hot et al., 2017). Thus, it seems possible that G12/13 participate in WNT4-induced stimulation of MuSC quiescence. Unfortunately, it was possible to study effects of WNT4 on G12/13-deficient MuSC, since, unlike ET-3 and NT, WNT4 does not exhibit pro-quiescence effects on MuSCs in vitro. The failure of WNT4 to maintain quiescence of MuSC in vitro is in contrast to its ability of RhoA activation in MuSCs in vivo within a restricted temporal window. Future studies, utilizing

genetic approaches to overexpress Wnt4 in *G1213^{scKO}* mice might help to answer the question whether the capability of WNT4 to induces MuSC quiescence also critically depends on activation of G12/13.

6.2 ET-3 and NT are effectors of the MuSC niche

NT and ET-3 are small peptides with diverse biological activities, encompassing stimulation of angiogenesis, regulation of food intake, and control of energy expenditure (Bek and McMillen, 2000; Davenport *et al.*, 2016; Gazquez et al., 2016; Siao *et al.*, 2021). A role for the regulation of MuSC was not known before. It is feasible that NT and ET-3 do not only have effects on MuSCs but also have an impact on other cell types within the MuSC niche, in particular since their receptors are also found in blood endothelial cells in proximity to MuSCs, suggesting a potential paracrine signaling mechanism. It will be also interesting to investigate whether NT and ET-3 involved in the recruitment of MuSCs or other niche cells for establishment of the characteristic microenvironment. Genetic inactivation of ET-3 and NT and their receptors in differerent cell types of the MuSC niche, will pave the way for a more comprehensive understanding of the biological functions of the tese peptides in skeletal muscles.

6.3 Inactivation of G12/13 in MuSCs depletes the stem cell pool and leads to increased sarcopenia during aging

Targeted ablation of G12/13 signaling in muscle stem cells (MuSCs) accelerates the onset of age-related sarcopenia, as evidenced by pronounced muscle atrophy in aged *G1213^{scKO}* mice. This phenotype strongly supports the pivotal role of MuSCs in mitigating age-related sarcopenia. Interestingly, G13 depletion in skeletal muscle fibers correlates with a shift in fiber type distribution, favoring an increase in oxidative-type myofibers, particularly type I and type IIa. Surprisingly, inactivation of G12/13 in juvenile MuSCs results in a significant reduction of type I fibers (Figure 7O-P), indicating different consequences of G12/13 inactivation in MuSCs compared to myofibers.

Therfore, I propose that fusion of G12/13-deficient, aberrantly activated MuSCs with adjacent myofibers alters the physiology of muscles. Incorporation of G12/13-deficient

progenitors into existing myofibers may disrupt intrinsic properties of myofibers, potentially perturbing their functions. Such perturbations may promote a phenotype switch away from type I fibers due to modulations in contractile protein expression or metabolic reprogramming. Furthermore, G12/13-deficient MuSCs may change the local paracrine landscape, altering the profile of secreted myokines, growth factors and cytokines. This altered secretome may contribute to the decline in muscle quality and functionality, observed in the aged *G1213*^{scKO} cohort. Persistent absence of G12/13 signaling may also trigger cellular senescence in aberrantly activated MuSCs, significantly altering the microenvironment surrounding adjacent myofibers through the Senescence-Associated Secretory Phenotype (SASP). SASP of senescent MuSCs may promote functional decline in adjacent myofibers, potentially accelerating sarcopenia through a pro-inflammatory and catabolic milieu. Lastly, fusion of constantly activated, G12/13-deficient MuSCs to neighboring myofibers may introduce defects into fibers that have been accumulated during constant activation, initiating or accelerating sarcopenia. Such processes may explain the decline in muscle functionality and enhanced sarcopenia during aging.

To elucidate these possibilities, comprehensive investigations are warranted to delineate the impact of G12/13 deficiency on muscle fiber type conversion, cellular senescence, and the overarching consequences of atypical MuSC fusion. The use of genetic lineage tracing methods, coupled with functional assays that assess muscle performance and regenerative potential, is essential to dissect the intricate interplay between MuSC biology, muscle fiber typing, and senescence

6.4 Activation of RhoA does not affect formation of protrusions in quiescent MuSCs

Recent studies suggest that cellular protrusions are crucial morphological features of quiescent MuSCs, characterized by high Rac1 activity and active filopodia formation (Kann et al., 2022). Interestingly, my findings demonstrate that RhoA activation does not affect Rac activity or contribute to the removal of protrusions in quiescent MuSCs, as claimed before. My experiments clearly demonstrated that activation of RhoA in *caRho* ^{scOE} mice does not affect the presence of protrusions compared to control MuSCs (Figure 14A-D). The study by Kann et al mainly used cell cycle-activated MuSCs, which raises the possibility

that cell cycle-activated and quiescent MuSCs have different mechanisms to organize the cytoskeleton. Some projections of quiescent MuSC contain cortical F-actin rings. Thus, it is plausible that RhoA, a key regulator of the F-actin cytoskeleton, controls F-actin dynamics during the growth of projections (Kann *et al.*, 2022; Ridley, 2015; Schaks et al., 2019). It is tempting to speculate that quiescent MuSCs possess a dynamic "protrusion-retraction switch", which is strongly dependent on the state of MuSCs. Protrusions in MuSCs may serve as sensory-like components, adjusting their length and number of filopodia in response to changes in mechanical force, stiffness, or biochemical cues within the muscle microenvironment, thus maintaining signal strength and preventing premature awakening of quiescent MuSCs. However, when muscle injury or stimuli surpass a certain threshold, projections are permanently lost, leading to a loss of sensitivity in MuSCs and triggering their entry into a highly contracted state, activating the regulatory program for cell cycle progression. RhoA and Rac1, as critical components for regulation of contraction and protrusion, are simultaneously expressed in quiescent MuSCs. Upon injury or persistent external stimuli exceeding the threshold, RhoA may accumulate rapidly and reorganize F-actin cytoskeletons within a brief time window, thereby mediating MuSC activation. While these studies underscore the importance of the projections in maintaining MuSC quiescence, they have yet to explore the underlying functional mechanisms deeply. In order to shed light on the specific roles of these projections in quiescent MuSC, future research should aim to dynamically monitor and track MuSC activity or the changes of RhoA/Rac1 activities in MuSC. Such investigations will undoubtedly help elucidate the precise functional mechanisms of these projections in quiescent MuSC.

6.5 Age-related decline in G12/13-dependent GPCR signaling is closly asscciated with the progressive loss of MuSC stemness during aging

The maintenance of stem cell quiescence is paramount for ensuring long-term tissue homeostasis and safeguarding the stem cell reservoir against premature depletion under diverse physiological stresses (Arai and Suda, 2008). However, as individuals age, the quiescence of MuSCs becomes progressively lost, leading to a decline in the regenerative potential of muscles (Blau et al., 2015). Various theories have been raised to explain the loss of quiescence in aging MuSC, one widely accepted mechanism involves the downregulation of Sprouty1 expression within aged MuSCs, leading to an inability to resist

the excessive stimulation by FGF2 from aged myofibers, consequently failing to maintain a quiescent state and resulting in the continual depletion of the MuSC pool (Chakkalakal et al., 2012). We hypothesize that that the gradual loss of MuSC quiescence during aging depends to a large degree on inability to sustain continuous activation of G12/13-dependent GPCR signaling pathways. Notably, the expression levels of *Edn3, Ednrb,* and *Ntsr2* in MuSCs decrease with age under homeostatic conditions, indicating a decline in G12/13-transduced GPCR signaling (Figure4 J). Possible factors contributing to this decline might be caused by malfunctions of the MuSC niche, reducing production of ligands or components crucial for GPCR signaling, as well as alterations in other quiescence-promoting signals (e.g., Notch and Wnt signaling) within the MuSC niche (Brack et al., 2007; Liu et al., 2018). Consequently, the activity of G12/13-dependent GPCR signaling pathways in MuSCs will diminish with age, eventually impairing MuSC quiescence. Since GPCRs are common target for drug design, we propose that G12/13-coupled GPCRs specific to quiescence are promising therapeutic targets for preventing age-related depletion of MuSCs. Preventing premature MuSC activation during aging has the potential to maintain muscle mass, physical mobilty and enhance the regenerative capacity of aged skeletal muscle. Further investigations into this signaling axis in aged MuSCs will improve the understanding of the mechanisms underlying the age-associated decline in stemness.

6.6 Future directions

The findings of this thesis have significantly advanced our understanding of the role G12/13-coupled GPCR signaling plays in maintaining muscle stem cell (MuSC) quiescence, providing a foundation for future research in this field. One critical area for further exploration involves the crosstalk between GPCR signaling and other quiescence-promoting pathways. Although this study has concentrated on G12/13-coupled GPCRs, MuSC quiescence is known to be influenced by a network of signaling pathways, including Notch, Wnt, and Hedgehog. Investigating the molecular interplay between these pathways and G12/13-coupled GPCR signaling is imperative for a holistic understanding of MuSC quiescence and activation. This approach will not only unravel the complex regulatory networks governing MuSC behavior but also identify novel targets for therapeutic interventions.

Another promising direction for future research lies in characterizing the role of GPCR signaling for aging of MuSCs. According to my results, it seems likely that an age-related decline in GPCR signaling contributes to the loss of MuSC functions during aging. However, the mechanisms underlying this decline are not fully understood. Longitudinal studies that track changes in GPCR expression and activity across different age groups, coupled with investigations into alterations within the MuSC niche, are crucial. These studies will provide valuable insights into the aging process of MuSCs and may reveal strategies for rejuvenating aged MuSCs through targeted modulation of GPCR signaling.

The therapeutic potential of targeting G12/13-coupled GPCRs in muscle diseases such as Duchenne muscular dystrophy (DMD) and other myopathies is another intriguing aspect that merits further exploration. Investigating how GPCR signaling is affected in these pathological conditions and whether modulation of this pathway can ameliorate disease symptoms or progression can lead to novel therapeutic strategies. Furthermore, the development of specific pharmacological modulators for G12/13-coupled GPCRs is a critical step towards harnessing their therapeutic potential. The discovery and optimization of small molecules or biologics that can selectively target these GPCRs would enable the enhancement of MuSC quiescence and regenerative capacity.

Incorporating advanced techniques such as in vivo imaging, genetic lineage tracing, and single-cell transcriptomics will also enhance our understanding of MuSC behavior in a physiological context. These techniques allow dynamic monitoring and real-time analysis of MuSCs, providing deeper insights into the effects of GPCR signaling on MuSC quiescence, activation, and differentiation.

Lastly, the therapeutic potential of NT and ET-3, identified in this thesis as novel ligands that promote MuSC quiescence, is a attractive avenue for research. Developing delivery systems for targeted administration of these ligands to the MuSC niche and assessing their effects in preclinical models of muscle injury and aging may lead to novel treatments for muscle-related diseases and conditions associated with aging.

In summary, this work provides a comprehensive understanding of GPCR-mediated regulation in MuSCs and lays the groundwork for future research to unravel the

complexities of MuSC biology and developing targeted therapies to maintain muscle health and functionality throughout the lifespan. The therapeutic potential of NT and ET-3 as novel ligands promoting MuSC quiescence offers new opportunities for the treatment of muscle-related diseases and age-related conditions.

7. Reference

Alfaro, L.A., Dick, S.A., Siegel, A.L., Anonuevo, A.S., McNagny, K.M., Megeney, L.A., Cornelison, D.D., and Rossi, F.M. (2011). CD34 promotes satellite cell motility and entry into proliferation to facilitate efficient skeletal muscle regeneration. Stem Cells *29*, 2030-2041. 10.1002/stem.759.

Amano, M., Nakayama, M., and Kaibuchi, K. (2010). Rho-kinase/ROCK: A key regulator of the cytoskeleton and cell polarity. Cytoskeleton (Hoboken) *67*, 545-554. 10.1002/cm.20472.

Arai, F., and Suda, T. (2008). Quiescent stem cells in the niche. In StemBook. 10.3824/stembook.1.6.1.

Arthofer, E., Hot, B., Petersen, J., Strakova, K., Jager, S., Grundmann, M., Kostenis, E., Gutkind, J.S., and Schulte, G. (2016). WNT Stimulation Dissociates a Frizzled 4 Inactive-State Complex with Galpha12/13. Mol Pharmacol *90*, 447-459. 10.1124/mol.116.104919.

Asakura, A., Seale, P., Girgis-Gabardo, A., and Rudnicki, M.A. (2002). Myogenic specification of side population cells in skeletal muscle. J Cell Biol *159*, 123-134. 10.1083/jcb.200202092.

Attwood, T.K., and Findlay, J.B.C. (1994). Fingerprinting G-protein-coupled receptors. Protein Engineering, Design and Selection *7*, 195-203. 10.1093/protein/7.2.195.

Auvergne, R., Wu, C., Connell, A., Au, S., Cornwell, A., Osipovitch, M., Benraiss, A., Dangelmajer, S., Guerrero-Cazares, H., Quinones-Hinojosa, A., and Goldman, S.A. (2016). PAR1 inhibition suppresses the self-renewal and growth of A2B5-defined glioma progenitor cells and their derived gliomas in vivo. Oncogene *35*, 3817-3828. 10.1038/onc.2015.452.

Baghdadi, M.B., Castel, D., Machado, L., Fukada, S.I., Birk, D.E., Relaix, F., Tajbakhsh, S., and Mourikis, P. (2018a). Reciprocal signalling by Notch-Collagen V-CALCR retains muscle stem cells in their niche. Nature *557*, 714-718. 10.1038/s41586-018-0144-9.

Baghdadi, M.B., Firmino, J., Soni, K., Evano, B., Di Girolamo, D., Mourikis, P., Castel, D., and Tajbakhsh, S. (2018b). Notch-Induced miR-708 Antagonizes Satellite Cell Migration and Maintains Quiescence. Cell Stem Cell *23*, 859-868.e855. 10.1016/j.stem.2018.09.017.

Bek, E.L., and McMillen, M.A. (2000). Endothelins are angiogenic. J Cardiovasc Pharmacol *36*, S135-139. 10.1097/00005344-200036051-00043.

Bernardi, H., Gay, S., Fedon, Y., Vernus, B., Bonnieu, A., and Bacou, F. (2011). Wnt4 activates the canonical beta-catenin pathway and regulates negatively myostatin: functional implication in myogenesis. American journal of physiology. Cell physiology *300*, C1122-1138. 10.1152/ajpcell.00214.2010.

Birdwell, C., Fiskus, W., Kadia, T.M., DiNardo, C.D., Mill, C.P., and Bhalla, K.N. (2021). EVI1 dysregulation: impact on biology and therapy of myeloid malignancies. Blood Cancer J *11*, 64. 10.1038/s41408-021-00457-9.

Blau, H.M., Cosgrove, B.D., and Ho, A.T. (2015). The central role of muscle stem cells in regenerative failure with aging. Nat Med *21*, 854-862. 10.1038/nm.3918.

Bober, E., Brand-Saberi, B., Ebensperger, C., Wilting, J., Balling, R., Paterson, B.M., Arnold, H.H., and Christ, B. (1994). Initial steps of myogenesis in somites are independent of influence from axial structures. Development *120*, 3073-3082. 10.1242/dev.120.11.3073.

Brack, A.S., Conboy, M.J., Roy, S., Lee, M., Kuo, C.J., Keller, C., and Rando, T.A. (2007). Increased Wnt signaling during aging alters muscle stem cell fate and increases fibrosis. Science *317*, 807-810. 10.1126/science.1144090.

Brockmann, M., Blomen, V.A., Nieuwenhuis, J., Stickel, E., Raaben, M., Bleijerveld, O.B., Altelaar, A.F.M., Jae, L.T., and Brummelkamp, T.R. (2017). Genetic wiring maps of single-cell protein states reveal an off-switch for GPCR signalling. Nature *546*, 307-311. 10.1038/nature22376.

Bruno, G., Cencetti, F., Bernacchioni, C., Donati, C., Blankenbach, K.V., Thomas, D., Meyer Zu Heringdorf, D., and Bruni, P. (2018). Bradykinin mediates myogenic differentiation in murine myoblasts through the involvement of SK1/Spns2/S1P2 axis. Cell Signal *45*, 110-121. 10.1016/j.cellsig.2018.02.001.

Burkin, D.J., and Kaufman, S.J. (1999). The alpha7beta1 integrin in muscle development and disease. Cell Tissue Res *296*, 183-190. 10.1007/s004410051279.

Castellani, L., Salvati, E., Alema, S., and Falcone, G. (2006). Fine regulation of RhoA and Rock is required for skeletal muscle differentiation. J Biol Chem *281*, 15249-15257. 10.1074/jbc.M601390200.
Chakkalakal, J.V., Jones, K.M., Basson, M.A., and Brack, A.S. (2012). The aged niche disrupts muscle stem cell quiescence. Nature *490*, 355-360. 10.1038/nature11438.
Chang, N.C., Chevalier, F.P., and Rudnicki, M.A. (2016). Satellite Cells in Muscular Dystrophy - Lost in Polarity. Trends Mol Med *22*, 479-496. 10.1016/j.molmed.2016.04.002.
Chang, T.H., Primig, M., Hadchouel, J., Tajbakhsh, S., Rocancourt, D., Fernandez, A., Kappler, R., Scherthan, H., and Buckingham, M. (2004). An enhancer directs differential expression of the linked Mrf4 and Myf5 myogenic regulatory genes in the mouse. Dev Biol *269*, 595-608. 10.1016/j.ydbio.2004.02.013.
Chechekhin, V.I., Kulebyakin, K.Y., Kokaev, R.I., and Tyurin-Kuzmin, P.A. (2022). GPCRs in the regulation of the functional activity of multipotent mesenchymal stromal cells. Front Cell Dev Biol *10*, 953374. 10.3389/fcell.2022.953374.
Chermnykh, E., Kalabusheva, E., and Vorotelyak, E. (2018). Extracellular Matrix as a Regulator of Epidermal Stem Cell Fate. Int J Mol Sci *19*. 10.3390/ijms19041003.
Congreve, M., de Graaf, C., Swain, N.A., and Tate, C.G. (2020). Impact of GPCR Structures on Drug Discovery. Cell *181*, 81-91. 10.1016/j.cell.2020.03.003.
Cornelison, D.D., Filla, M.S., Stanley, H.M., Rapraeger, A.C., and Olwin, B.B. (2001). Syndecan-3 and syndecan-4 specifically mark skeletal muscle satellite cells and are implicated in satellite cell maintenance and muscle regeneration. Dev Biol *239*, 79-94. 10.1006/dbio.2001.0416.
Cornelison, D.D., and Wold, B.J. (1997). Single-cell analysis of regulatory gene expression in quiescent and activated mouse skeletal muscle satellite cells. Dev Biol *191*, 270-283. 10.1006/dbio.1997.8721.
Daadi, M.M. (2019). Differentiation of Neural Stem Cells Derived from Induced Pluripotent Stem Cells into Dopaminergic Neurons. Methods Mol Biol *1919*, 89-96. 10.1007/978-1-4939-9007-8_7.
Daga, S., Rosenberger, A., Quehenberger, F., Krisper, N., Prietl, B., Reinisch, A., Zebisch, A., Sill, H., and Wolfler, A. (2019). High GPR56 surface expression correlates with a leukemic stem cell gene signature in CD34-positive AML. Cancer Med *8*, 1771-1778. 10.1002/cam4.2053.
Davenport, A.P. (2002). International Union of Pharmacology. XXIX. Update on endothelin receptor nomenclature. Pharmacol Rev *54*, 219-226. 10.1124/pr.54.2.219.
Davenport, A.P., Hyndman, K.A., Dhaun, N., Southan, C., Kohan, D.E., Pollock, J.S., Pollock, D.M., Webb, D.J., and Maguire, J.J. (2016). Endothelin. Pharmacol Rev *68*, 357-418. 10.1124/pr.115.011833.
De Belly, H., Paluch, E.K., and Chalut, K.J. (2022). Interplay between mechanics and signalling in regulating cell fate. Nature reviews. Molecular cell biology *23*, 465-480. 10.1038/s41580-022-00472-z.
Dellavalle, A., Maroli, G., Covarello, D., Azzoni, E., Innocenzi, A., Perani, L., Antonini, S., Sambasivan, R., Brunelli, S., Tajbakhsh, S., and Cossu, G. (2011). Pericytes resident in postnatal skeletal muscle differentiate into muscle fibres and generate satellite cells. Nat Commun *2*, 499. 10.1038/ncomms1508.
Dietrich, P.A., Yang, C., Leung, H.H., Lynch, J.R., Gonzales, E., Liu, B., Haber, M., Norris, M.D., Wang, J., and Wang, J.Y. (2014). GPR84 sustains aberrant beta-catenin signaling in leukemic stem cells for maintenance of MLL leukemogenesis. Blood *124*, 3284-3294. 10.1182/blood-2013-10-532523.
Dobreva, G., and Braun, T. (2010). The yin and yang of polycomb repression in regenerating muscle. Cell Stem Cell *7*, 422-424. 10.1016/j.stem.2010.09.005.
Donati, C., Cencetti, F., and Bruni, P. (2013). Sphingosine 1-phosphate axis: a new leader actor in skeletal muscle biology. Front Physiol *4*, 338. 10.3389/fphys.2013.00338.
Dong, F., Sun, X., Liu, W., Ai, D., Klysik, E., Lu, M.F., Hadley, J., Antoni, L., Chen, L., Baldini, A., et al. (2006). Pitx2 promotes development of splanchnic mesoderm-derived branchiomeric muscle. Development *133*, 4891-4899. 10.1242/dev.02693.

Doze, V.A., and Perez, D.M. (2012). G-protein-coupled receptors in adult neurogenesis. Pharmacol Rev *64*, 645-675. 10.1124/pr.111.004762.
Doze, V.A., and Perez, D.M. (2013). GPCRs in stem cell function. Prog Mol Biol Transl Sci *115*, 175-216. 10.1016/B978-0-12-394587-7.00005-1.
Eliazer, S., Muncie, J.M., Christensen, J., Sun, X., D'Urso, R.S., Weaver, V.M., and Brack, A.S. (2019). Wnt4 from the Niche Controls the Mechano-Properties and Quiescent State of Muscle Stem Cells. Cell Stem Cell. 10.1016/j.stem.2019.08.007.
Fedorov, Y.V., Jones, N.C., and Olwin, B.B. (1998). Regulation of myogenesis by fibroblast growth factors requires beta-gamma subunits of pertussis toxin-sensitive G proteins. Mol Cell Biol *18*, 5780-5787. 10.1128/MCB.18.10.5780.
Flock, T., Hauser, A.S., Lund, N., Gloriam, D.E., Balaji, S., and Babu, M.M. (2017). Selectivity determinants of GPCR-G-protein binding. Nature *545*, 317-322. 10.1038/nature22070.
Forcales, S.V., Albini, S., Giordani, L., Malecova, B., Cignolo, L., Chernov, A., Coutinho, P., Saccone, V., Consalvi, S., Williams, R., et al. (2012). Signal-dependent incorporation of MyoD-BAF60c into Brg1-based SWI/SNF chromatin-remodelling complex. Embo j *31*, 301-316. 10.1038/emboj.2011.391.
Fortier, M., Figeac, N., White, R.B., Knopp, P., and Zammit, P.S. (2013). Sphingosine-1-phosphate receptor 3 influences cell cycle progression in muscle satellite cells. Dev Biol *382*, 504-516. 10.1016/j.ydbio.2013.07.006.
Francetic, T., and Li, Q. (2011). Skeletal myogenesis and Myf5 activation. Transcription *2*, 109-114. 10.4161/trns.2.3.15829.
Franz, T., Kothary, R., Surani, M.A., Halata, Z., and Grim, M. (1993). The Splotch mutation interferes with muscle development in the limbs. Anat Embryol (Berl) *187*, 153-160. 10.1007/bf00171747.
Fu, X., Zhuang, C.L., and Hu, P. (2022). Regulation of muscle stem cell fate. Cell Regen *11*, 40. 10.1186/s13619-022-00142-7.
Fuchs, E., and Blau, H.M. (2020). Tissue Stem Cells: Architects of Their Niches. Cell Stem Cell *27*, 532-556. 10.1016/j.stem.2020.09.011.
Fukada, S., Uezumi, A., Ikemoto, M., Masuda, S., Segawa, M., Tanimura, N., Yamamoto, H., Miyagoe-Suzuki, Y., and Takeda, S. (2007). Molecular signature of quiescent satellite cells in adult skeletal muscle. Stem Cells *25*, 2448-2459. 10.1634/stemcells.2007-0019.
Fulco, M., Schiltz, R.L., Iezzi, S., King, M.T., Zhao, P., Kashiwaya, Y., Hoffman, E., Veech, R.L., and Sartorelli, V. (2003). Sir2 regulates skeletal muscle differentiation as a potential sensor of the redox state. Mol Cell *12*, 51-62. 10.1016/s1097-2765(03)00226-0.
Gage, P.J., and Camper, S.A. (1997). Pituitary homeobox 2, a novel member of the bicoid-related family of homeobox genes, is a potential regulator of anterior structure formation. Human molecular genetics *6*, 457-464. 10.1093/hmg/6.3.457.
Gazquez, E., Watanabe, Y., Broders-Bondon, F., Paul-Gilloteaux, P., Heysch, J., Baral, V., Bondurand, N., and Dufour, S. (2016). Endothelin-3 stimulates cell adhesion and cooperates with beta1-integrins during enteric nervous system ontogenesis. Sci Rep *6*, 37877. 10.1038/srep37877.
Geisler, S., Berod, A., Zahm, D.S., and Rostene, W. (2006). Brain neurotensin, psychostimulants, and stress--emphasis on neuroanatomical substrates. Peptides *27*, 2364-2384. 10.1016/j.peptides.2006.03.037.
Geloso, M.C., Corvino, V., Di Maria, V., Marchese, E., and Michetti, F. (2015). Cellular targets for neuropeptide Y-mediated control of adult neurogenesis. Front Cell Neurosci *9*, 85. 10.3389/fncel.2015.00085.
Gensch, N., Borchardt, T., Schneider, A., Riethmacher, D., and Braun, T. (2008). Different autonomous myogenic cell populations revealed by ablation of Myf5-expressing cells during mouse embryogenesis. Development *135*, 1597-1604. 10.1242/dev.019331.
Gilbert, P.M., Havenstrite, K.L., Magnusson, K.E., Sacco, A., Leonardi, N.A., Kraft, P., Nguyen, N.K., Thrun, S., Lutolf, M.P., and Blau, H.M. (2010). Substrate elasticity regulates skeletal muscle stem cell self-renewal in culture. Science *329*, 1078-1081. 10.1126/science.1191035.

Giordani, L., and Puri, P.L. (2013). Epigenetic control of skeletal muscle regeneration: Integrating genetic determinants and environmental changes. Febs j *280*, 4014-4025. 10.1111/febs.12383.
Gopinath, S.D., Narumiya, S., and Dhawan, J. (2007). The RhoA effector mDiaphanous regulates MyoD expression and cell cycle progression via SRF-dependent and SRF-independent pathways. Journal of cell science *120*, 3086-3098. 10.1242/jcs.006619.
Goulding, M., Lumsden, A., and Paquette, A.J. (1994). Regulation of Pax-3 expression in the dermomyotome and its role in muscle development. Development *120*, 957-971. 10.1242/dev.120.4.957.
Guerci, A., Lahoute, C., Hébrard, S., Collard, L., Graindorge, D., Favier, M., Cagnard, N., Batonnet-Pichon, S., Précigout, G., Garcia, L., et al. (2012). Srf-dependent paracrine signals produced by myofibers control satellite cell-mediated skeletal muscle hypertrophy. Cell Metab *15*, 25-37. 10.1016/j.cmet.2011.12.001.
Gunther, S., Kim, J., Kostin, S., Lepper, C., Fan, C.M., and Braun, T. (2013). Myf5-positive satellite cells contribute to Pax7-dependent long-term maintenance of adult muscle stem cells. Cell Stem Cell *13*, 590-601. 10.1016/j.stem.2013.07.016.
Gupta, M.K., Papay, R.S., Jurgens, C.W., Gaivin, R.J., Shi, T., Doze, V.A., and Perez, D.M. (2009). alpha1-Adrenergic receptors regulate neurogenesis and gliogenesis. Mol Pharmacol *76*, 314-326. 10.1124/mol.109.057307.
Hamann, J., Aust, G., Arac, D., Engel, F.B., Formstone, C., Fredriksson, R., Hall, R.A., Harty, B.L., Kirchhoff, C., Knapp, B., et al. (2015). International Union of Basic and Clinical Pharmacology. XCIV. Adhesion G protein-coupled receptors. Pharmacol Rev *67*, 338-367. 10.1124/pr.114.009647.
Hicks, M.R., and Pyle, A.D. (2022). The emergence of the stem cell niche. Trends Cell Biol. 10.1016/j.tcb.2022.07.003.
Ho, A.T.V., Palla, A.R., Blake, M.R., Yucel, N.D., Wang, Y.X., Magnusson, K.E.G., Holbrook, C.A., Kraft, P.E., Delp, S.L., and Blau, H.M. (2017a). Prostaglandin E2 is essential for efficacious skeletal muscle stem-cell function, augmenting regeneration and strength. Proc Natl Acad Sci U S A *114*, 6675-6684. 10.1073/pnas.1705420114.
Ho, S.Y., Ling, T.Y., Lin, H.Y., Liou, J.T., Liu, F.C., Chen, I.C., Lee, S.W., Hsu, Y., Lai, D.M., and Liou, H.H. (2017b). SDF-1/CXCR4 Signaling Maintains Stemness Signature in Mouse Neural Stem/Progenitor Cells. Stem Cells Int *2017*, 2493752. 10.1155/2017/2493752.
Holst, B., Holliday, N.D., Bach, A., Elling, C.E., Cox, H.M., and Schwartz, T.W. (2004). Common structural basis for constitutive activity of the ghrelin receptor family. The Journal of biological chemistry *279*, 53806-53817. 10.1074/jbc.M407676200.
Hot, B., Valnohova, J., Arthofer, E., Simon, K., Shin, J., Uhlen, M., Kostenis, E., Mulder, J., and Schulte, G. (2017). FZD(10)-Galpha(13) signalling axis points to a role of FZD(10) in CNS angiogenesis. Cell Signal *32*, 93-103. 10.1016/j.cellsig.2017.01.023.
Husted, A.S., Trauelsen, M., Rudenko, O., Hjorth, S.A., and Schwartz, T.W. (2017). GPCR-Mediated Signaling of Metabolites. Cell Metab *25*, 777-796. 10.1016/j.cmet.2017.03.008.
Hutcheson, D.A., Zhao, J., Merrell, A., Haldar, M., and Kardon, G. (2009). Embryonic and fetal limb myogenic cells are derived from developmentally distinct progenitors and have different requirements for beta-catenin. Genes Dev *23*, 997-1013. 10.1101/gad.1769009.
Inoue, A., Raimondi, F., Kadji, F.M.N., Singh, G., Kishi, T., Uwamizu, A., Ono, Y., Shinjo, Y., Ishida, S., Arang, N., et al. (2019). Illuminating G-Protein-Coupling Selectivity of GPCRs. Cell *177*, 1933-1947 e1925. 10.1016/j.cell.2019.04.044.
Ivan, J., Major, E., Sipos, A., Kovacs, K., Horvath, D., Tamas, I., Bay, P., Dombradi, V., and Lontay, B. (2017). The Short-Chain Fatty Acid Propionate Inhibits Adipogenic Differentiation of Human Chorion-Derived Mesenchymal Stem Cells Through the Free Fatty Acid Receptor 2. Stem Cells Dev *26*, 1724-1733. 10.1089/scd.2017.0035.
Jiang, S., Fu, Y., Williams, J., Wood, J., Pandarinathan, L., Avraham, S., Makriyannis, A., Avraham, S., and Avraham, H.K. (2007). Expression and function of cannabinoid receptors CB1 and CB2 and their cognate cannabinoid ligands in murine embryonic stem cells. PLoS One *2*, e641. 10.1371/journal.pone.0000641.

Joe, A.W., Yi, L., Natarajan, A., Le Grand, F., So, L., Wang, J., Rudnicki, M.A., and Rossi, F.M. (2010). Muscle injury activates resident fibro/adipogenic progenitors that facilitate myogenesis. Nat Cell Biol *12*, 153-163. 10.1038/ncb2015.
Juan, A.H., Derfoul, A., Feng, X., Ryall, J.G., Dell'Orso, S., Pasut, A., Zare, H., Simone, J.M., Rudnicki, M.A., and Sartorelli, V. (2011). Polycomb EZH2 controls self-renewal and safeguards the transcriptional identity of skeletal muscle stem cells. Genes Dev *25*, 789-794. 10.1101/gad.2027911.
Kanisicak, O., Mendez, J.J., Yamamoto, S., Yamamoto, M., and Goldhamer, D.J. (2009). Progenitors of skeletal muscle satellite cells express the muscle determination gene, MyoD. Dev Biol *332*, 131-141. 10.1016/j.ydbio.2009.05.554.
Kann, A.P., Hung, M., Wang, W., Nguyen, J., Gilbert, P.M., Wu, Z., and Krauss, R.S. (2022). An injury-responsive Rac-to-Rho GTPase switch drives activation of muscle stem cells through rapid cytoskeletal remodeling. Cell Stem Cell *29*, 933-947 e936. 10.1016/j.stem.2022.04.016.
Kassar-Duchossoy, L., Giacone, E., Gayraud-Morel, B., Jory, A., Gomès, D., and Tajbakhsh, S. (2005). Pax3/Pax7 mark a novel population of primitive myogenic cells during development. Genes Dev *19*, 1426-1431. 10.1101/gad.345505.
Kelly, R.G., Jerome-Majewska, L.A., and Papaioannou, V.E. (2004). The del22q11.2 candidate gene Tbx1 regulates branchiomeric myogenesis. Human molecular genetics *13*, 2829-2840. 10.1093/hmg/ddh304.
Kestler, H.A., and Kuhl, M. (2008). From individual Wnt pathways towards a Wnt signalling network. Philos Trans R Soc Lond B Biol Sci *363*, 1333-1347. 10.1098/rstb.2007.2251.
Kippin, T.E., Kapur, S., and van der Kooy, D. (2005). Dopamine specifically inhibits forebrain neural stem cell proliferation, suggesting a novel effect of antipsychotic drugs. J Neurosci *25*, 5815-5823. 10.1523/JNEUROSCI.1120-05.2005.
Kong, Y., Wang, H., Lin, T., and Wang, S. (2014). Sphingosine-1-phosphate/S1P receptors signaling modulates cell migration in human bone marrow-derived mesenchymal stem cells. Mediators Inflamm *2014*, 565369. 10.1155/2014/565369.
Krishnan, A. (2015). Evolution of the G protein-coupled receptor signaling system : Genomic and phylogenetic analyses*.* PhD dissertation.
Kuang, S., Kuroda, K., Le Grand, F., and Rudnicki, M.A. (2007). Asymmetric self-renewal and commitment of satellite stem cells in muscle. Cell *129*, 999-1010. 10.1016/j.cell.2007.03.044.
LaBarge, M.A., and Blau, H.M. (2002). Biological progression from adult bone marrow to mononucleate muscle stem cell to multinucleate muscle fiber in response to injury. Cell *111*, 589-601. 10.1016/s0092-8674(02)01078-4.
Lagha, M., Sato, T., Bajard, L., Daubas, P., Esner, M., Montarras, D., Relaix, F., and Buckingham, M. (2008). Regulation of skeletal muscle stem cell behavior by Pax3 and Pax7. Cold Spring Harb Symp Quant Biol *73*, 307-315. 10.1101/sqb.2008.73.006.
Lee, J.Y., Qu-Petersen, Z., Cao, B., Kimura, S., Jankowski, R., Cummins, J., Usas, A., Gates, C., Robbins, P., Wernig, A., and Huard, J. (2000). Clonal isolation of muscle-derived cells capable of enhancing muscle regeneration and bone healing. J Cell Biol *150*, 1085-1100. 10.1083/jcb.150.5.1085.
Li, W., Wei, S., Liu, C., Song, M., Wu, H., and Yang, Y. (2016). Regulation of the osteogenic and adipogenic differentiation of bone marrow-derived stromal cells by extracellular uridine triphosphate: The role of P2Y2 receptor and ERK1/2 signaling. Int J Mol Med *37*, 63-73. 10.3892/ijmm.2015.2400.
Lin, J.H., Chang, H.H., Lee, W.S., Ting, P.C., Luo, Y.P., and Yang, K.T. (2021). Palmitic Acid Methyl Ester Enhances Adipogenic Differentiation in Rat Adipose Tissue-Derived Mesenchymal Stem Cells through a G Protein-Coupled Receptor-Mediated Pathway. Stem Cells Int *2021*, 9938649. 10.1155/2021/9938649.
Liu, B., and Wu, D. (2003). The first inner loop of endothelin receptor type B is necessary for specific coupling to Galpha 13. The Journal of biological chemistry *278*, 2384-2387. 10.1074/jbc.M208683200.

Liu, G.Y., Liu, J., Wang, Y.L., Liu, Y., Shao, Y., Han, Y., Qin, Y.R., Xiao, F.J., Li, P.F., Zhao, L.J., et al. (2016). Adipose-Derived Mesenchymal Stem Cells Ameliorate Lipid Metabolic Disturbance in Mice. Stem Cells Transl Med *5*, 1162-1170. 10.5966/sctm.2015-0239.
Liu, L., Charville, G.W., Cheung, T.H., Yoo, B., Santos, P.J., Schroeder, M., and Rando, T.A. (2018). Impaired Notch Signaling Leads to a Decrease in p53 Activity and Mitotic Catastrophe in Aged Muscle Stem Cells. Cell Stem Cell *23*, 544-556 e544. 10.1016/j.stem.2018.08.019.
Liu, L., Cheung, T.H., Charville, G.W., Hurgo, B.M., Leavitt, T., Shih, J., Brunet, A., and Rando, T.A. (2013). Chromatin modifications as determinants of muscle stem cell quiescence and chronological aging. Cell Rep *4*, 189-204. 10.1016/j.celrep.2013.05.043.
Loh, K.C., Leong, W.I., Carlson, M.E., Oskouian, B., Kumar, A., Fyrst, H., Zhang, M., Proia, R.L., Hoffman, E.P., and Saba, J.D. (2012). Sphingosine-1-phosphate enhances satellite cell activation in dystrophic muscles through a S1PR2/STAT3 signaling pathway. PLoS One *7*, e37218. 10.1371/journal.pone.0037218.
Lu, J.R., Bassel-Duby, R., Hawkins, A., Chang, P., Valdez, R., Wu, H., Gan, L., Shelton, J.M., Richardson, J.A., and Olson, E.N. (2002). Control of facial muscle development by MyoR and capsulin. Science *298*, 2378-2381. 10.1126/science.1078273.
Luo, F., Su, Y., Zhang, Z., and Li, J. (2022). Bone marrow mesenchymal stem cells promote the progression of prostate cancer through the SDF-1/CXCR4 axis in vivo and vitro. Clin Transl Oncol *24*, 892-901. 10.1007/s12094-021-02740-4.
Mal, A., Sturniolo, M., Schiltz, R.L., Ghosh, M.K., and Harter, M.L. (2001). A role for histone deacetylase HDAC1 in modulating the transcriptional activity of MyoD: inhibition of the myogenic program. Embo j *20*, 1739-1753. 10.1093/emboj/20.7.1739.
Mazella, J. (2001). Sortilin/neurotensin receptor-3: a new tool to investigate neurotensin signaling and cellular trafficking? Cell Signal *13*, 1-6. 10.1016/s0898-6568(00)00130-3.
McCudden, C.R., Hains, M.D., Kimple, R.J., Siderovski, D.P., and Willard, F.S. (2005). G-protein signaling: back to the future. Cell Mol Life Sci *62*, 551-577. 10.1007/s00018-004-4462-3.
McKellar, D.W., Walter, L.D., Song, L.T., Mantri, M., Wang, M.F.Z., De Vlaminck, I., and Cosgrove, B.D. (2021). Large-scale integration of single-cell transcriptomic data captures transitional progenitor states in mouse skeletal muscle regeneration. Commun Biol *4*, 1280. 10.1038/s42003-021-02810-x.
McKinsey, T.A., Zhang, C.L., Lu, J., and Olson, E.N. (2000). Signal-dependent nuclear export of a histone deacetylase regulates muscle differentiation. Nature *408*, 106-111. 10.1038/35040593.
Melendez, J., Stengel, K., Zhou, X., Chauhan, B.K., Debidda, M., Andreassen, P., Lang, R.A., and Zheng, Y. (2011). RhoA GTPase Is Dispensable for Actomyosin Regulation but Is Essential for Mitosis in Primary Mouse Embryonic Fibroblasts*. Journal of Biological Chemistry *286*, 15132-15137. https://doi.org/10.1074/jbc.C111.229336.
Messina, G., Biressi, S., Monteverde, S., Magli, A., Cassano, M., Perani, L., Roncaglia, E., Tagliafico, E., Starnes, L., Campbell, C.E., et al. (2010). Nfix regulates fetal-specific transcription in developing skeletal muscle. Cell *140*, 554-566. 10.1016/j.cell.2010.01.027.
Messina, G., and Cossu, G. (2009). The origin of embryonic and fetal myoblasts: a role of Pax3 and Pax7. Genes & Development *23*, 902-905. 10.1101/gad.1797009.
Minetti, G.C., Feige, J.N., Bombard, F., Heier, A., Morvan, F., Nurnberg, B., Leiss, V., Birnbaumer, L., Glass, D.J., and Fornaro, M. (2014). Galphai2 signaling is required for skeletal muscle growth, regeneration, and satellite cell proliferation and differentiation. Mol Cell Biol *34*, 619-630. 10.1128/MCB.00957-13.
Mitchell, K.J., Pannerec, A., Cadot, B., Parlakian, A., Besson, V., Gomes, E.R., Marazzi, G., and Sassoon, D.A. (2010). Identification and characterization of a non-satellite cell muscle resident progenitor during postnatal development. Nat Cell Biol *12*, 257-266. 10.1038/ncb2025.
Moers, A., Nieswandt, B., Massberg, S., Wettschureck, N., Grüner, S., Konrad, I., Schulte, V., Aktas, B., Gratacap, M.P., Simon, M.I., et al. (2003). G13 is an essential mediator of platelet activation in hemostasis and thrombosis. Nat Med *9*, 1418-1422. 10.1038/nm943.

Mohamed-Ahmed, S., Fristad, I., Lie, S.A., Suliman, S., Mustafa, K., Vindenes, H., and Idris, S.B. (2018). Adipose-derived and bone marrow mesenchymal stem cells: a donor-matched comparison. Stem Cell Res Ther *9*, 168. 10.1186/s13287-018-0914-1.
Mohle, R., and Drost, A.C. (2012). G protein-coupled receptor crosstalk and signaling in hematopoietic stem and progenitor cells. Ann N Y Acad Sci *1266*, 63-67. 10.1111/j.1749-6632.2012.06559.x.
Montarras, D., Morgan, J., Collins, C., Relaix, F., Zaffran, S., Cumano, A., Partridge, T., and Buckingham, M. (2005). Direct isolation of satellite cells for skeletal muscle regeneration. Science *309*, 2064-2067. 10.1126/science.1114758.
Moreno, M., Pedrosa, L., Pare, L., Pineda, E., Bejarano, L., Martinez, J., Balasubramaniyan, V., Ezhilarasan, R., Kallarackal, N., Kim, S.H., et al. (2017). GPR56/ADGRG1 Inhibits Mesenchymal Differentiation and Radioresistance in Glioblastoma. Cell Rep *21*, 2183-2197. 10.1016/j.celrep.2017.10.083.
Nagata, Y., Partridge, T.A., Matsuda, R., and Zammit, P.S. (2006). Entry of muscle satellite cells into the cell cycle requires sphingolipid signaling. J Cell Biol *174*, 245-253. 10.1083/jcb.200605028.
Ng, J.K., Kawakami, Y., Büscher, D., Raya, A., Itoh, T., Koth, C.M., Rodríguez Esteban, C., Rodríguez-León, J., Garrity, D.M., Fishman, M.C., and Izpisúa Belmonte, J.C. (2002). The limb identity gene Tbx5 promotes limb initiation by interacting with Wnt2b and Fgf10. Development *129*, 5161-5170. 10.1242/dev.129.22.5161.
Nichols, A.S., Floyd, D.H., Bruinsma, S.P., Narzinski, K., and Baranski, T.J. (2013). Frizzled receptors signal through G proteins. Cell Signal *25*, 1468-1475. 10.1016/j.cellsig.2013.03.009.
O'Hayre, M., Degese, M.S., and Gutkind, J.S. (2014). Novel insights into G protein and G protein-coupled receptor signaling in cancer. Curr Opin Cell Biol *27*, 126-135. 10.1016/j.ceb.2014.01.005.
Olguín, H.C., and Pisconti, A. (2012). Marking the tempo for myogenesis: Pax7 and the regulation of muscle stem cell fate decisions. J Cell Mol Med *16*, 1013-1025. 10.1111/j.1582-4934.2011.01348.x.
Palacios, D., Mozzetta, C., Consalvi, S., Caretti, G., Saccone, V., Proserpio, V., Marquez, V.E., Valente, S., Mai, A., Forcales, S.V., et al. (2010). TNF/p38α/polycomb signaling to Pax7 locus in satellite cells links inflammation to the epigenetic control of muscle regeneration. Cell Stem Cell *7*, 455-469. 10.1016/j.stem.2010.08.013.
Pannerec, A., Formicola, L., Besson, V., Marazzi, G., and Sassoon, D.A. (2013). Defining skeletal muscle resident progenitors and their cell fate potentials. Development *140*, 2879-2891. 10.1242/dev.089326.
Pant, T., Juric, M., Bosnjak, Z.J., and Dhanasekaran, A. (2021). Recent Insight on the Non-coding RNAs in Mesenchymal Stem Cell-Derived Exosomes: Regulatory and Therapeutic Role in Regenerative Medicine and Tissue Engineering. Front Cardiovasc Med *8*, 737512. 10.3389/fcvm.2021.737512.
Parise, G., McKinnell, I.W., and Rudnicki, M.A. (2008). Muscle satellite cell and atypical myogenic progenitor response following exercise. Muscle Nerve *37*, 611-619. 10.1002/mus.20995.
Pedro, M.P., Lund, K., and Iglesias-Bartolome, R. (2020). The landscape of GPCR signaling in the regulation of epidermal stem cell fate and skin homeostasis. Stem Cells. 10.1002/stem.3273.
Perez, A.L., Bachrach, E., Illigens, B.M., Jun, S.J., Bagden, E., Steffen, L., Flint, A., McGowan, F.X., Del Nido, P., Montecino-Rodriguez, E., et al. (2009). CXCR4 enhances engraftment of muscle progenitor cells. Muscle Nerve *40*, 562-572. 10.1002/mus.21317.
Polesskaya, A., Duquet, A., Naguibneva, I., Weise, C., Vervisch, A., Bengal, E., Hucho, F., Robin, P., and Harel-Bellan, A. (2000). CREB-binding protein/p300 activates MyoD by acetylation. The Journal of biological chemistry *275*, 34359-34364. 10.1074/jbc.M003815200.
Puri, P.L., Iezzi, S., Stiegler, P., Chen, T.T., Schiltz, R.L., Muscat, G.E., Giordano, A., Kedes, L., Wang, J.Y., and Sartorelli, V. (2001). Class I histone deacetylases sequentially interact with MyoD and pRb during skeletal myogenesis. Mol Cell *8*, 885-897. 10.1016/s1097-2765(01)00373-2.
Rao, T.N., Marks-Bluth, J., Sullivan, J., Gupta, M.K., Chandrakanthan, V., Fitch, S.R., Ottersbach, K., Jang, Y.C., Piao, X., Kulkarni, R.N., et al. (2015). High-level Gpr56 expression is dispensable for

the maintenance and function of hematopoietic stem and progenitor cells in mice. Stem Cell Res *14*, 307-322. 10.1016/j.scr.2015.02.001.
Ratajczak, M.Z., Majka, M., Kucia, M., Drukala, J., Pietrzkowski, Z., Peiper, S., and Janowska-Wieczorek, A. (2003). Expression of functional CXCR4 by muscle satellite cells and secretion of SDF-1 by muscle-derived fibroblasts is associated with the presence of both muscle progenitors in bone marrow and hematopoietic stem/progenitor cells in muscles. Stem Cells *21*, 363-371. 10.1634/stemcells.21-3-363.
Relaix, F., Bencze, M., Borok, M.J., Der Vartanian, A., Gattazzo, F., Mademtzoglou, D., Perez-Diaz, S., Prola, A., Reyes-Fernandez, P.C., Rotini, A., and Taglietti, t. (2021). Perspectives on skeletal muscle stem cells. Nat Commun *12*, 692. 10.1038/s41467-020-20760-6.
Relaix, F., Montarras, D., Zaffran, S., Gayraud-Morel, B., Rocancourt, D., Tajbakhsh, S., Mansouri, A., Cumano, A., and Buckingham, M. (2006). Pax3 and Pax7 have distinct and overlapping functions in adult muscle progenitor cells. *172*, 91-102. 10.1083/jcb.200508044.
Rezza, A., Wang, Z., Sennett, R., Qiao, W., Wang, D., Heitman, N., Mok, K.W., Clavel, C., Yi, R., Zandstra, P., et al. (2016). Signaling Networks among Stem Cell Precursors, Transit-Amplifying Progenitors, and their Niche in Developing Hair Follicles. Cell Rep *14*, 3001-3018. 10.1016/j.celrep.2016.02.078.
Ridley, A.J. (2015). Rho GTPase signalling in cell migration. Curr Opin Cell Biol *36*, 103-112. 10.1016/j.ceb.2015.08.005.
Rodrigues, R.S., Lourenco, D.M., Paulo, S.L., Mateus, J.M., Ferreira, M.F., Mouro, F.M., Moreira, J.B., Ribeiro, F.F., Sebastiao, A.M., and Xapelli, S. (2019). Cannabinoid Actions on Neural Stem Cells: Implications for Pathophysiology. Molecules *24*. 10.3390/molecules24071350.
Rosenbaum, D.M., Rasmussen, S.G.F., and Kobilka, B.K. (2009). The structure and function of G-protein-coupled receptors. Nature *459*, 356-363. 10.1038/nature08144.
Rothe, J., Thor, D., Winkler, J., Knierim, A.B., Binder, C., Huth, S., Kraft, R., Rothemund, S., Schoneberg, T., and Promel, S. (2019). Involvement of the Adhesion GPCRs Latrophilins in the Regulation of Insulin Release. Cell Rep *26*, 1573-1584 e1575. 10.1016/j.celrep.2019.01.040.
Rudnicki, M.A., Le Grand, F., McKinnell, I., and Kuang, S. (2008). The molecular regulation of muscle stem cell function. Cold Spring Harb Symp Quant Biol *73*, 323-331. 10.1101/sqb.2008.73.064.
Rudnicki, M.A., Schnegelsberg, P.N.J., Stead, R.H., Braun, T., Arnold, H.-H., and Jaenisch, R. (1993). MyoD or Myf-5 is required for the formation of skeletal muscle. Cell *75*, 1351-1359. https://doi.org/10.1016/0092-8674(93)90621-V.
Sacco, A., Doyonnas, R., Kraft, P., Vitorovic, S., and Blau, H.M. (2008). Self-renewal and expansion of single transplanted muscle stem cells. Nature *456*, 502-506. 10.1038/nature07384.
Saito, Y., Kaneda, K., Suekane, A., Ichihara, E., Nakahata, S., Yamakawa, N., Nagai, K., Mizuno, N., Kogawa, K., Miura, I., et al. (2013). Maintenance of the hematopoietic stem cell pool in bone marrow niches by EVI1-regulated GPR56. Leukemia *27*, 1637-1649. 10.1038/leu.2013.75.
Saleh, A., Subramaniam, G., Raychaudhuri, S., and Dhawan, J. (2019). Cytoplasmic sequestration of the RhoA effector mDiaphanous1 by Prohibitin2 promotes muscle differentiation. Scientific Reports *9*, 8302. 10.1038/s41598-019-44749-4.
Sambasivan, R., Yao, R., Kissenpfennig, A., Van Wittenberghe, L., Paldi, A., Gayraud-Morel, B., Guenou, H., Malissen, B., Tajbakhsh, S., and Galy, A. (2011). Pax7-expressing satellite cells are indispensable for adult skeletal muscle regeneration. Development *138*, 3647-3656. 10.1242/dev.067587.
Santos-Zas, I., Gurriaran-Rodriguez, U., Cid-Diaz, T., Figueroa, G., Gonzalez-Sanchez, J., Bouzo-Lorenzo, M., Mosteiro, C.S., Senaris, J., Casanueva, F.F., Casabiell, X., et al. (2016). beta-Arrestin scaffolds and signaling elements essential for the obestatin/GPR39 system that determine the myogenic program in human myoblast cells. Cell Mol Life Sci *73*, 617-635. 10.1007/s00018-015-1994-z.
Schaks, M., Giannone, G., and Rottner, K. (2019). Actin dynamics in cell migration. Essays Biochem *63*, 483-495. 10.1042/ebc20190015.

Seale, P., Sabourin, L.A., Girgis-Gabardo, A., Mansouri, A., Gruss, P., and Rudnicki, M.A. (2000). Pax7 Is Required for the Specification of Myogenic Satellite Cells. Cell *102*, 777-786. https://doi.org/10.1016/S0092-8674(00)00066-0.
Sénéchal, C., Fujita, R., Jamet, S., Maiga, A., Dort, J., Orfi, Z., Dumont, N.A., Bouvier, M., and Crist, C. (2022). The adhesion G-protein-coupled receptor Gpr116 is essential to maintain the skeletal muscle stem cell pool. Cell Rep *41*, 111645. 10.1016/j.celrep.2022.111645.
Serra, C., Palacios, D., Mozzetta, C., Forcales, S.V., Morantte, I., Ripani, M., Jones, D.R., Du, K., Jhala, U.S., Simone, C., and Puri, P.L. (2007). Functional interdependence at the chromatin level between the MKK6/p38 and IGF1/PI3K/AKT pathways during muscle differentiation. Mol Cell *28*, 200-213. 10.1016/j.molcel.2007.08.021.
Shen, B., Estevez, B., Xu, Z., Kreutz, B., Karginov, A., Bai, Y., Qian, F., Norifumi, U., Mosher, D., and Du, X. (2015). The interaction of Galpha13 with integrin beta1 mediates cell migration by dynamic regulation of RhoA. Mol Biol Cell *26*, 3658-3670. 10.1091/mbc.E15-05-0274.
Siao, A.C., Shih, L.J., Lin, Y.Y., Tsuei, Y.W., Kuo, Y.C., Ku, H.C., Chuu, C.P., Hsiao, P.J., and Kao, Y.H. (2021). Investigation of the Molecular Mechanisms by Which Endothelin-3 Stimulates Preadipocyte Growth. Front Endocrinol (Lausanne) *12*, 661828. 10.3389/fendo.2021.661828.
Siehler, S. (2009). Regulation of RhoGEF proteins by G12/13-coupled receptors. Br J Pharmacol *158*, 41-49. 10.1111/j.1476-5381.2009.00121.x.
Simone, C., Forcales, S.V., Hill, D.A., Imbalzano, A.N., Latella, L., and Puri, P.L. (2004). p38 pathway targets SWI-SNF chromatin-remodeling complex to muscle-specific loci. Nat Genet *36*, 738-743. 10.1038/ng1378.
Smith, P., Azzam, M., and Hinck, L. (2017). Extracellular Regulation of the Mitotic Spindle and Fate Determinants Driving Asymmetric Cell Division. Results and problems in cell differentiation *61*, 351-373. 10.1007/978-3-319-53150-2_16.
Sriram, K., and Insel, P.A. (2018). G Protein-Coupled Receptors as Targets for Approved Drugs: How Many Targets and How Many Drugs? Mol Pharmacol *93*, 251-258. 10.1124/mol.117.111062.
Sternweis, P.C., Carter, A.M., Chen, Z., Danesh, S.M., Hsiung, Y.F., and Singer, W.D. (2007). Regulation of Rho guanine nucleotide exchange factors by G proteins. Adv Protein Chem *74*, 189-228. 10.1016/s0065-3233(07)74006-8.
Szustak, M., and Gendaszewska-Darmach, E. (2020). Extracellular Nucleotides Selectively Induce Migration of Chondrocytes and Expression of Type II Collagen. Int J Mol Sci *21*. 10.3390/ijms21155227.
Tajbakhsh, S., Rocancourt, D., and Buckingham, M. (1996). Muscle progenitor cells failing to respond to positional cues adopt non-myogenic fates in myf-5 null mice. Nature *384*, 266-270. 10.1038/384266a0.
Till, J.E., and Mc, C.E. (1961). A direct measurement of the radiation sensitivity of normal mouse bone marrow cells. Radiat Res *14*, 213-222.
Tischner, D., Grimm, M., Kaur, H., Staudenraus, D., Carvalho, J., Looso, M., Gunther, S., Wanke, F., Moos, S., Siller, N., et al. (2017). Single-cell profiling reveals GPCR heterogeneity and functional patterning during neuroinflammation. JCI insight *2*. 10.1172/jci.insight.95063.
Ullah, I., Subbarao, R.B., and Rho, G.J. (2015). Human mesenchymal stem cells - current trends and future prospective. Biosci Rep *35*. 10.1042/BSR20150025.
Urtatiz, O., and Van Raamsdonk, C.D. (2016). Gnaq and Gna11 in the Endothelin Signaling Pathway and Melanoma. Front Genet *7*, 59. 10.3389/fgene.2016.00059.
Veltri, A., Lang, C., and Lien, W.H. (2018). Concise Review: Wnt Signaling Pathways in Skin Development and Epidermal Stem Cells. Stem Cells *36*, 22-35. 10.1002/stem.2723.
Verma, M., Asakura, Y., Murakonda, B.S.R., Pengo, T., Latroche, C., Chazaud, B., McLoon, L.K., and Asakura, A. (2018). Muscle Satellite Cell Cross-Talk with a Vascular Niche Maintains Quiescence via VEGF and Notch Signaling. Cell Stem Cell *23*, 530-543 e539. 10.1016/j.stem.2018.09.007.
Wagstaff, M., Coke, B., Hodgkiss, G.R., and Morgan, R.G. (2022). Targeting beta-catenin in acute myeloid leukaemia: past, present, and future perspectives. Biosci Rep *42*. 10.1042/BSR20211841.

Watanabe, N., Kato, T., Fujita, A., Ishizaki, T., and Narumiya, S. (1999). Cooperation between mDia1 and ROCK in Rho-induced actin reorganization. Nat Cell Biol *1*, 136-143. 10.1038/11056.
Wettschureck, N., Rütten, H., Zywietz, A., Gehring, D., Wilkie, T.M., Chen, J., Chien, K.R., and Offermanns, S. (2001). Absence of pressure overload induced myocardial hypertrophy after conditional inactivation of Galphaq/Galpha11 in cardiomyocytes. Nat Med *7*, 1236-1240. 10.1038/nm1101-1236.
White, R.B., Biérinx, A.S., Gnocchi, V.F., and Zammit, P.S. (2010). Dynamics of muscle fibre growth during postnatal mouse development. BMC Dev Biol *10*, 21. 10.1186/1471-213x-10-21.
Woodhouse, S., Pugazhendhi, D., Brien, P., and Pell, J.M. (2013). Ezh2 maintains a key phase of muscle satellite cell expansion but does not regulate terminal differentiation. Journal of cell science *126*, 565-579. 10.1242/jcs.114843.
Yablonka-Reuveni, Z., Day, K., Vine, A., and Shefer, G. (2008). Defining the transcriptional signature of skeletal muscle stem cells. J Anim Sci *86*, E207-216. 10.2527/jas.2007-0473.
Yamaguchi, M., Watanabe, Y., Ohtani, T., Uezumi, A., Mikami, N., Nakamura, M., Sato, T., Ikawa, M., Hoshino, M., Tsuchida, K., et al. (2015). Calcitonin Receptor Signaling Inhibits Muscle Stem Cells from Escaping the Quiescent State and the Niche. Cell Rep *13*, 302-314. 10.1016/j.celrep.2015.08.083.
Yin, H., Price, F., and Rudnicki, M.A. (2013). Satellite cells and the muscle stem cell niche. Physiol Rev *93*, 23-67. 10.1152/physrev.00043.2011.
Yoshida, T., Galvez, S., Tiwari, S., Rezk, B.M., Semprun-Prieto, L., Higashi, Y., Sukhanov, S., Yablonka-Reuveni, Z., and Delafontaine, P. (2013). Angiotensin II inhibits satellite cell proliferation and prevents skeletal muscle regeneration. The Journal of biological chemistry *288*, 23823-23832. 10.1074/jbc.M112.449074.
Yoshida, T., Huq, T.S., and Delafontaine, P. (2014). Angiotensin type 2 receptor signaling in satellite cells potentiates skeletal muscle regeneration. The Journal of biological chemistry *289*, 26239-26248. 10.1074/jbc.M114.585521.
Yu, O.M., and Brown, J.H. (2015). G Protein-Coupled Receptor and RhoA-Stimulated Transcriptional Responses: Links to Inflammation, Differentiation, and Cell Proliferation. Mol Pharmacol *88*, 171-180. 10.1124/mol.115.097857.
Zacharias, A.L., Lewandoski, M., Rudnicki, M.A., and Gage, P.J. (2011). Pitx2 is an upstream activator of extraocular myogenesis and survival. Dev Biol *349*, 395-405. 10.1016/j.ydbio.2010.10.028.
Zammit, P.S., Golding, J.P., Nagata, Y., Hudon, V., Partridge, T.A., and Beauchamp, J.R. (2004). Muscle satellite cells adopt divergent fates: a mechanism for self-renewal? J Cell Biol *166*, 347-357. 10.1083/jcb.200312007.
Zhang, H., Pasolli, H.A., and Fuchs, E. (2011). Yes-associated protein (YAP) transcriptional coactivator functions in balancing growth and differentiation in skin. Proc Natl Acad Sci U S A *108*, 2270-2275. 10.1073/pnas.1019603108.
Zhang, L., Noguchi, Y.T., Nakayama, H., Kaji, T., Tsujikawa, K., Ikemoto-Uezumi, M., Uezumi, A., Okada, Y., Doi, T., Watanabe, S., et al. (2019). The CalcR-PKA-Yap1 Axis Is Critical for Maintaining Quiescence in Muscle Stem Cells. Cell Rep *29*, 2154-2163 e2155. 10.1016/j.celrep.2019.10.057.
Zhang, T., Gunther, S., Looso, M., Kunne, C., Kruger, M., Kim, J., Zhou, Y., and Braun, T. (2015a). Prmt5 is a regulator of muscle stem cell expansion in adult mice. Nat Commun *6*, 7140. 10.1038/ncomms8140.
Zhang, T., Günther, S., Looso, M., Künne, C., Krüger, M., Kim, J., Zhou, Y., and Braun, T. (2015b). Prmt5 is a regulator of muscle stem cell expansion in adult mice. Nature Communications *6*, 7140. 10.1038/ncomms8140.
Zhang, Y., Depond, M., He, L., Foudi, A., Kwarteng, E.O., Lauret, E., Plo, I., Desterke, C., Dessen, P., Fujii, N., et al. (2016). CXCR4/CXCL12 axis counteracts hematopoietic stem cell exhaustion through selective protection against oxidative stress. Sci Rep *6*, 37827. 10.1038/srep37827.
Zhang, Z., Guan, N., Li, T., Mais, D.E., and Wang, M. (2012). Quality control of cell-based high-throughput drug screening. Acta Pharmaceutica Sinica B *2*, 429-438. 10.1016/j.apsb.2012.03.006.

Zhao, X., and Moore, D.L. (2018). Neural stem cells: developmental mechanisms and disease modeling. Cell Tissue Res *371*, 1-6. 10.1007/s00441-017-2738-1.
Zismanov, V., Chichkov, V., Colangelo, V., Jamet, S., Wang, S., Syme, A., Antonis, and Crist, C. (2016). Phosphorylation of eIF2α Is a Translational Control Mechanism Regulating Muscle Stem Cell Quiescence and Self-Renewal. Cell Stem Cell *18*, 79-90. 10.1016/j.stem.2015.09.020.

8. APPENDIX

8.1 Abbreviations

%	Percent
℃	Degree Celsius
A	Adenine
ATP	Adenosine triphosphate
bp	Base pairs
BSA	Bovine serum albumin
C	Cytosine
CDK	Cyclin-dependent kinase
cDNA	Complementary DNA
ChIP	Chromatin immunoprecipitation
cm	Centimeter
CMV	Cytomegalovirus
Co-IP	Co-immunopricipitation
CpG	Cytosine-guanine dinucleotide
CREB	cAMP response element-binding protein
CTX	Cobra cardiotoxin
CXCR-4	C-X-C chemokine receptor type 4
DAPI	4',6-diamidino-2-phenylindole
DMD	Duchenne muscular dystrophy
DMEM	Dulbecco's Modified Eagle Medium

DMSO	Dimethyl sulfoxide
DNA	Deoxyribonucleic acid
DNMT	DNA methyltransferase
DTA	Diphtheria toxin A
DTT	Dithiothreitol
E. coli	*Escherichia coli*
ECL	Enhanced chemi-luminescence
ECM	Extracellular matrix
EDL	Extensor digitorum longus
EDTA	Ethylenediaminetetraacetic acid
EdU	5-ethynyl-2'-deoxyuridine
ES	Embryonic stem cell
FAPs	Fibro-adipogenic progenitors
FCS	Fetal calf serum
FGF	Fibroblast growth factor
FACS	Fluorescence-Activated Cell Sorting
g	Gram
G	Guanine
g	Gravitational acceleration
GAPDH	Glyceraldehyde 3-phosphate dehydrogenase

GFP	Green fluorescent protein
h	Hour
H&E	Hematoxylin and eosin
HBS	HEPES Buffered Saline
HDAC	Histone deacetylases
HE	Hematoxylin and eosin
HEPES	4-(2-hydroxyethyl)-1-piperazineethanesulfonic acid
HRP	Horseradish peroxidase
HSA	Human skeletal actin
IF	Immunofluorescence
IGF	Insulin-like growth factor
IgG	Immunoglobulin G
IP	Immunoprecipitation
JNK	c-Jun N-terminal kinases
kb	kilo-base pairs
kDa	kilodalton
kg	kilogram
KO	Knock Out
M	molar
MEF2	Myocyte enhancer factor 2
min	Minute
ml	milliliter
mm	millimeter

mM	millimolar
MPI	Max-Planck Institute
Mrf4	myogenic regulatory factor 4
mRNA	messenger RNA
MS	Mass spectrometry
Myf5	Myogenic factor 5
MyoD	Myogenic differentiation
NFκB	Nuclear factor kappa-light-chain-enhancer of activated B cells
NP-40	Nonidet P-40
NSC	neural stem cell
P300	E1A binding protein p300
Pax3	Pair box transcription factor 3
Pax7	Pair box transcription factor 7
PBS	Phosphate Buffered Saline
PCAF	P300/CBP-associated factor
PcG	Polycomb-group
PCR	Polymerase chain reaction
P/S	Penicillin Streptomycin
PFA	Paraformaldehyde
Pitx2	Pituitary homeobox 2
PMSF	Phenyl methyl sulfonyl fluoride
Pol II	RNA Polymerase II
Prp8	pre-mRNA processing factor 8

qPCR	quantitative PCR
rDNA	Ribosomal DNA
RNA	Ribonucleic acid
rpm	Rotations per minute
rRNA	Ribosomal RNA
RT	Room temperature
RT-qPCR	Quantitative reverse transcription polymerase chain reaction
s	Second
SC	MuSC
SDS	Sodium dodecyl sulfate
SDS-PAGE	Sodium dodecyl sulfate polyacrylamide gel electrophoresis
shRNA	Small hairpin RNA
T	Thymine
TA	Tibialis anterior
TBS	Tris-Buffered Saline
Tbx1	T-box transcription factor 1
TES	Transcription end site
TFBS	Transcription factor binding sites
TrxG	Trithorax group
TSS	Transcription start site
Tween 20	Polyoxyethylene-sorbitan-monolaurate

V	Volt
WT	Wild type
EGFP	Enhanced green fluorescent protein
µg	micro gram
µl	micro liter
µM	micro molar
µm	micro meter

Acknowledgments

This work was carried out at Max Planck Institute for Heart and Lung Research in Bad Nauheim, Germany. I am sincerely grateful to my Ph.D. supervisor, Prof. Dr. Dr. Thomas Braun, for granting me this invaluable opportunity to pursue my doctoral studies. His profound knowledge and exceptional scientific insights left a lasting impression on me. Throughout my Ph.D. journey, he consistently supported and motivated me to develop innovative ideas for research projects, explore captivating techniques, and fearlessly establish collaborations with esteemed scientists.

I would like to extend my deepest gratitude to my second supervisor, Dr. Andre Schneider, for his unwavering encouragement and guidance throughout the course of this project. He consistently approached critical issues from a stimulating perspective, serving as an outstanding mentor and a dependable friend. His patience and diligence greatly facilitated the progress of this undertaking. Moreover, he taught me how to overcome failure both in scientific and everyday life. His optimistic outlook on life inspired me to persevere during the darkest moments.

I would also like to express my appreciation to Prof. Dr. Ingrid Fleming for her willingness to serve as my second examiner and for her valuable advice as a member of my thesis committee. I am immensely grateful to all the members of the AG Braun group for their support. I would like to extend special thanks to my colleagues and friends, particularly Dr. Jingjing Du, for their unwavering support. Working alongside these cherished friends has created indelible memories that will last a lifetime.

I am indebted to my beloved wife, Dr. Rui Li, whose support, companionship, and love have alleviated the hardships throughout this study. Her unwavering ability to uplift my spirits during moments of deep despair is truly remarkable.

Lastly, I would like to express my heartfelt gratitude to my parents and grandparents for their understanding and encouragement. With their unwavering support, I have been able to achieve all that I can. I dedicate this dissertation to them, as a token of my appreciation.